Clumping and Porosity in Massive Star Winds and How They Affect the Observed X-ray Emission

David Cohen
Swarthmore College

with Stan Owocki & Jon Sundqvist (U. Delaware) and Maurice Leutenegger (GSFC)

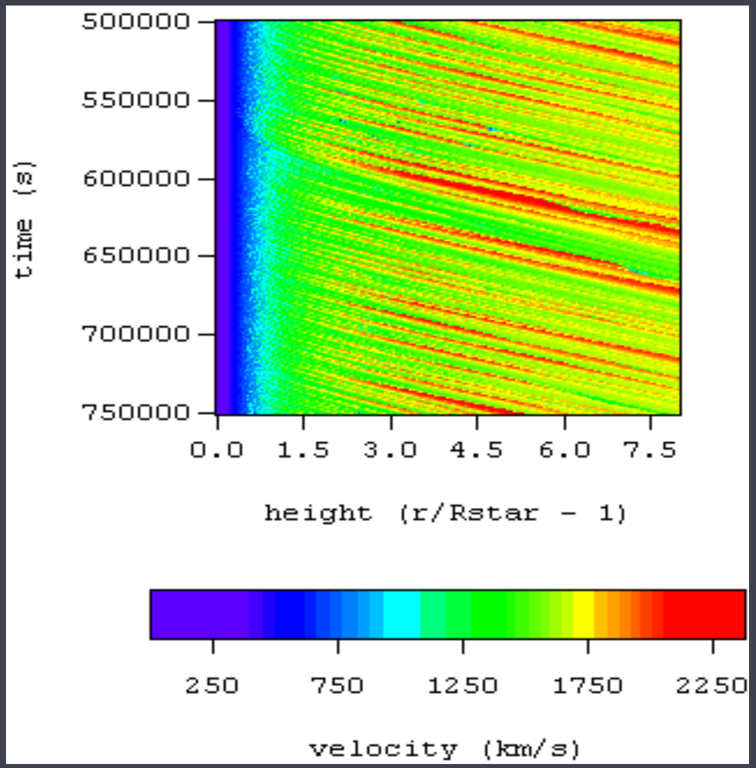

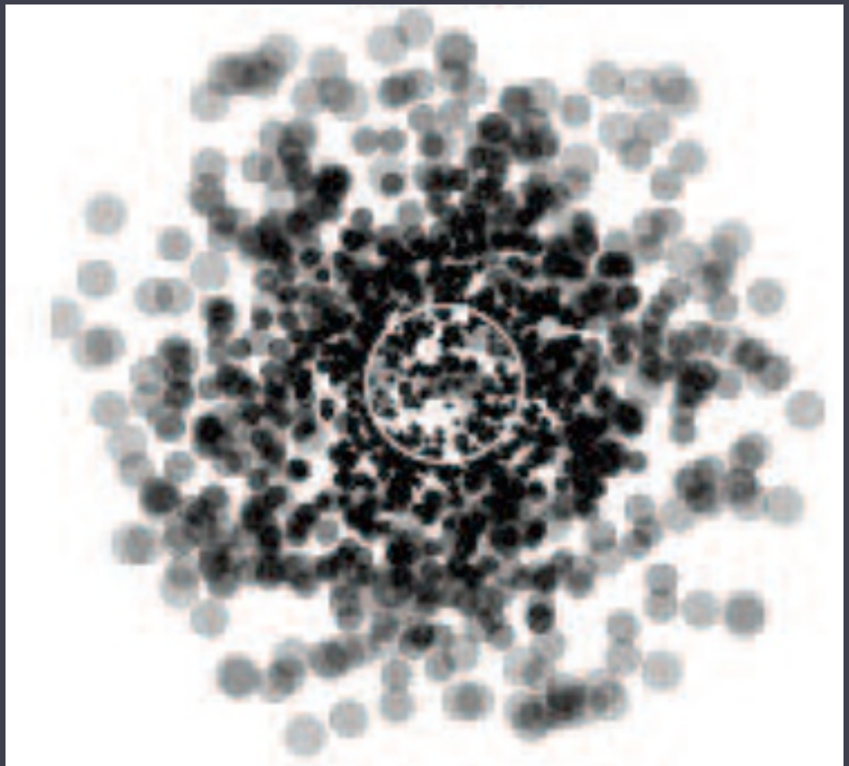

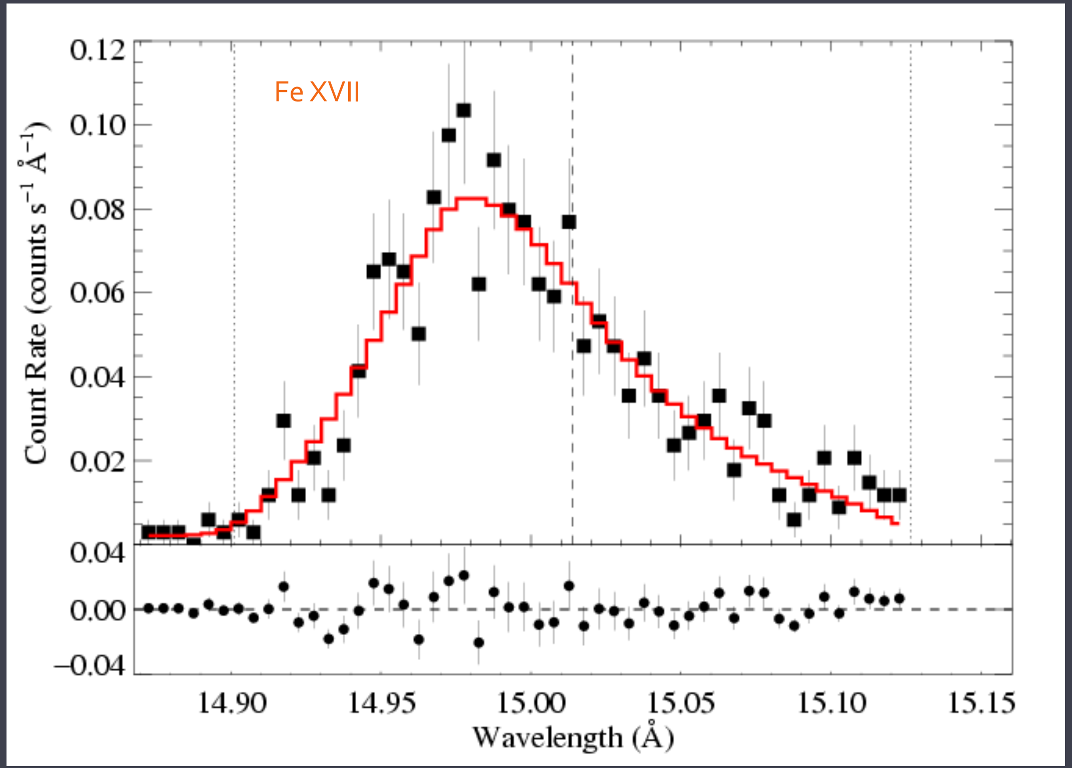

Outline: clumping and porosity

- Evidence for **clumping** in massive star winds

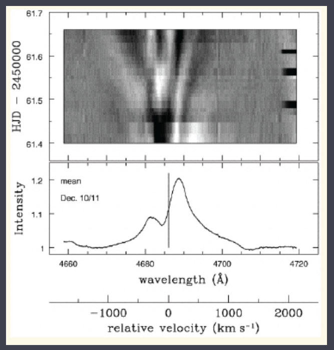

- Clumped winds are only **porous** if individual clumps are optically thick

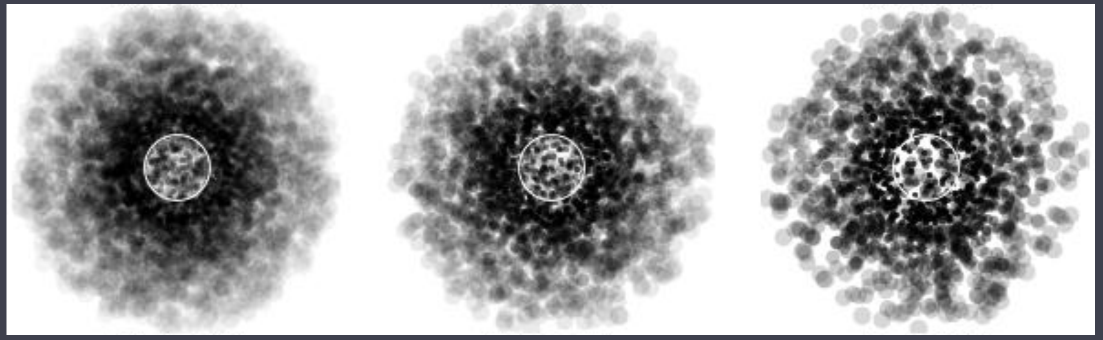

- The **porosity length** quantifies the effect of porosity

$h \equiv (n_{cl}A_{cl})^{-1} = L^3/\ell^2$ = *mean free path* between clumps

- If the porosity length is greater than $h \sim 1R_\star$, the overall transparency of the wind increases

Outline: clumping and porosity

X-ray line profiles

- For spherical clumps (**isotropic porosity**), porosity mimics a reduced mass-loss rate

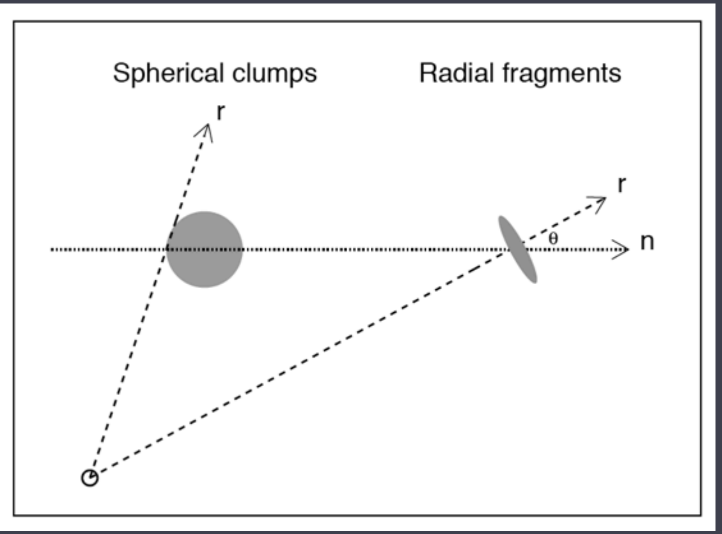

- For flattened clumps (**anisotropic porosity**), porosity leads to distinctive X-ray line profile shapes

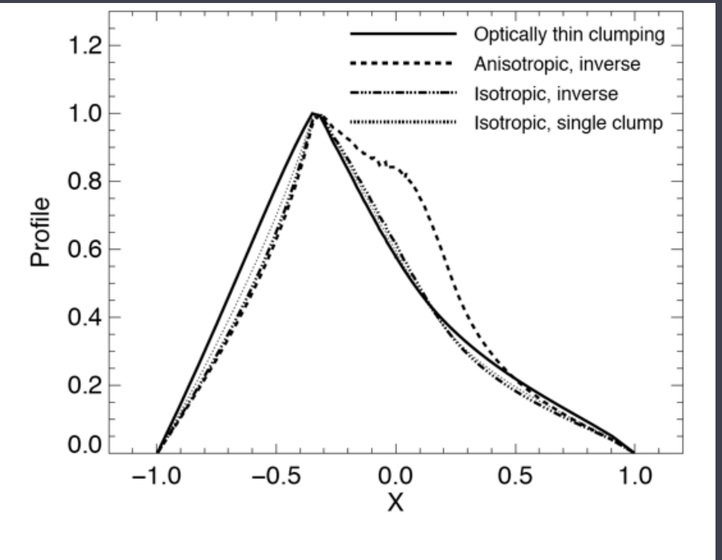

Figure 5. Line profiles for $h_\infty/R_\star = 1.0$ and $\tau_\star = 2.5$, using different effective opacity laws, as labelled.

- Observed X-ray profiles can place constraints on porosity, clumping, and the wind mass-loss rate

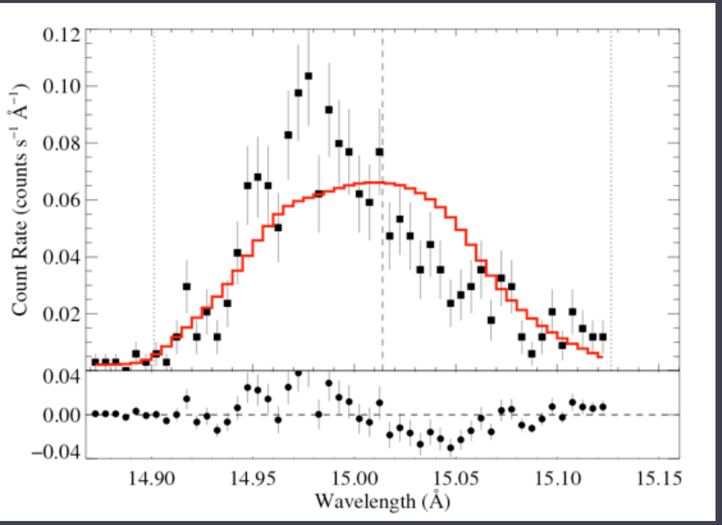

Evidence for clumping in massive stars

- theoretically expected from simulations of the line-driving instability (LDI)
- line profile variability
  - optical emission lines
  - UV absorption lines
  - polarization
- black troughs in UV resonance lines
- electron scattering wings
- UV doublet ratios
- different diagnostics, with different clumping sensitivities, give different mass-loss rates for the same star if clumping is neglected

Evidence for clumping in massive stars

- theoretically expected from simulations of the line-driving instability (LDI)
- line profile variability
  - optical emission lines
  - UV absorption lines
  - polarization
- black troughs in UV resonance lines
- electron scattering wings
- UV doublet ratios
- different diagnostics, with different clumping sensitivities, give different mass-loss rates for the same star if clumping is neglected

Numerical simulations of the line-driving instability (LDI)

self-excited instability

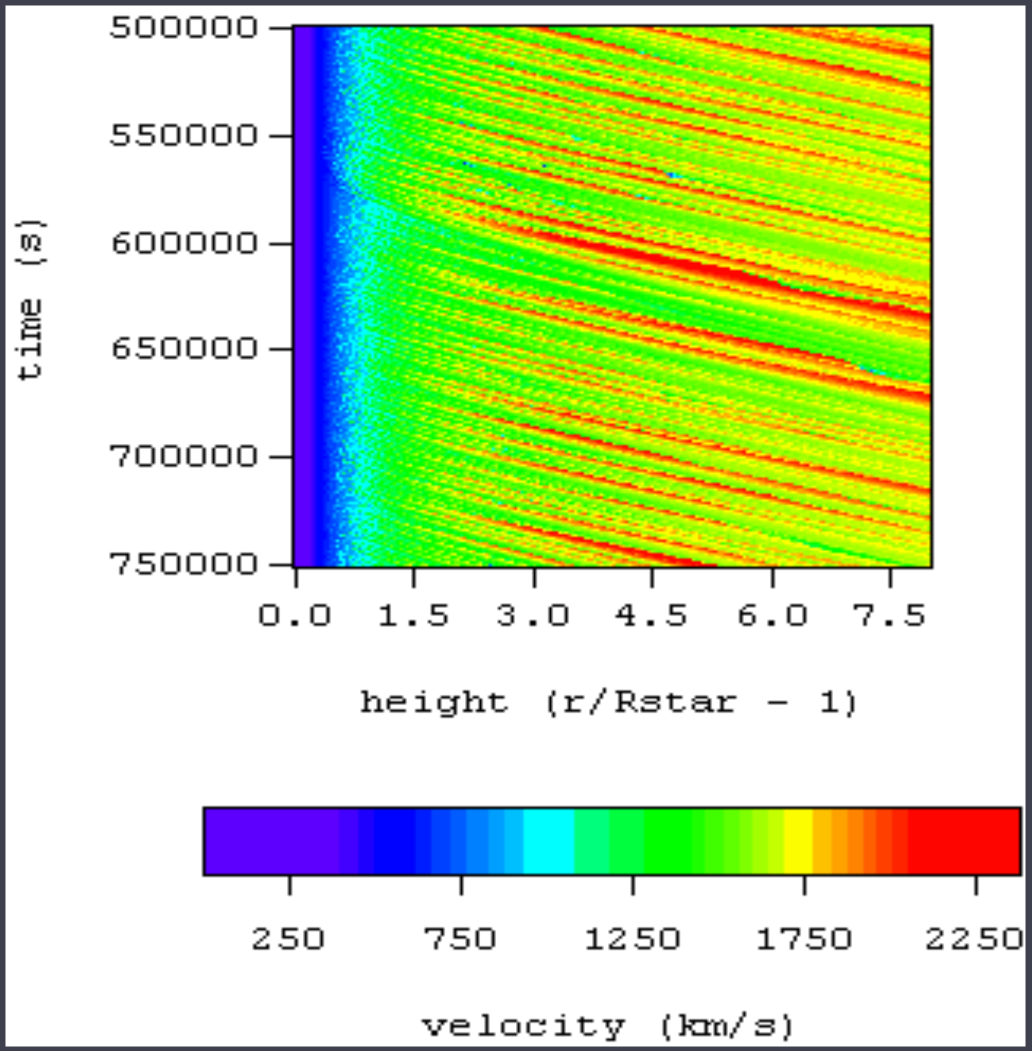

Owocki, Cooper, Cohen 1999

excited by turbulence at the wind base

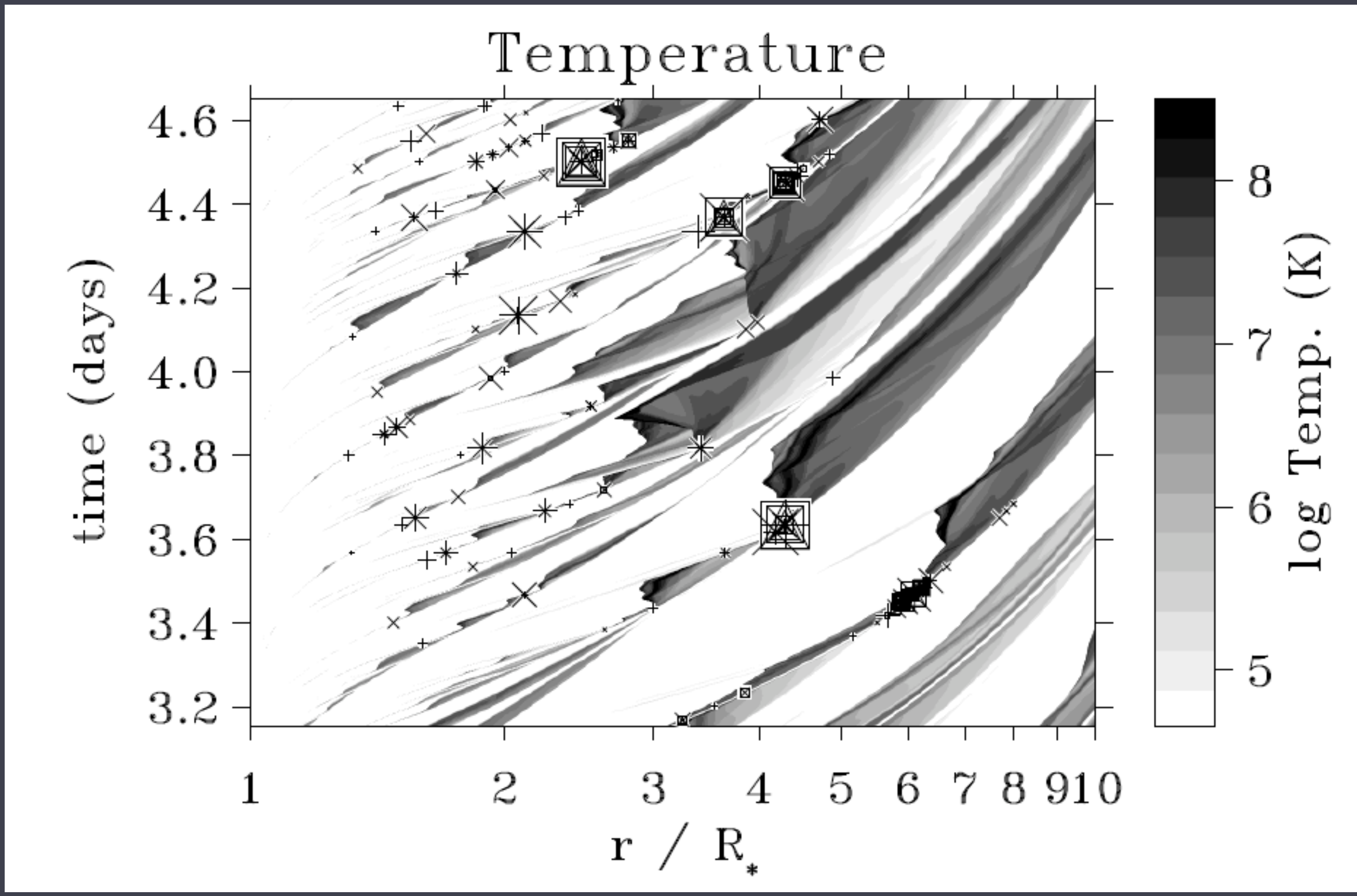

Feldmeier, Puls, & Pauldrach 1997

Dense clumps/shells form and advect through the wind

from a single time snap-shot

clumps

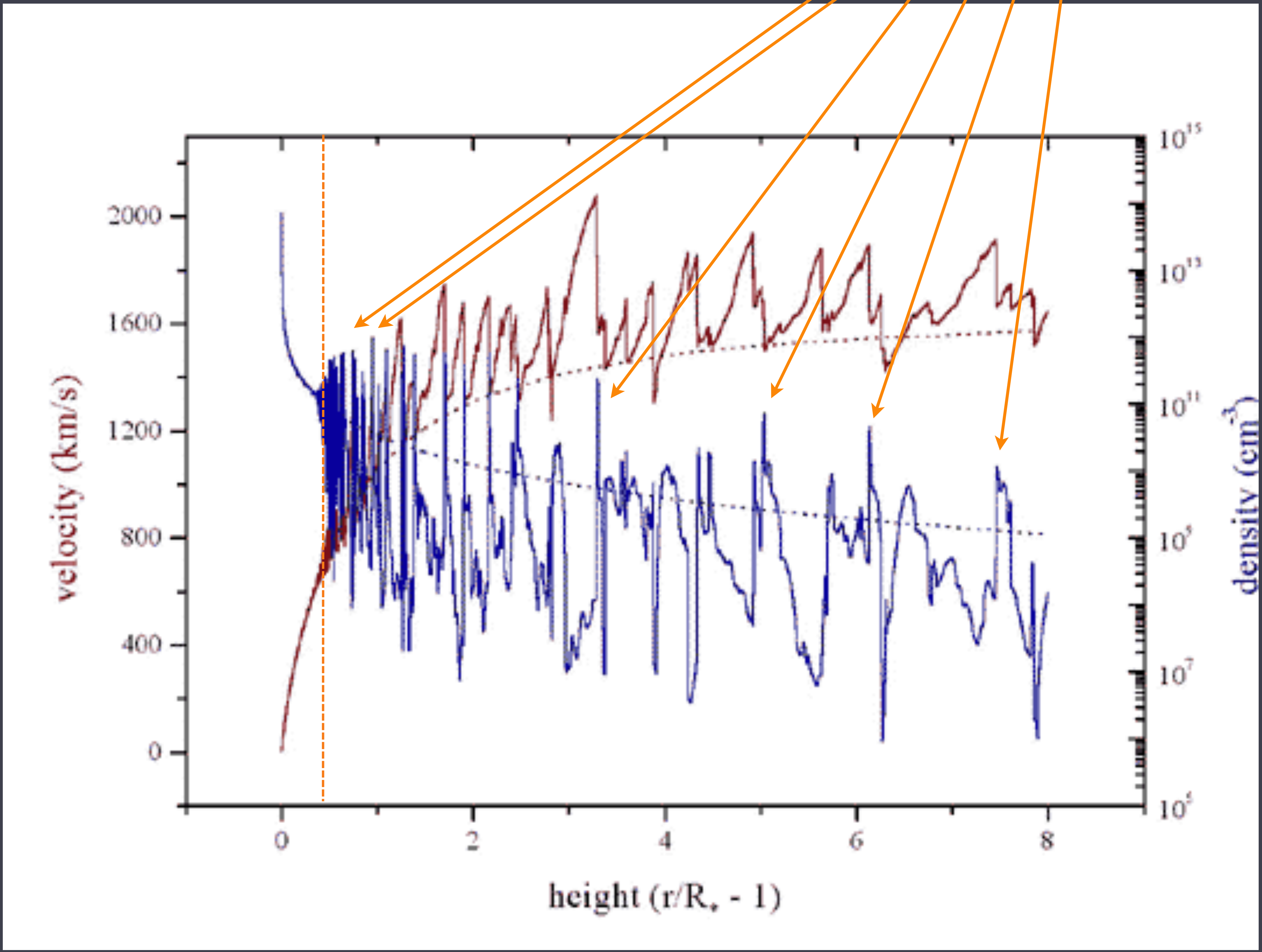

but keep in mind, limitations of 1-D simulations

clumps

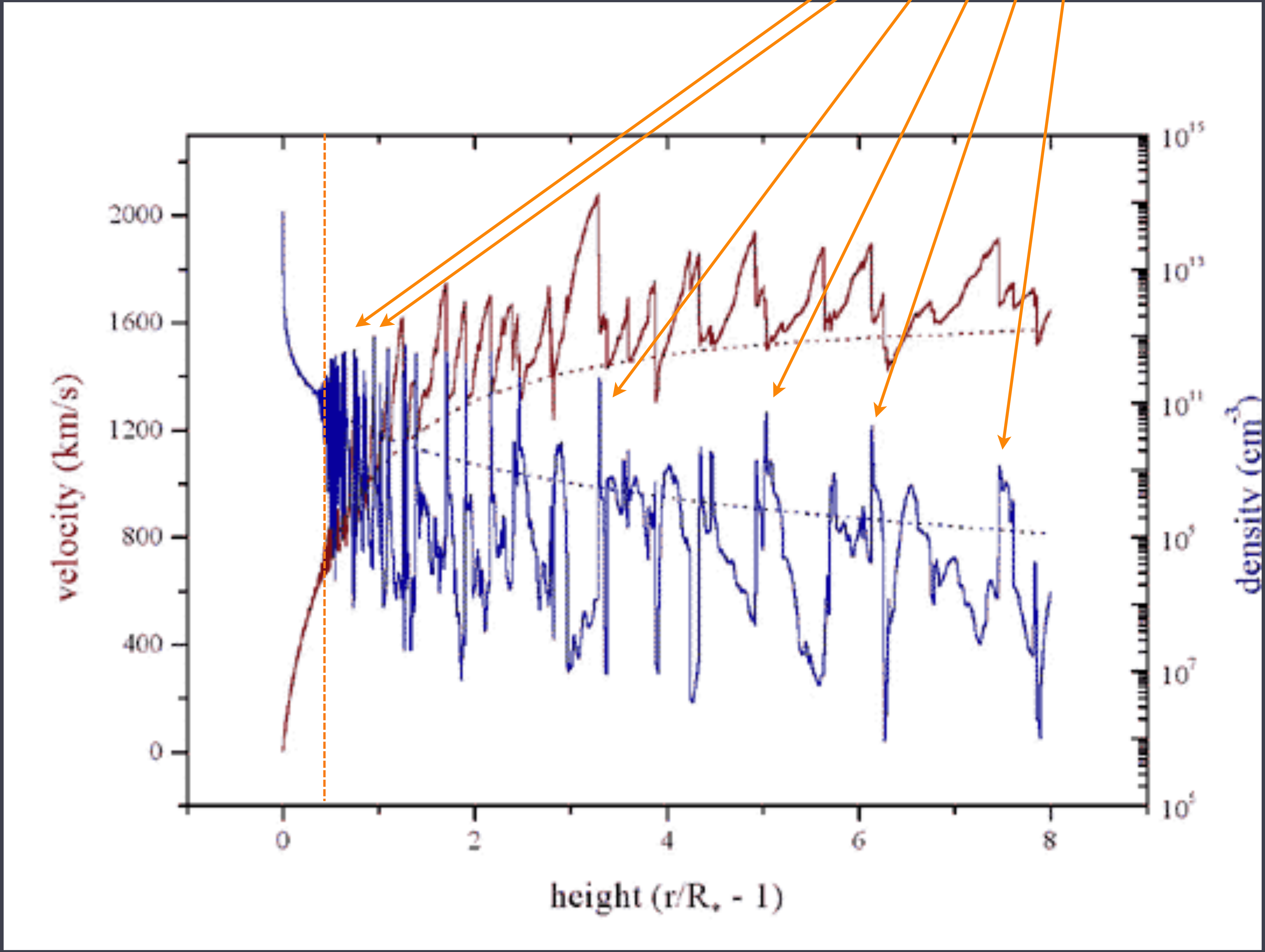

More realistic 2-D simulations: R-T like break-up; structure on quite *small scales*

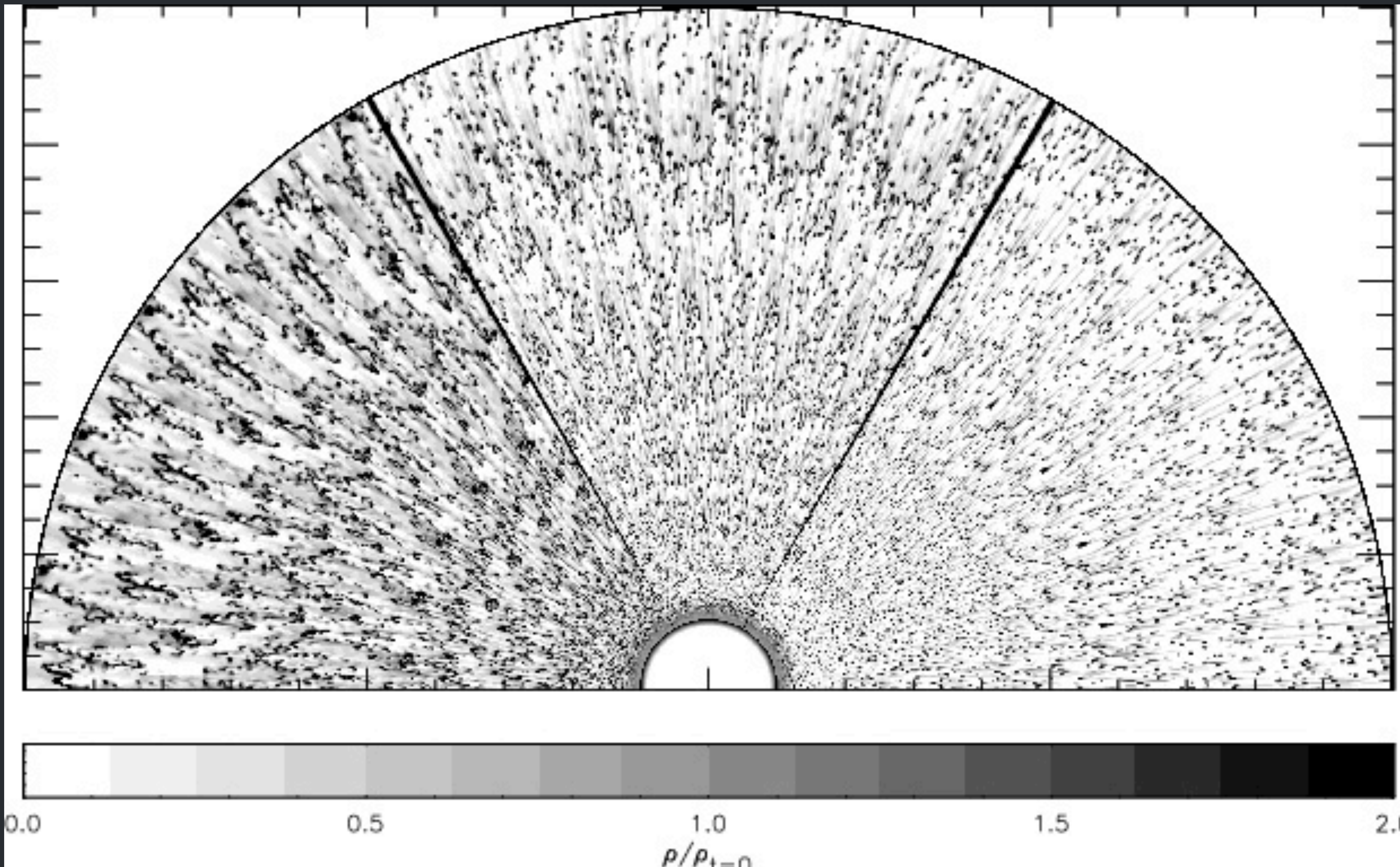

Dessart & Owocki 2003, *A&A*, 406, L1

Evidence for clumping in massive stars

- theoretically expected from simulations of the line-driving instability (LDI)
- line profile variability
  - optical emission lines
  - UV absorption lines
  - polarization
- black troughs in UV resonance lines
- electron scattering wings
- UV doublet ratios
- different diagnostics, with different clumping sensitivities, give different mass-loss rates for the same star if clumping is neglected

Hα variability - moving bumps - in WR stars

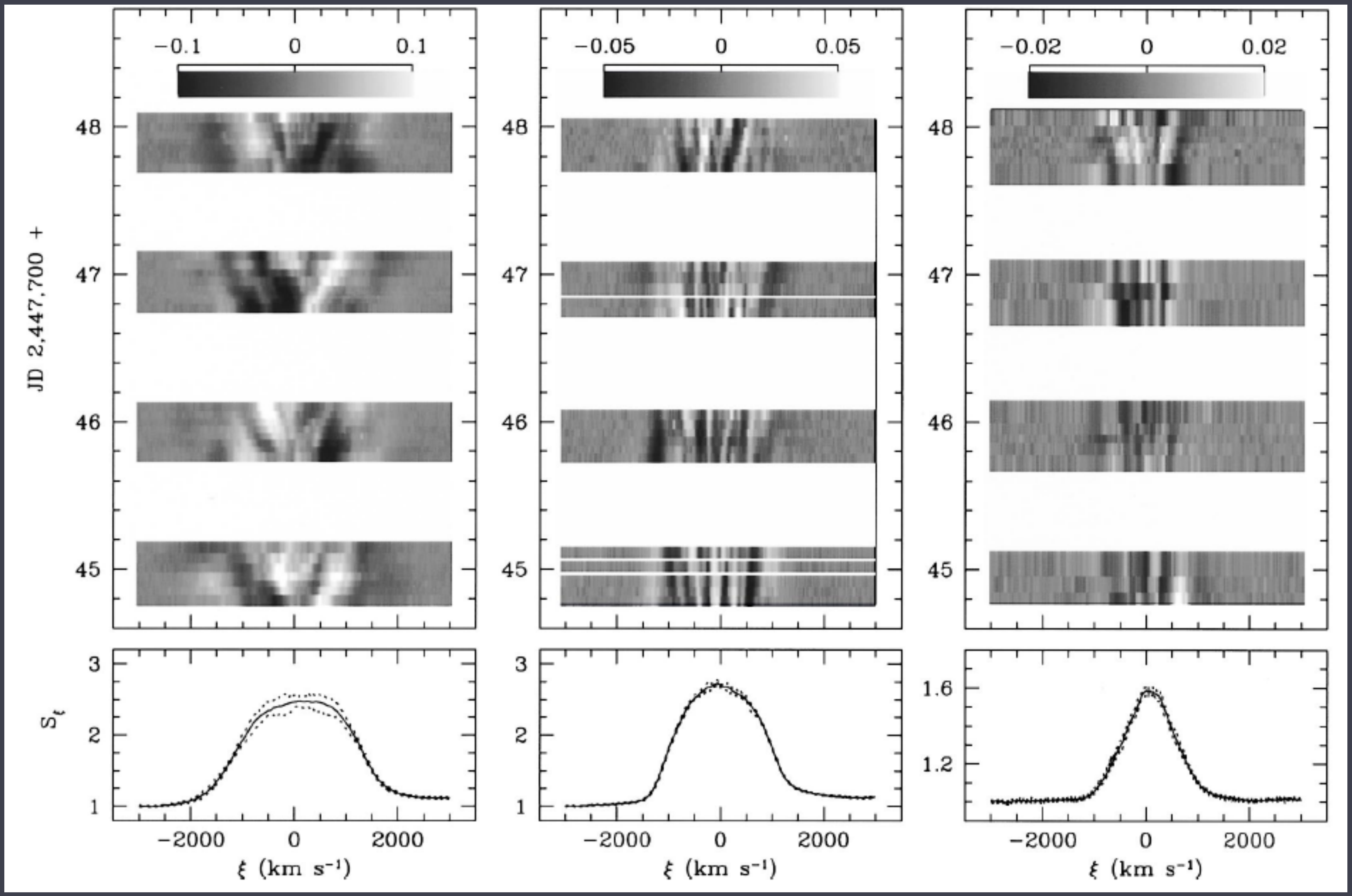

WR 134, 136, 138, from Lépine & Moffat 1999

and in ζ Pup (O4If)

moving spectral subpeaks

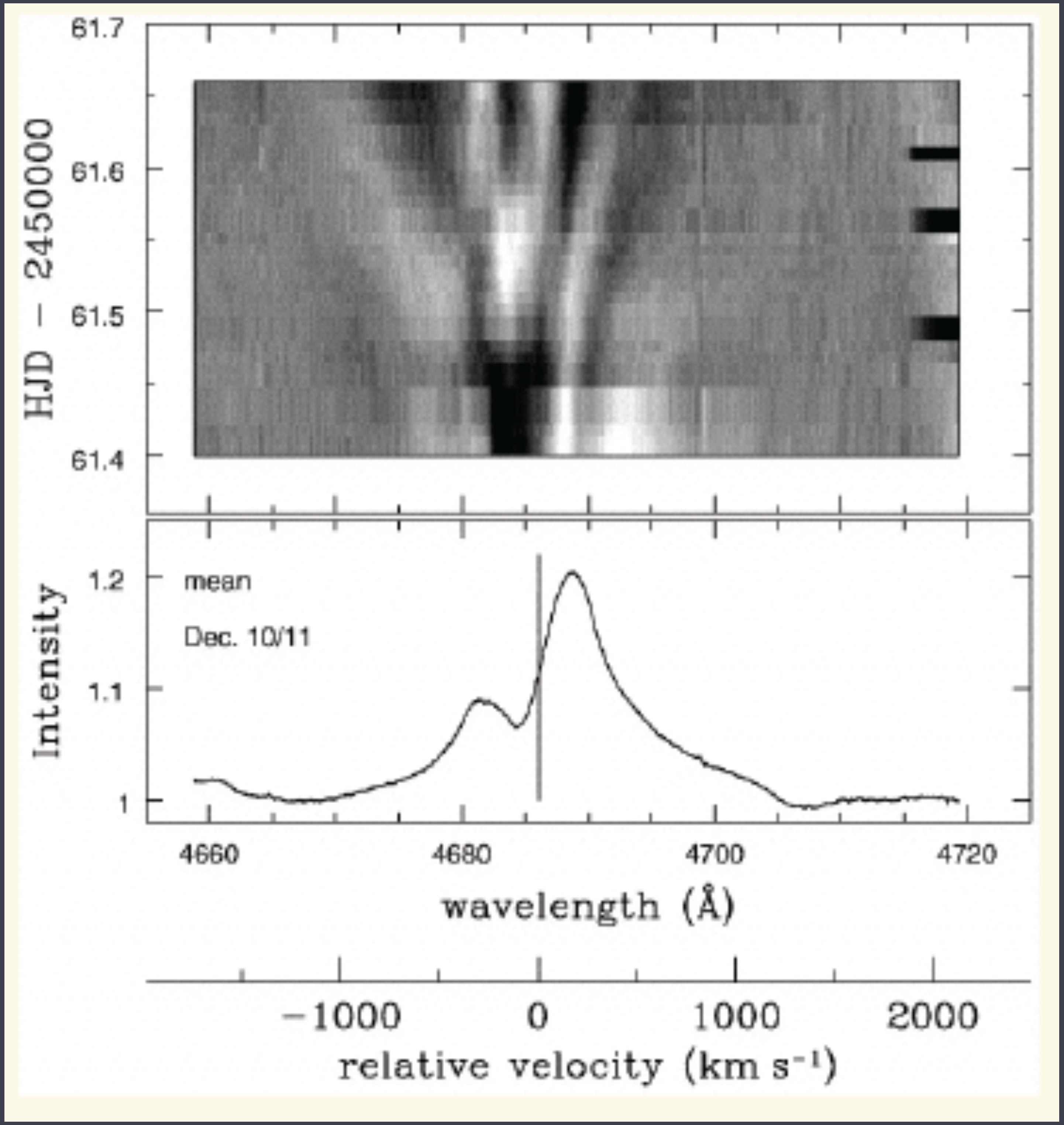

(Eversberg, Lépine, & Moffat 1998, Lépine & Moffat 2008)

Evidence for clumping in massive stars

- theoretically expected from simulations of the line-driving instability (LDI)
- line profile variability
  - optical emission lines
  - UV absorption lines
  - polarization
- black troughs in UV resonance lines
- electron scattering wings
- UV doublet ratios
- different diagnostics, with different clumping sensitivities, give different mass-loss rates for the same star if clumping is neglected

ζ Pup: without clumping, $\dot{M}$ discrepancies

for $\dot{M}$ = 7 X 10^{-6} M_{sun}/yr

Hα IR radio

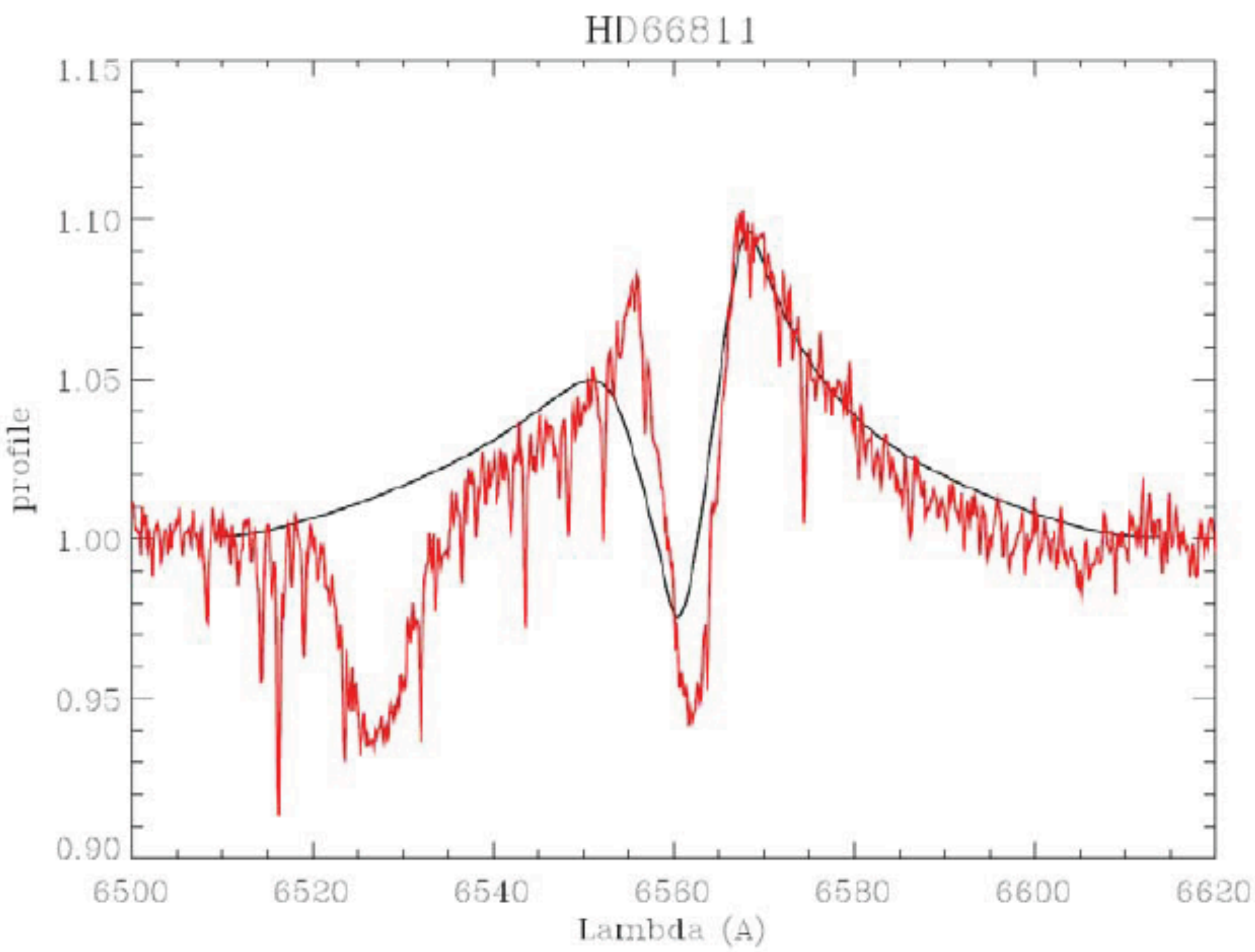

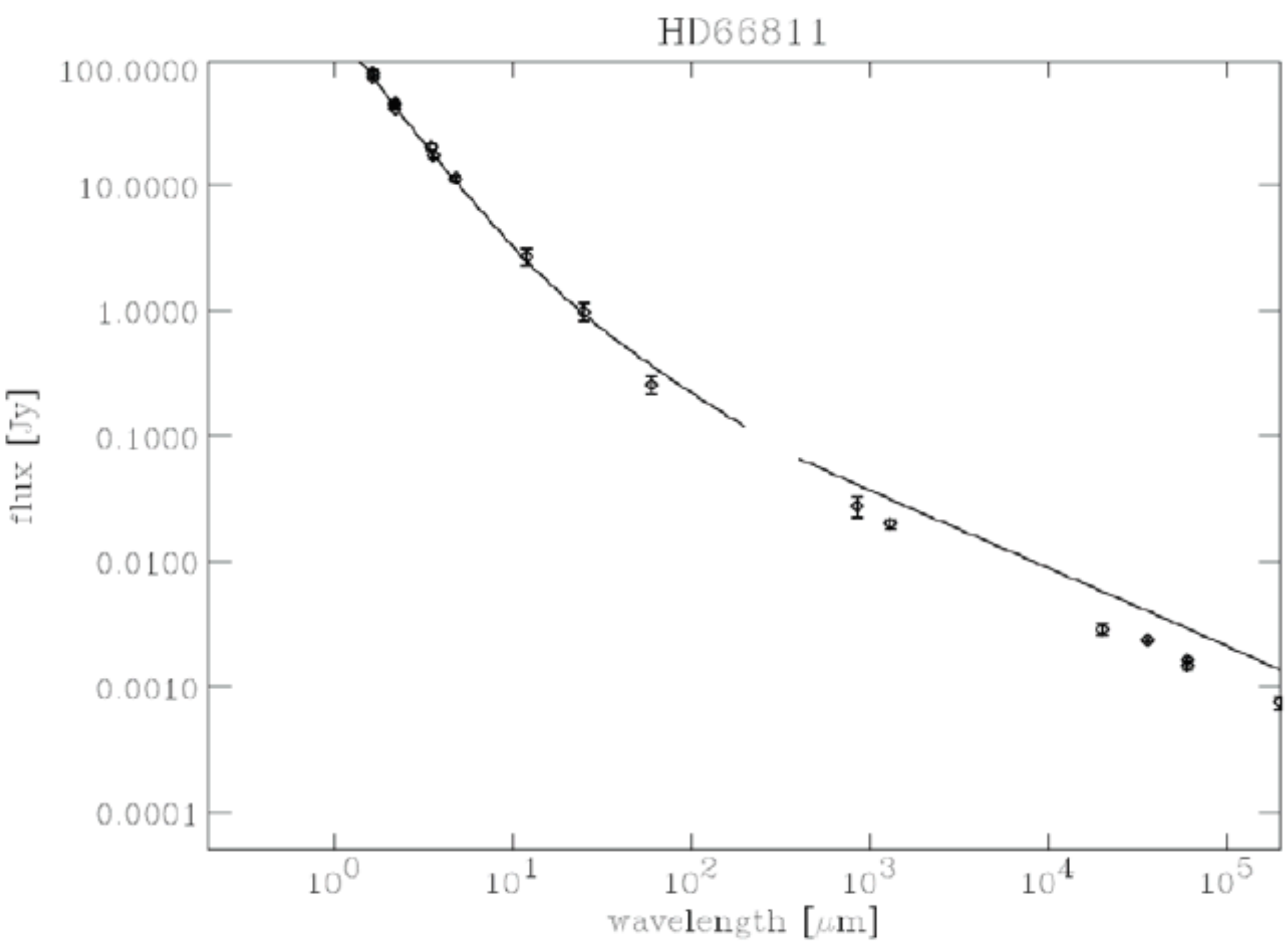

ζ Pup: without clumping, $\dot{M}$ discrepancies

for $\dot{M} = 7 \times 10^{-6}\ M_{sun}/yr$

Hα IR radio

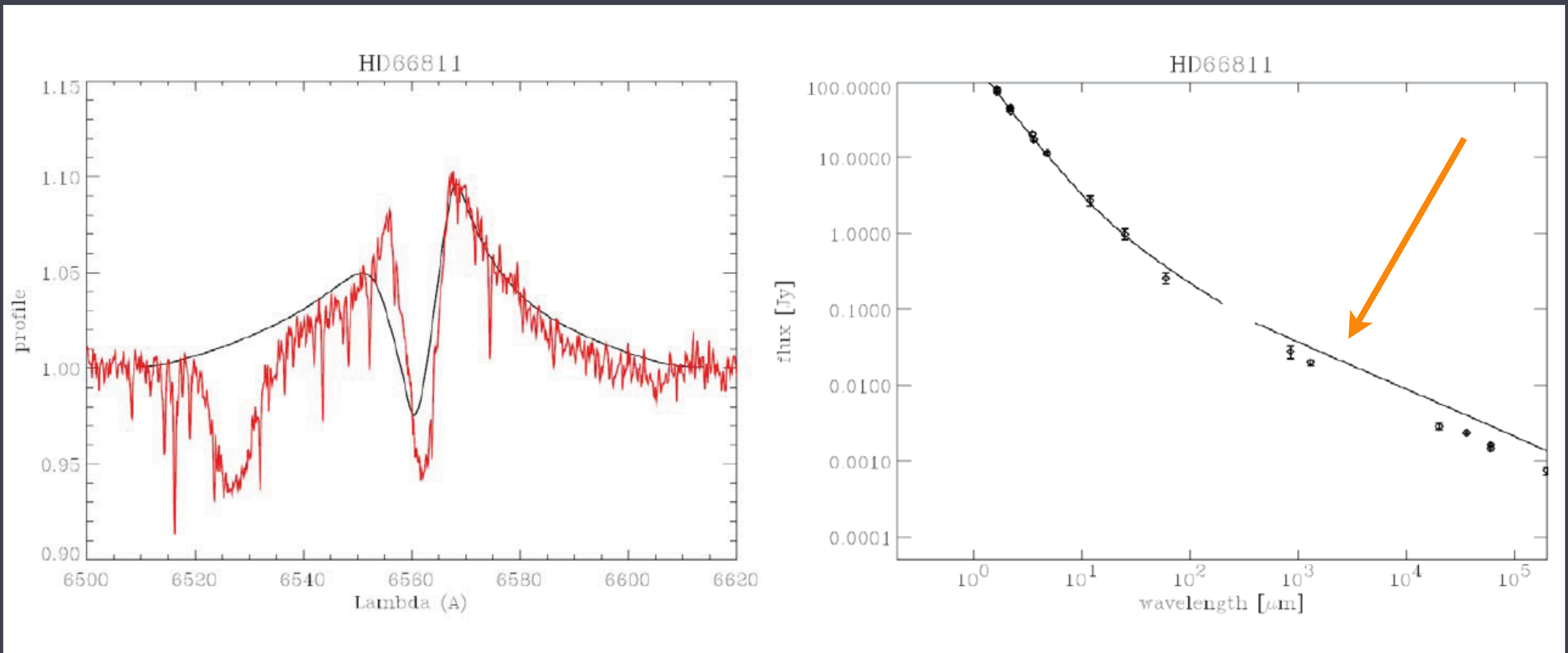

ζ Pup: without clumping, $\dot{M}$ discrepancies

for $\dot{M}$ = 4.2 X 10^{-6} M_{sun}/yr

Hα

IR

radio

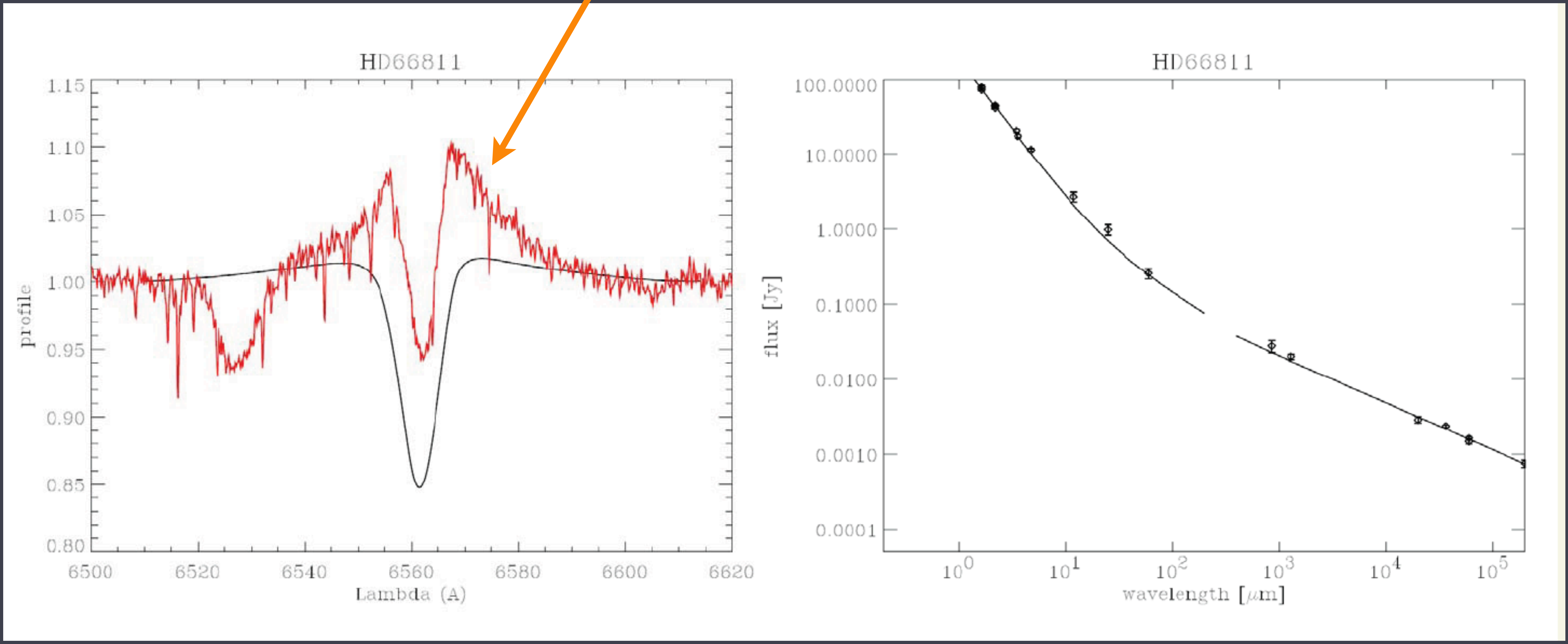

Clumping's effect

assumptions: optically thin clumps, void interclump medium

$$f_{cl} \equiv \langle\rho^2\rangle / \langle\rho\rangle^2$$

$$f_{cl} \equiv f_{vol}^{-1}$$

volume filling factor, f_{vol}

$$\rho_{cl} = f_{cl} \langle\rho\rangle$$

$$\dot{M}_{cl} \equiv \dot{M}_{smooth} / f_{cl}^{0.5}$$

ignoring clumping overestimates mass-loss rates by a factor of $\sqrt{f_{cl}}$

Clumping's effect

assumptions: optically thin clumps, void interclump medium

$$f_{cl} \equiv \langle\rho^2\rangle/\langle\rho\rangle^2$$

$$f_{cl} \equiv f_{vol}^{-1}$$

volume filling factor, f_{vol}

$$\rho_{cl} = f_{cl}\langle\rho\rangle$$

$$\dot{M}_{cl} \equiv \dot{M}_{smooth} / f_{cl}^{0.5}$$

ignoring clumping overestimates mass-loss rates by a factor of $\sqrt{f_{cl}}$

for *density squared* diagnostics

Aside/explanation

collisional processes (e.g. recombination (Hα) or free-free (IR, radio excess)) have intensities that scale as **ρ^2*Volume**

if clumps fill a fraction of the volume, the density of clumps exceeds the mean density by the same fraction, and the intensity scales as:

$$(\rho/f_{vol})^2 \times (f_{vol}\text{Volume}) \propto 1/f_{vol} = f_{cl}$$

and since $\dot{M} \propto \rho$ and measured intensity $\propto \rho^2$ then $\dot{M}$ will be overestimated by a factor of *sqrt*(f_{cl}) if clumping is ignored in the analysis of density-squared diagnostics

ζ Pup: *with* clumping

for $\dot{M} = 4.2 \times 10^{-6}\ M_{sun}/yr$

and no clumping in the radio regime (>10 $R_\star$)

but with clumping in the Hα regime (<1.5 $R_\star$)

Hα IR radio

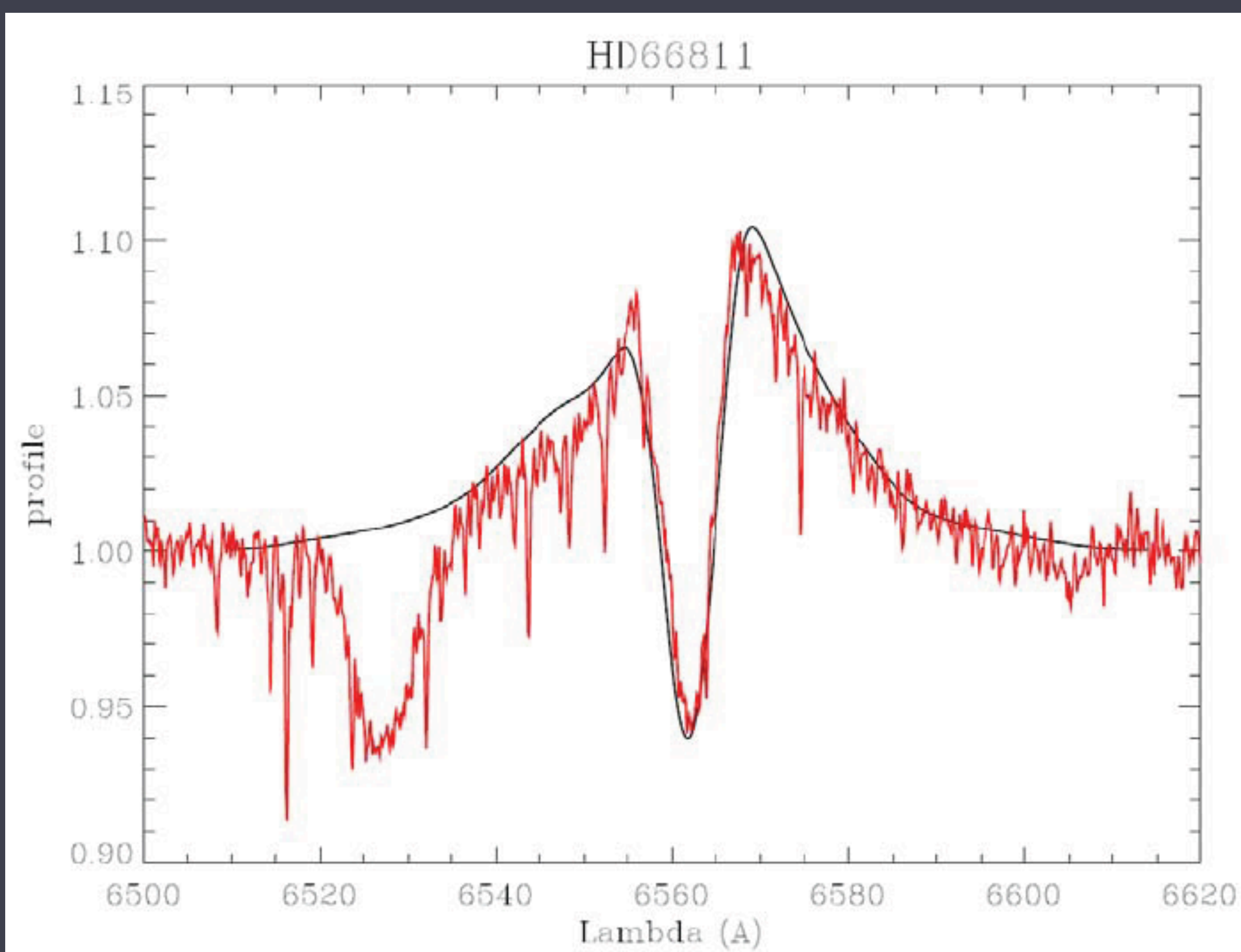

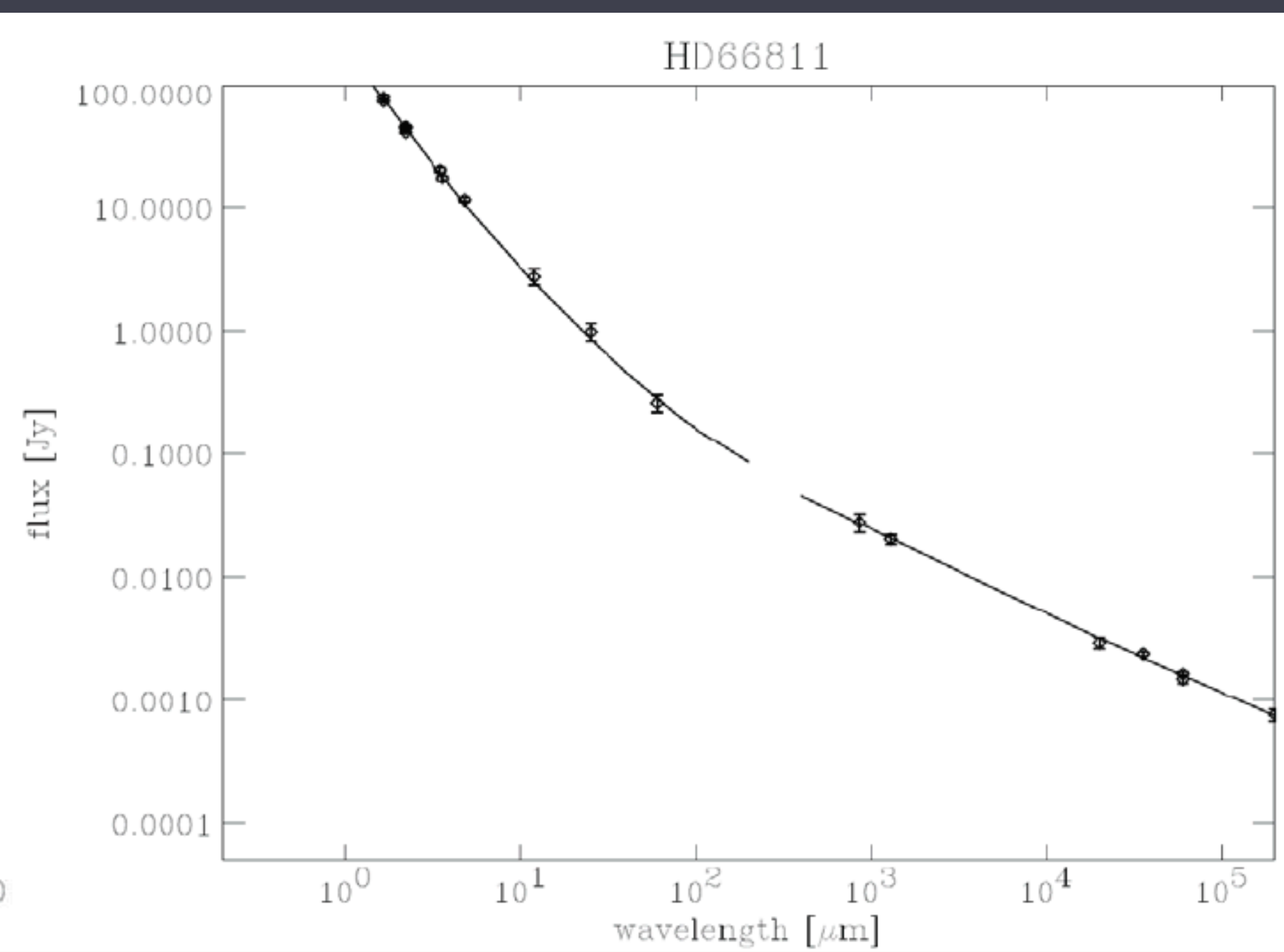

ζ Pup: radially varying clumping

for $\dot{M} = 4.2 \times 10^{-6}\ M_{sun}/yr$

$f_{cl} = 1$ @ $r < 1.12\ R_*$
$f_{cl} = 5.5$ @ $1.12 < r < 1.5\ R_*$
$f_{cl} = 3.1$ @ $1.5 < r < 2\ R_*$
$f_{cl} = 2$ @ $2 < r < 15\ R_*$
$f_{cl} = 1$ @ $r > 15\ R_*$

Hα IR radio

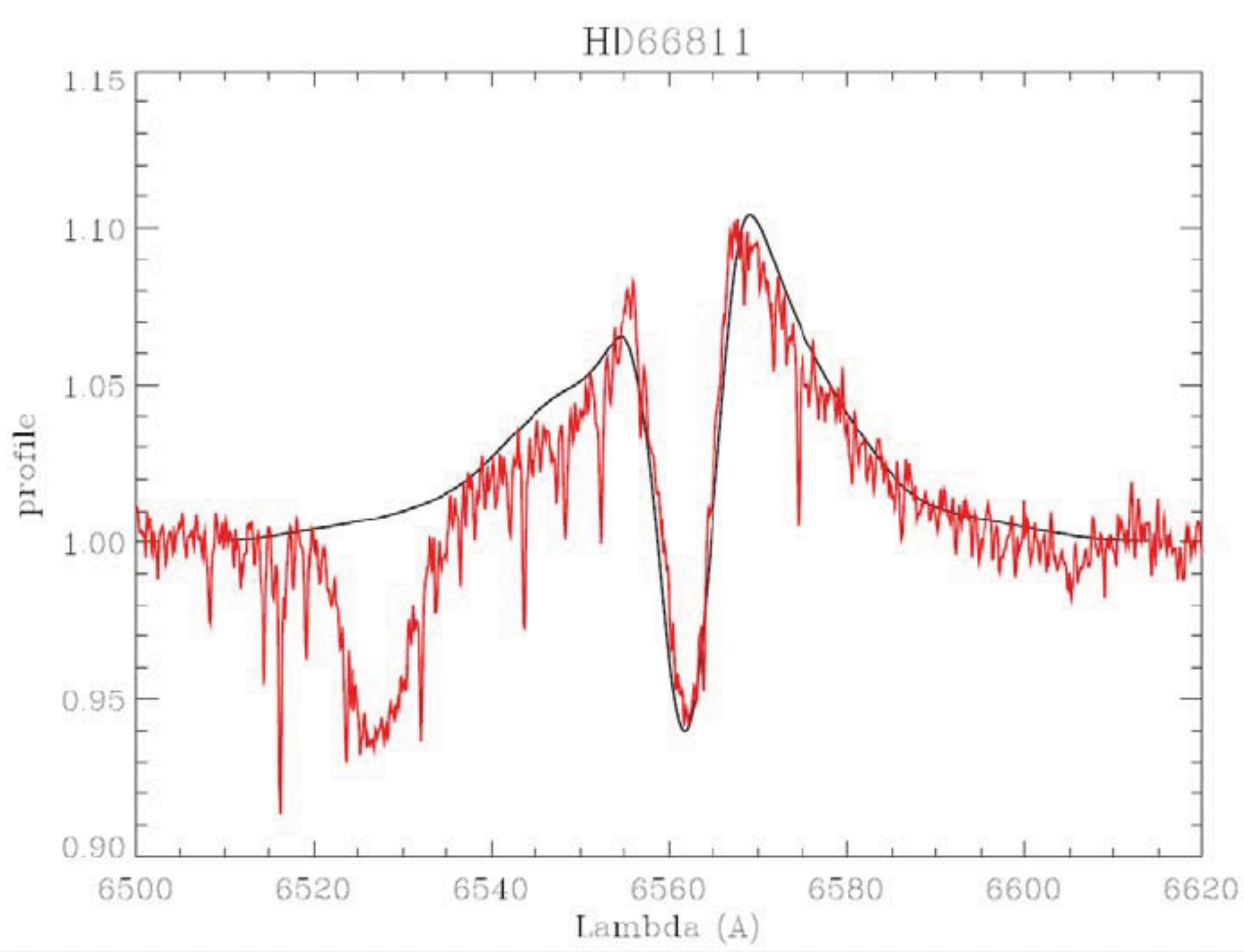

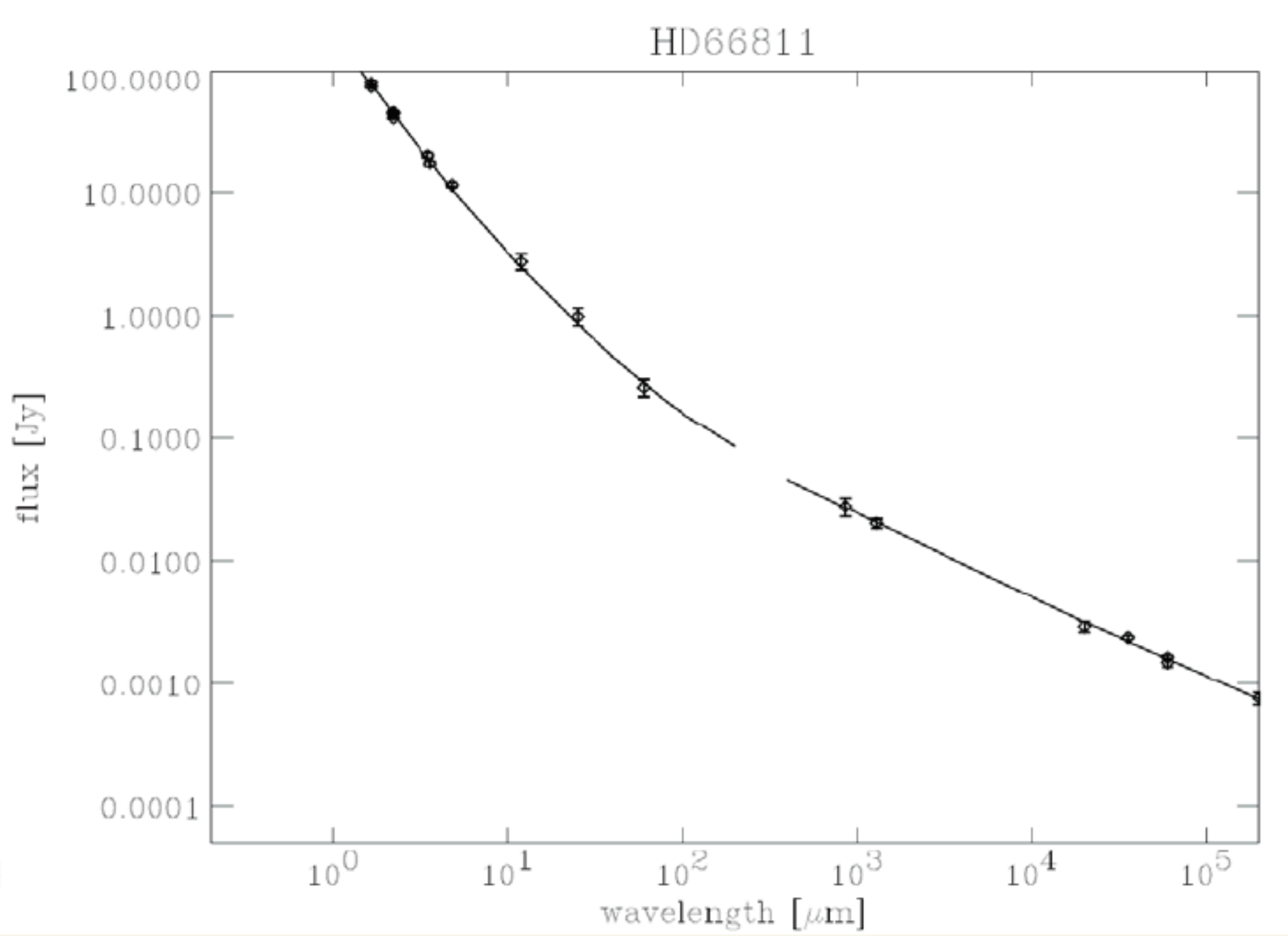

ζ Pup: radially varying clumping

for $\dot{M} = 4.2 \times 10^{-6}\ M_{sun}/yr$

$f_{cl} = 1$ @ $r < 1.12\ R_*$
$f_{cl} = 5.5$ @ $1.12 < r < 1.5\ R_*$
$f_{cl} = 3.1$ @ $1.5 < r < 2\ R_*$
$f_{cl} = 2$ @ $2 < r < 15\ R_*$
$f_{cl} = 1$ @ $r > 15\ R_*$

Note: one *family* of solutions; all f_{cl} can be scaled up by the same factor (and $\dot{M}$ scaled down, accordingly)

so $\dot{M} \leq 4.2 \times 10^{-6}\ M_{sun}/yr$

ζ Pup: radially varying clumping

for $\dot{M} = 4.2 \times 10^{-6}$ M_{sun}/yr

$f_{cl} = 1$ @ $r < 1.12\ R_*$

$f_{cl} = 5.5$ @ $1.12 < r < 1.5\ R_*$

$f_{cl} = 3.1$ @ $1.5 < r < 2\ R_*$

$f_{cl} = 2$ @ $2 < r < 15\ R_*$

$f_{cl} = 1$ @ $r > 15\ R_*$

Also: this is a general trend - clumping factors decrease with radius

Clumping

Key point: as long as the clumps are optically thin, only the clumping factor (their over-density) matters.

Their size scale, shape, etc are irrelevant!

Column density based diagnostics (e.g. some UV abs lines, X-ray emission lines and X-ray SEDs) are *unaffected* by *optically thin clumping*.

Visualizations of clumped winds

all have clump sizes $\ell = 0.1\ R_\star$ (at surface; increasing as r)

$f_{cl} = 1$ $f_{cl} \approx 2.5$ $f_{cl} \approx 5$

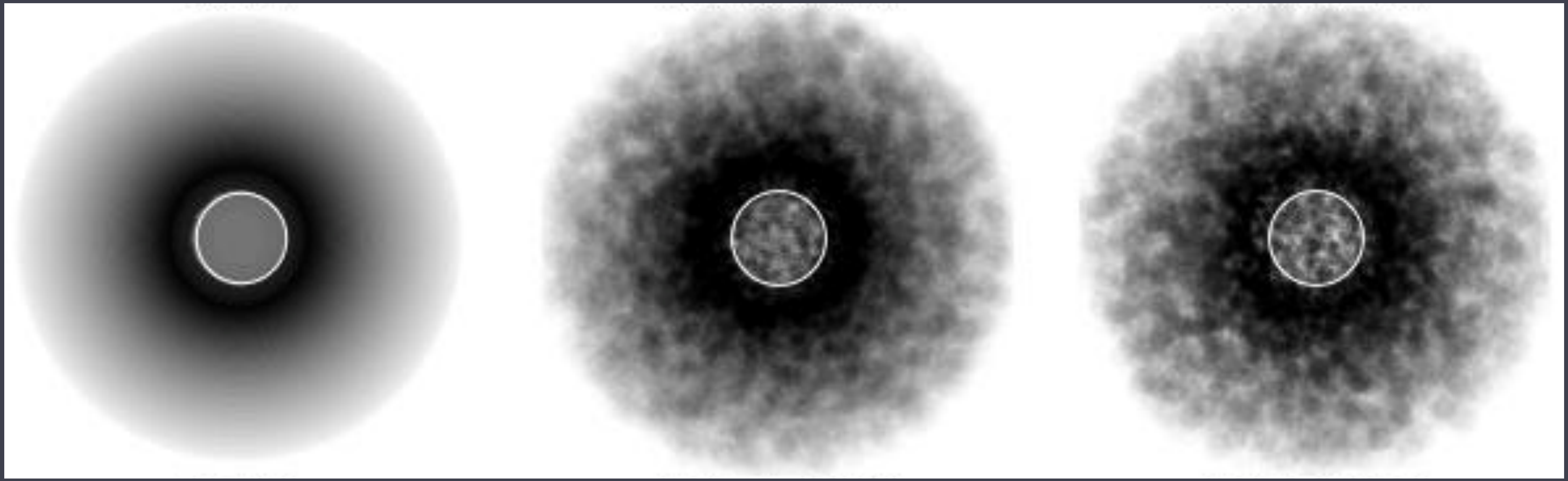

$f_{cl} \approx 10$ $f_{cl} \approx 20$ $f_{cl} \approx 40$

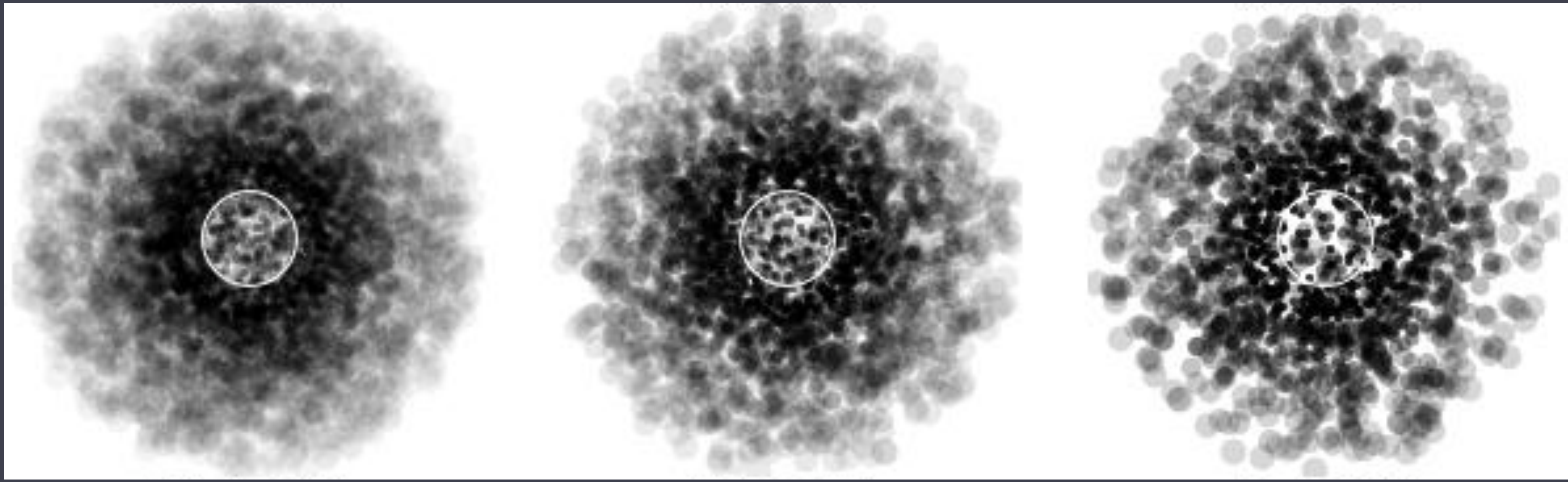

Visualizations of clumped winds

all have same clump sizes

bigger clumping factors = bigger volume over which matter in each clump is collected = more empty space

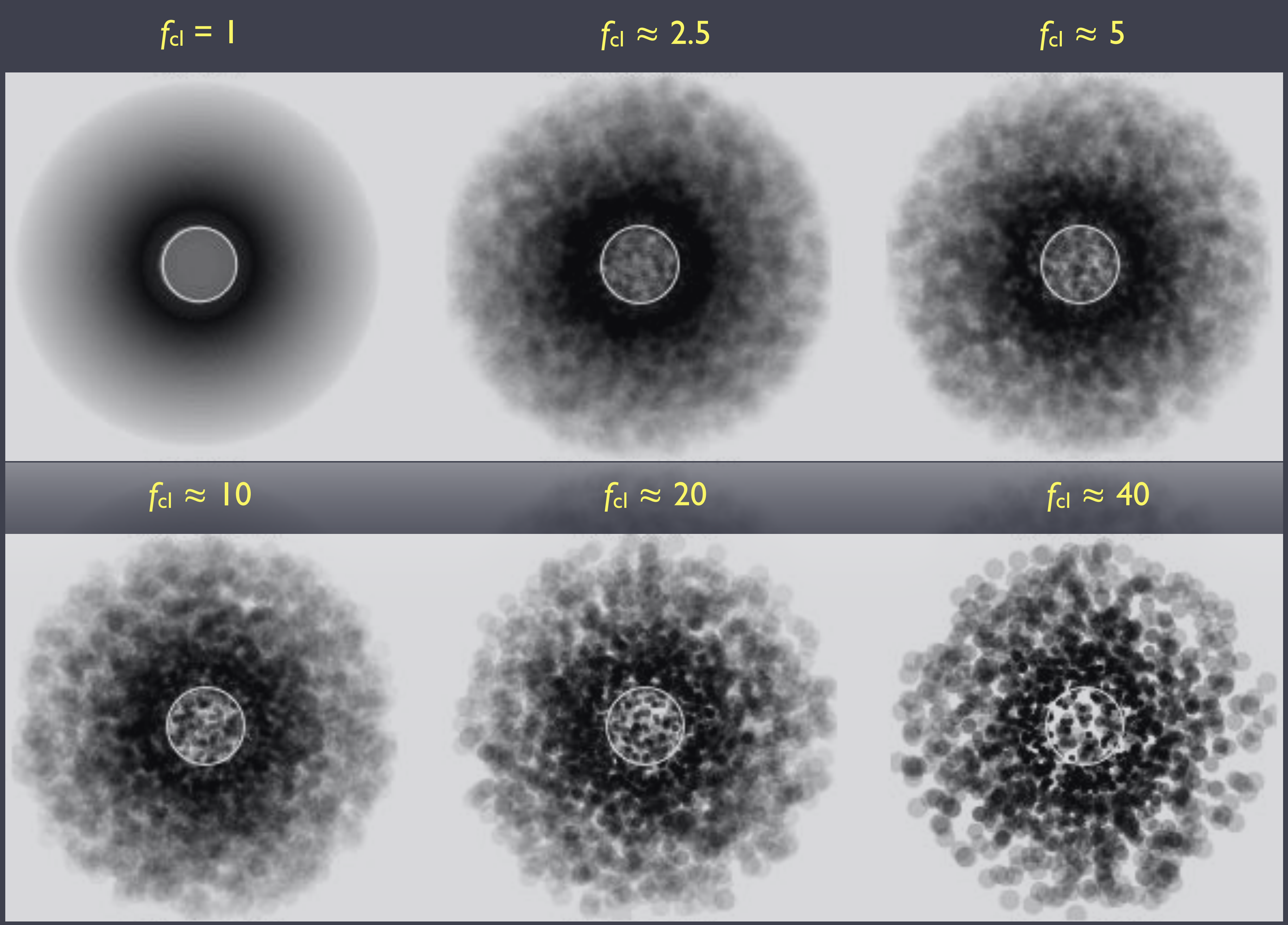

Porosity

optically thick clumps

enhances photon escape through evacuated channels

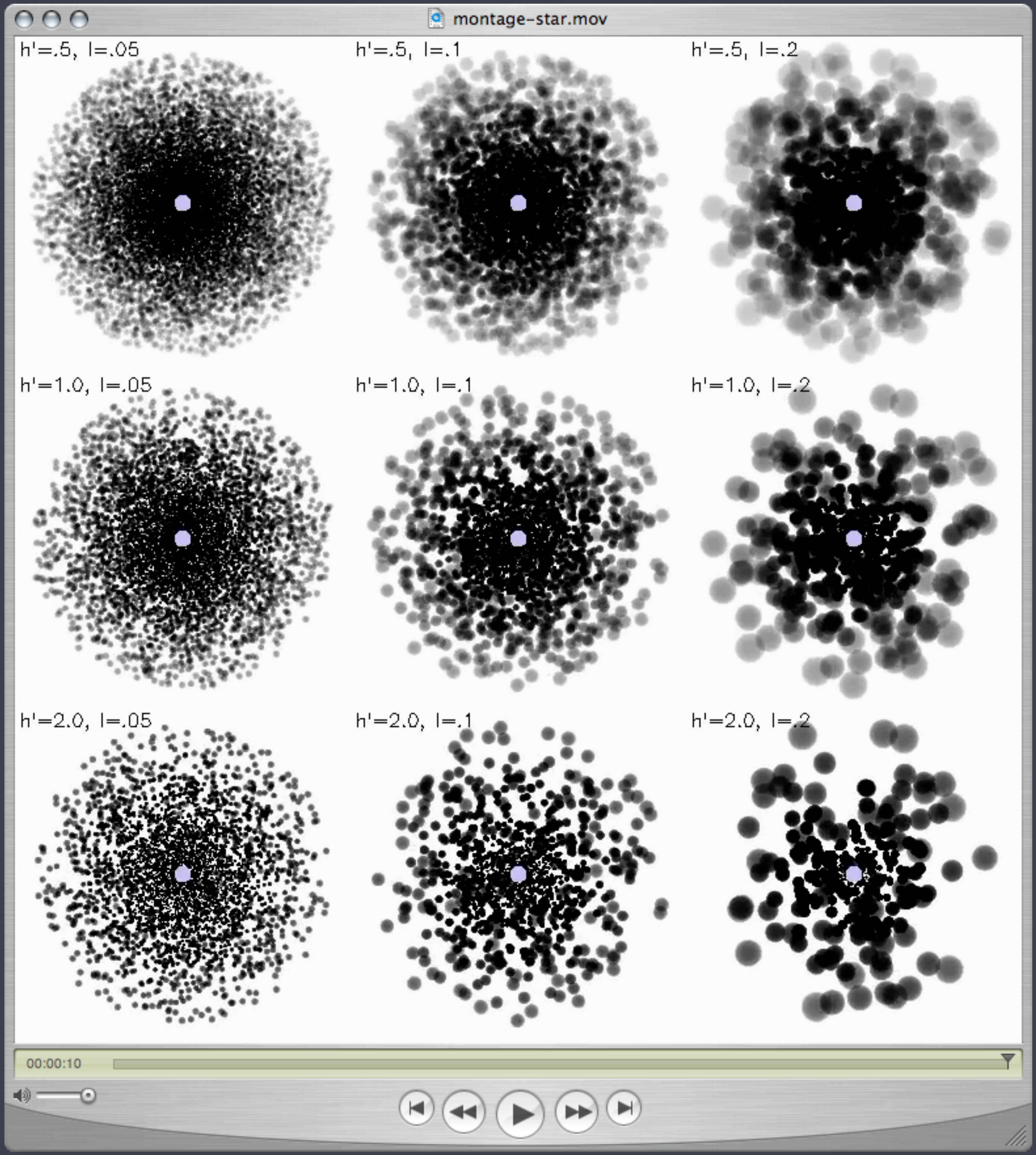

Porosity

optically thick clumps

Thus, porosity only exists if there's clumping

But, you *can* have clumping without having porosity

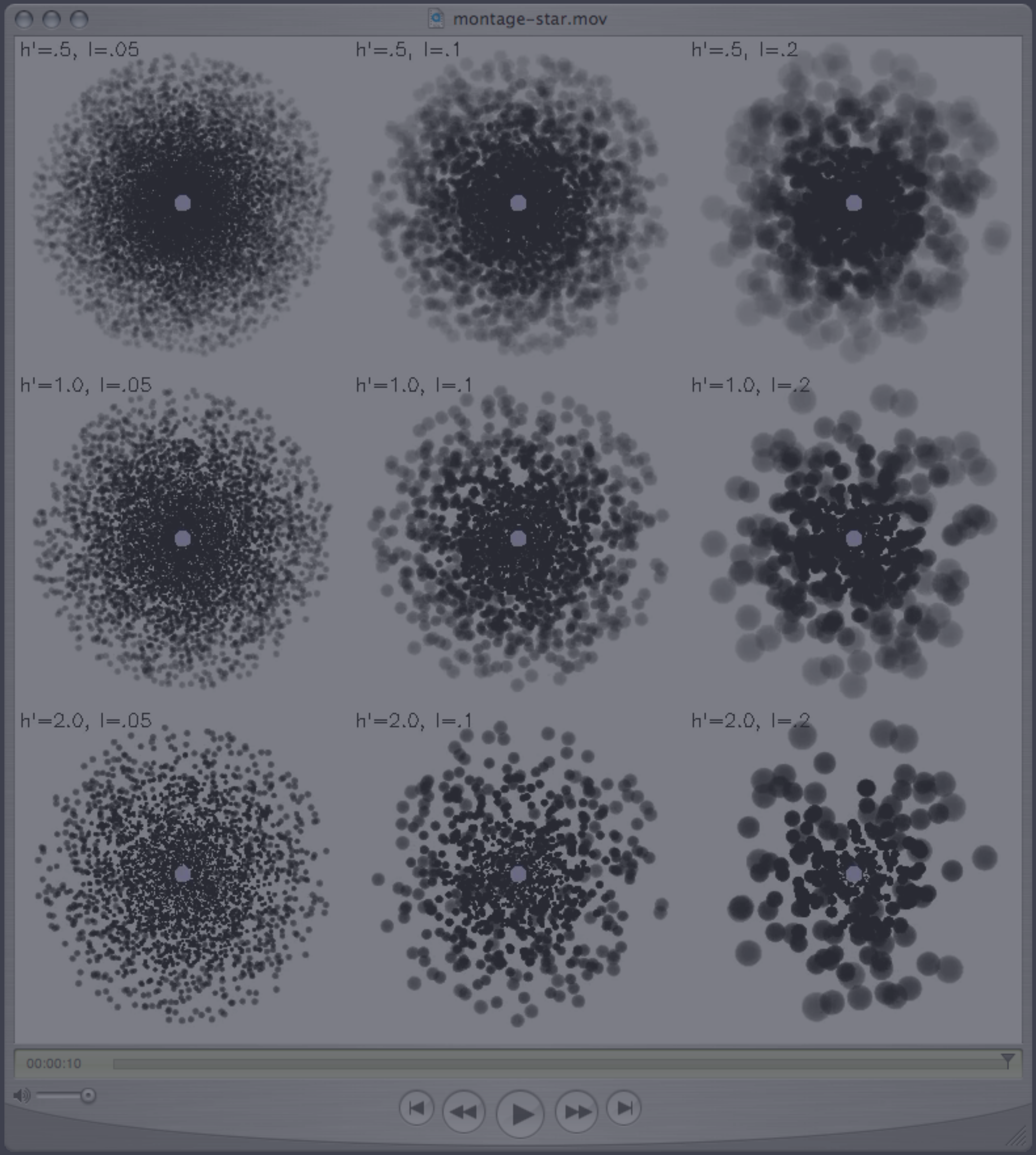

less porous

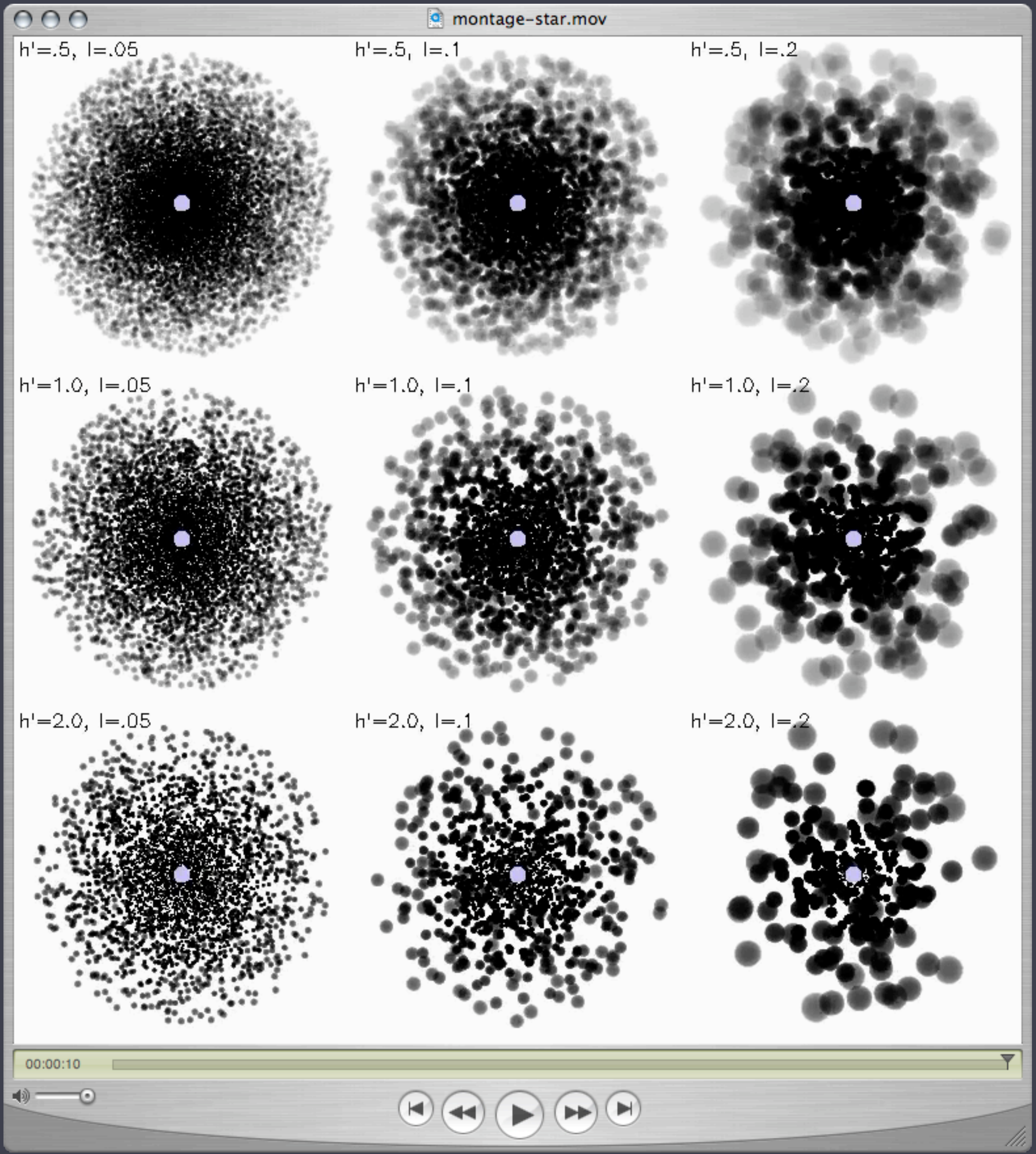

more porous

less porous

more porous

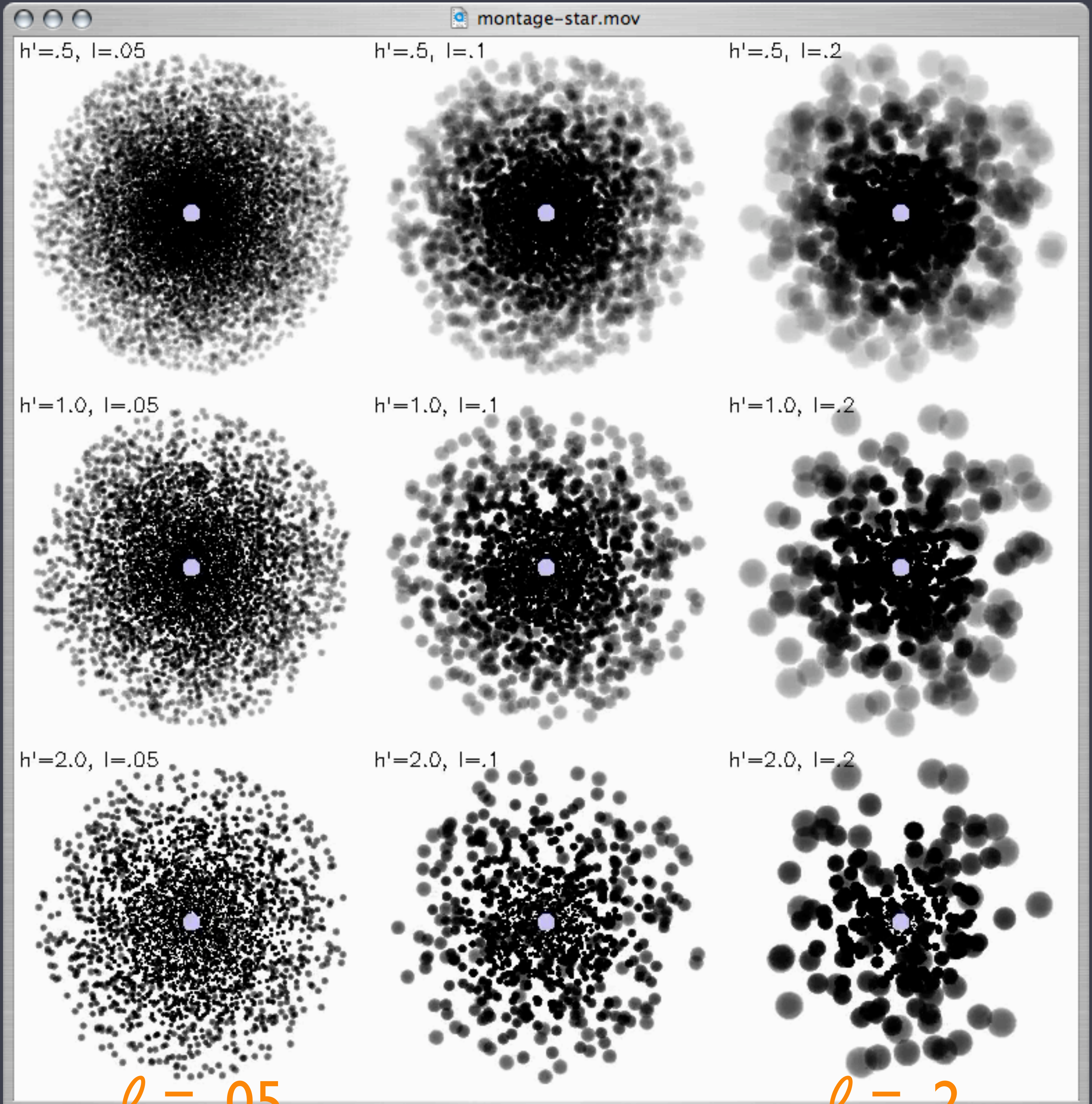

$\ell = .05$
small clumps

$\ell = .2$
big clumps

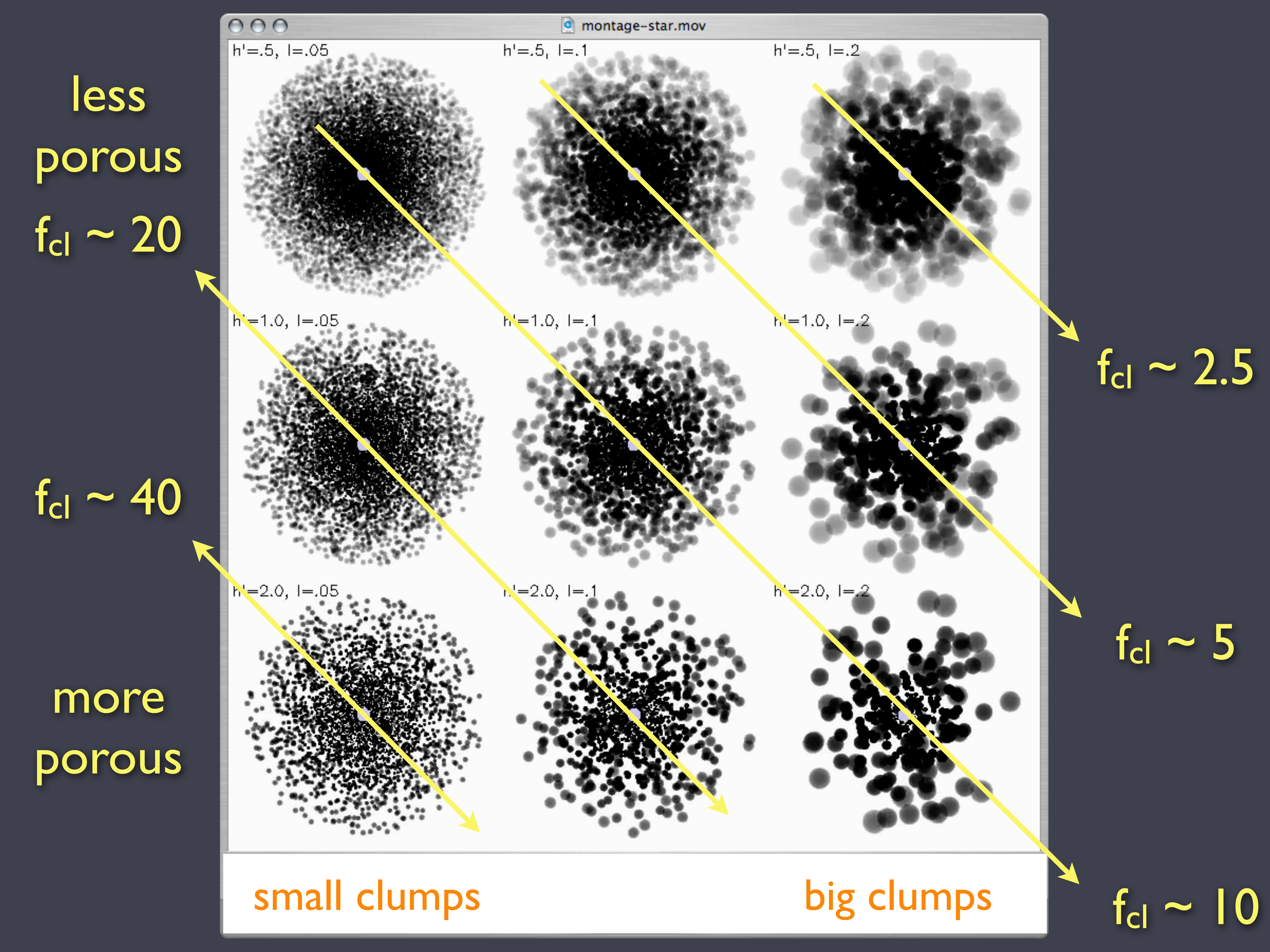

montage-star.mov
h'=.5, l=.05
h'=.5, l=.1
h'=.5, l=.2
h'=1.0, l=.05
h'=1.0, l=.1
h'=1.0, l=.2
h'=2.0, l=.05
h'=2.0, l=.1
h'=2.0, l=.2
less porous
$f_{cl} \sim 20$
$f_{cl} \sim 40$
more porous
$f_{cl} \sim 2.5$
$f_{cl} \sim 5$
$f_{cl} \sim 10$
small clumps
big clumps

Porosity length

The degree of porosity is characterized by the **porosity length**, h

less porous

h=0.5

$$h \equiv (n_{cl} A_{cl})^{-1} \; (= \textbf{mfp})$$

$$= L^3/\ell^2 = \ell/f_{vol} = \ell * f_{cl}$$

h=1

$$f_{vol} \equiv \ell^3/L^3 \text{ or } f_{cl} = L^3/\ell^3$$

h=2

more porous

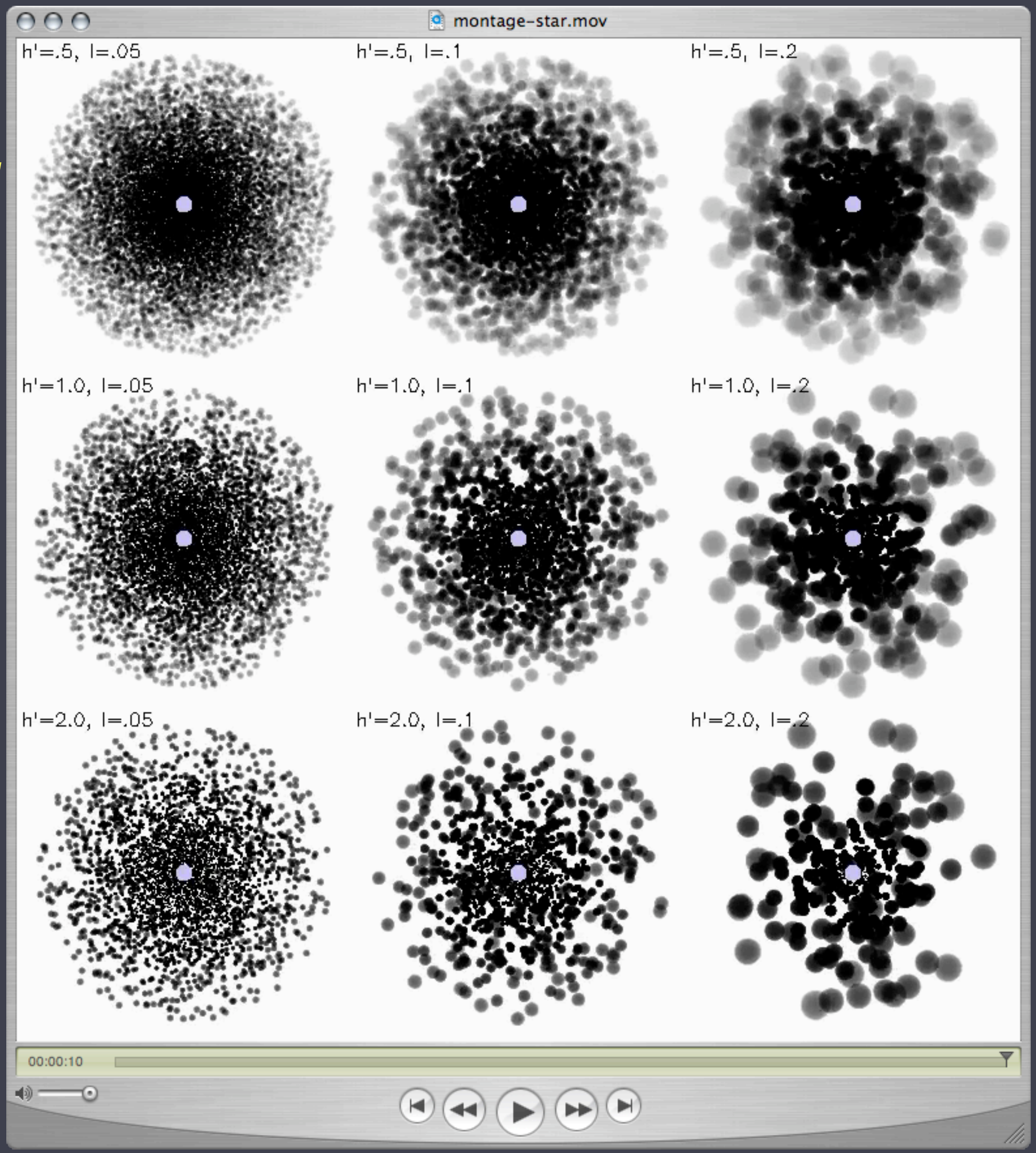

Summary of porosity considerations

porosity length, ***h*** = mean free path between clumps

porosity is only important if individual clumps are optically thick

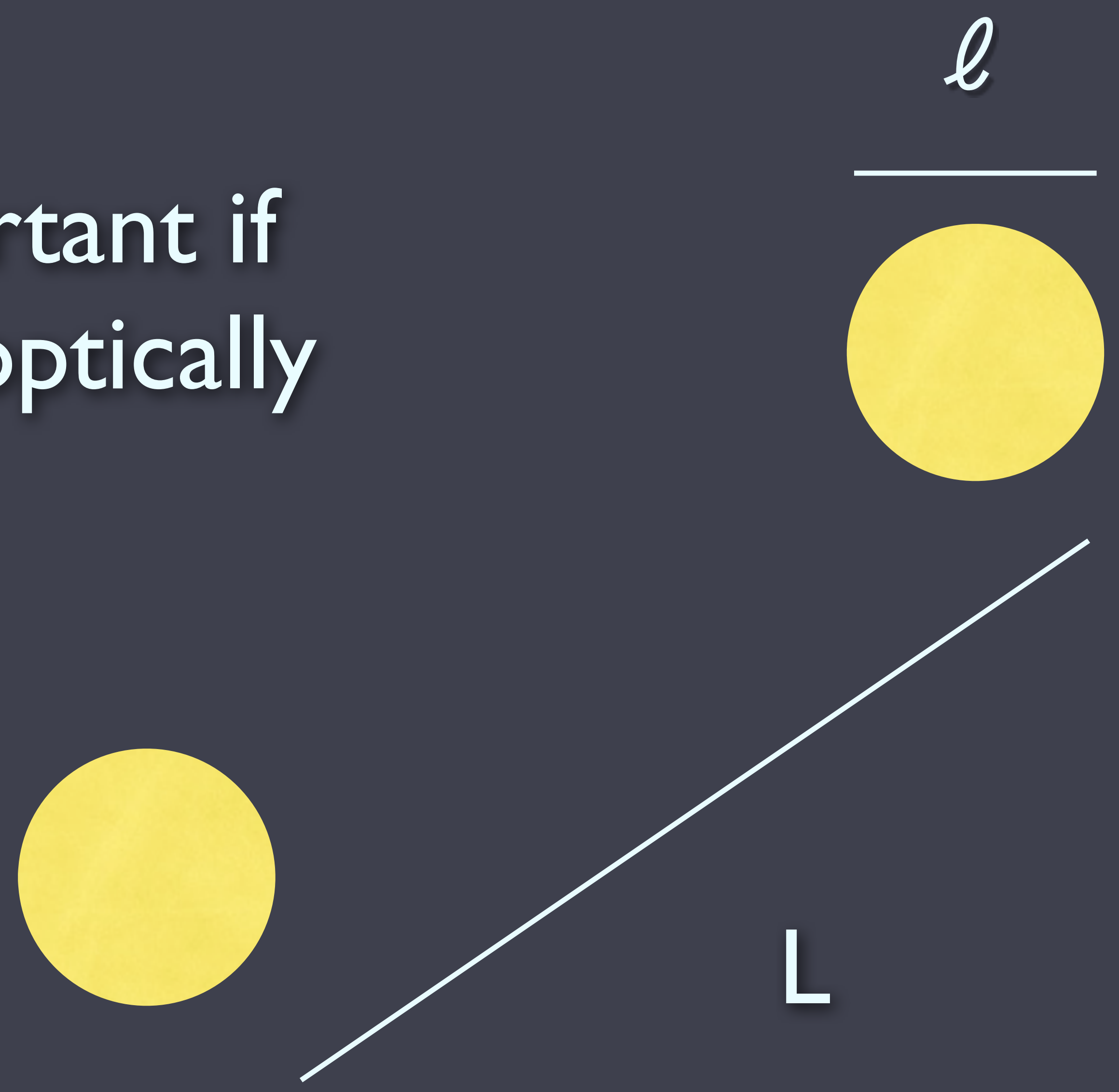

Quantitative treatment of porosity

porosity reduces the *effective opacity* of the wind

$$\kappa_{eff} \equiv \ell^2/m_{cl} \quad \text{vs.} \quad \kappa \equiv \sigma_{atom}/m_{atom}$$

$$\tau_{cl} = \kappa\rho_{cl}\ell = \kappa\langle\rho\rangle\ell f_{cl} = \kappa\langle\rho\rangle h$$

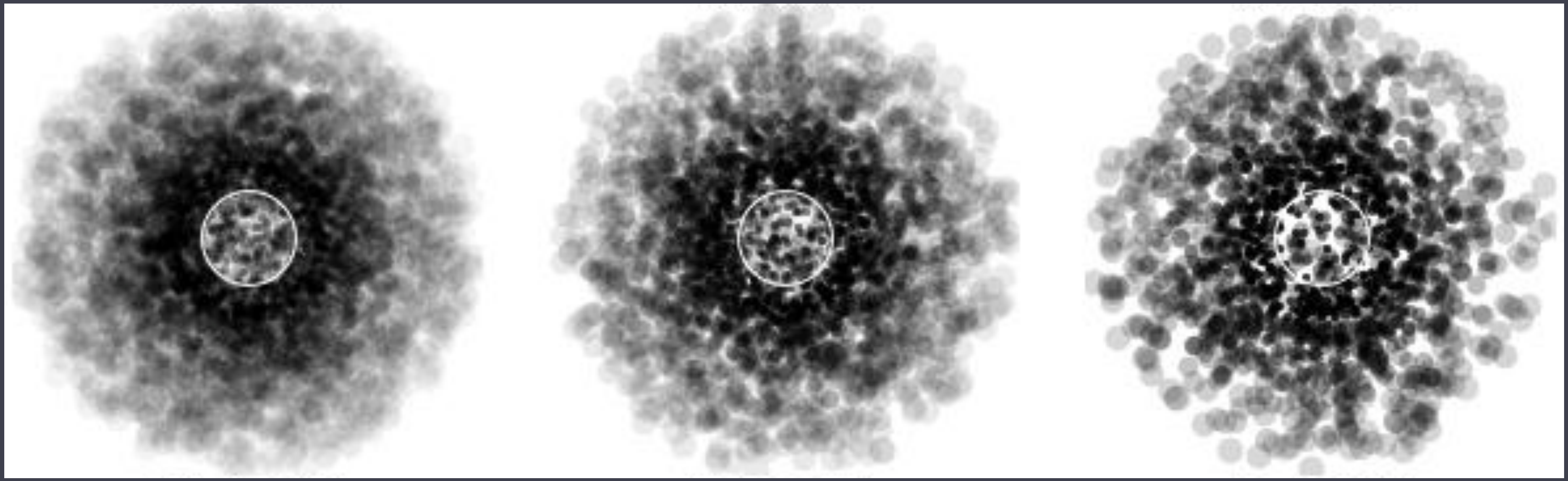

Quantitative treatment of porosity

porosity reduces the *effective opacity* of the wind

$$\kappa_{eff} \equiv \ell^2/m_{cl} \quad \text{vs.} \quad \kappa \equiv \sigma_{atom}/m_{atom}$$

$$\tau_{cl} = \kappa\rho_{cl}\,\ell = \kappa\langle\rho\rangle\,\ell\, f_{cl} = \kappa\langle\rho\rangle h$$

in radiation transport, simply replace κ with κ_{eff} where

$$\kappa_{eff} = \kappa/(1+\tau_{cl})$$

porosity length, *h*,
is the only new
parameter

Testing models of clumping and porosity with data

...or, measuring f_{cl} and h

Testing models of clumping and porosity with data

...or, measuring f_{cl} and h

first, consider emission line profiles, ignoring clumping and porosity for now

Line Asymmetry

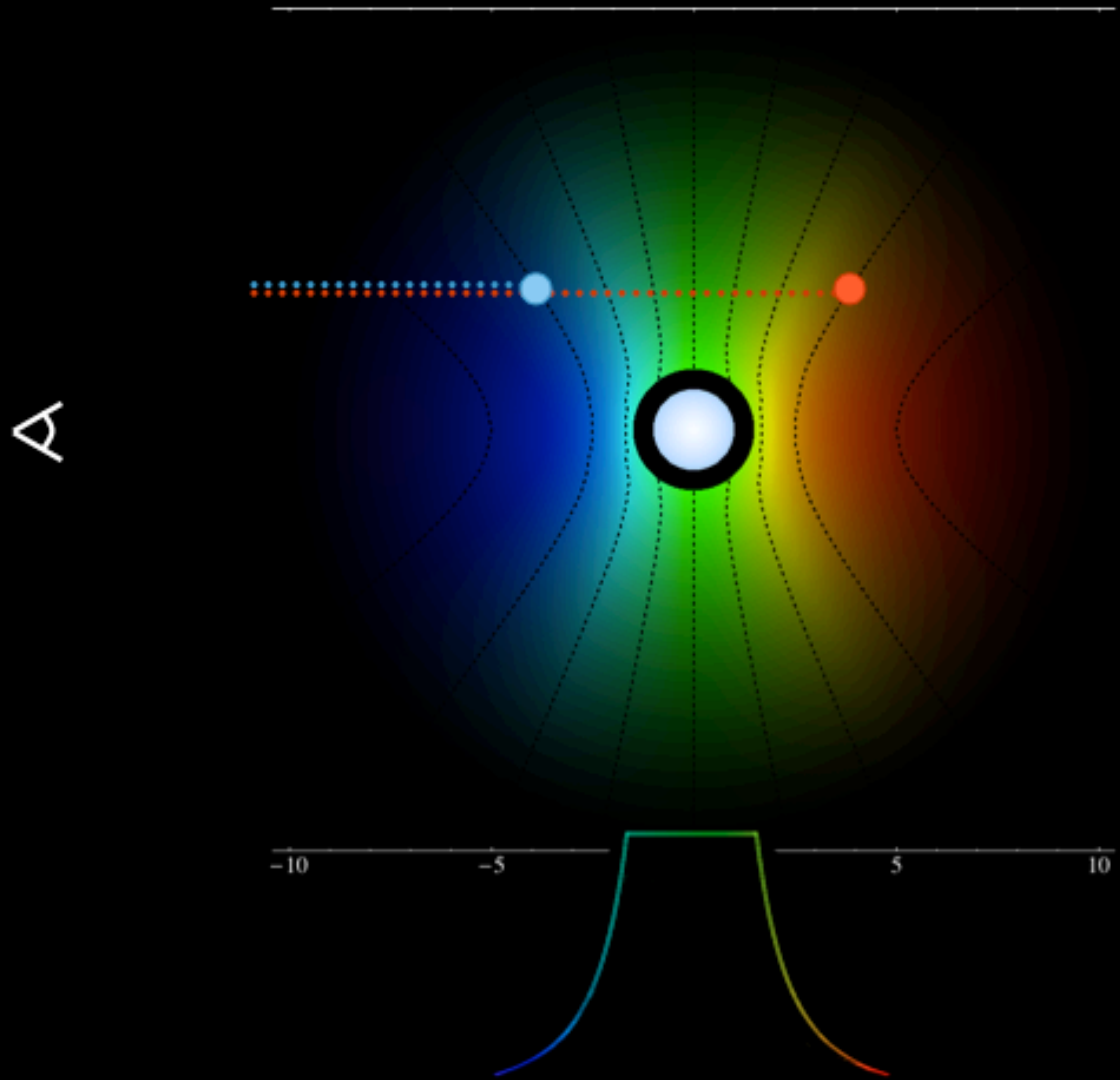

Line Asymmetry

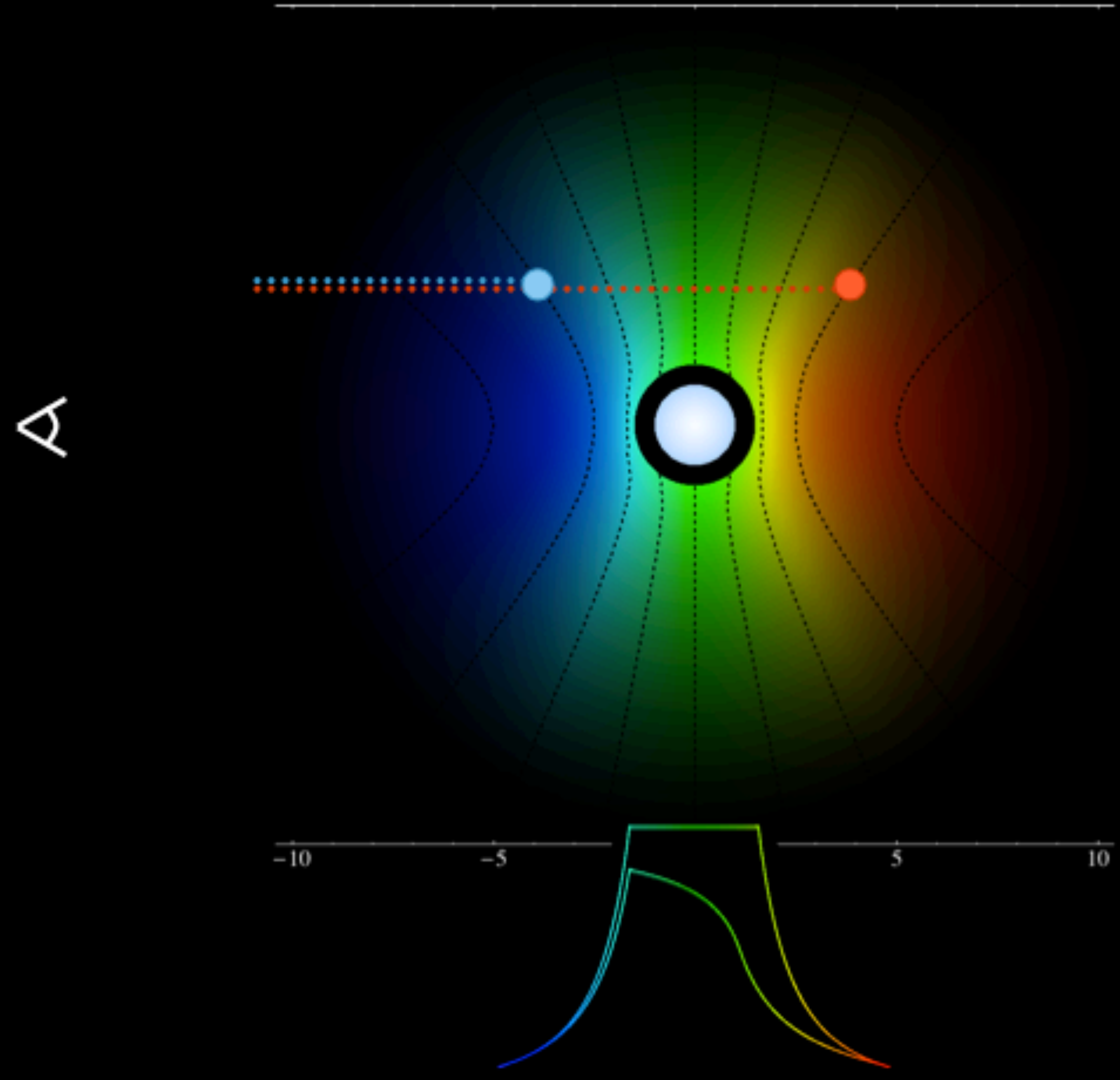

Line Asymmetry

$$\tau = \tau_* \int_z^\infty \frac{R_* dz'}{r'^2 (1 - {}^{R_*}\!/_{r'})^\beta}$$

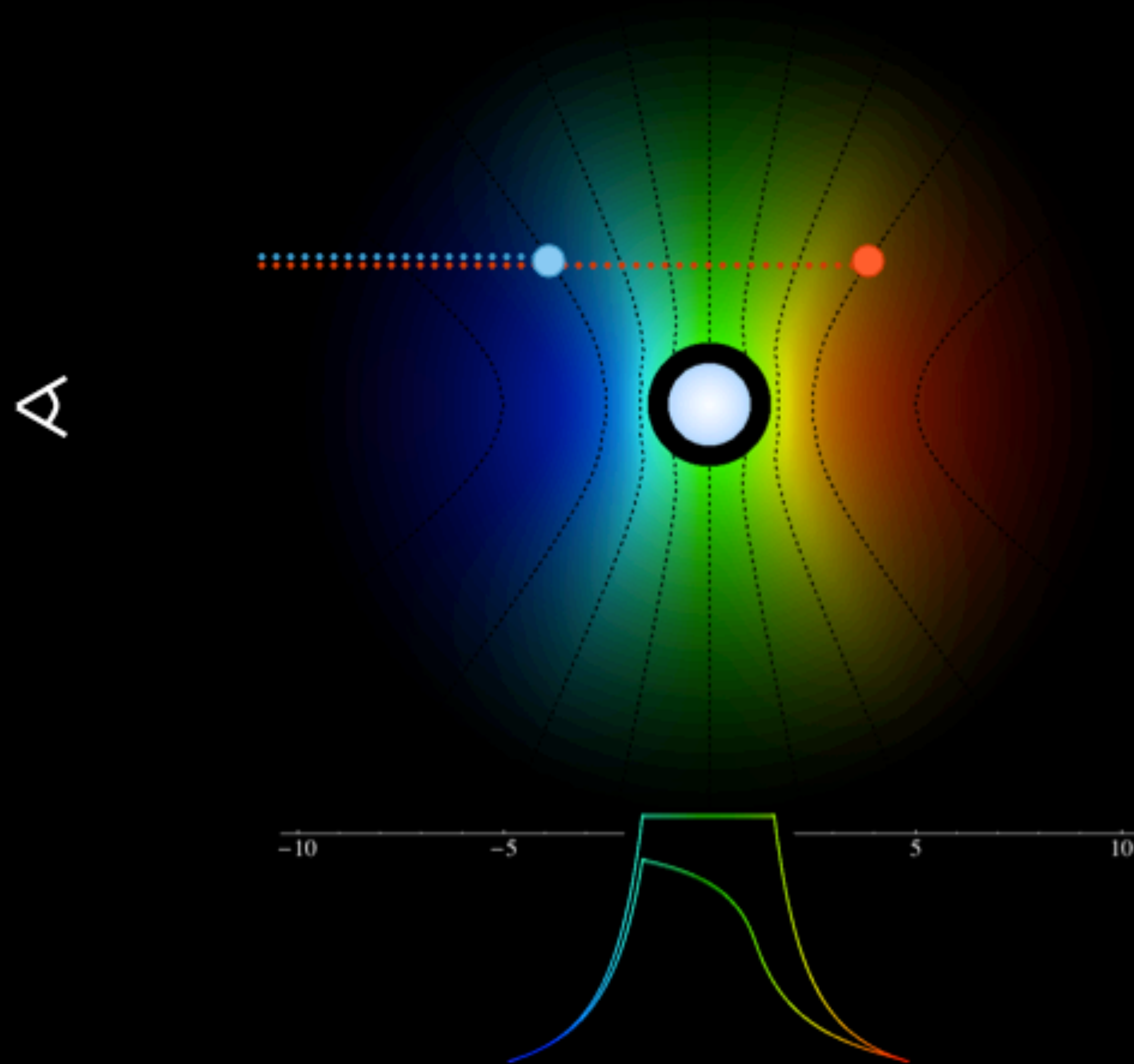

Wind Profile Model

$$\tau_* = \frac{\kappa \dot{M}}{4\pi R_* v_\infty}$$

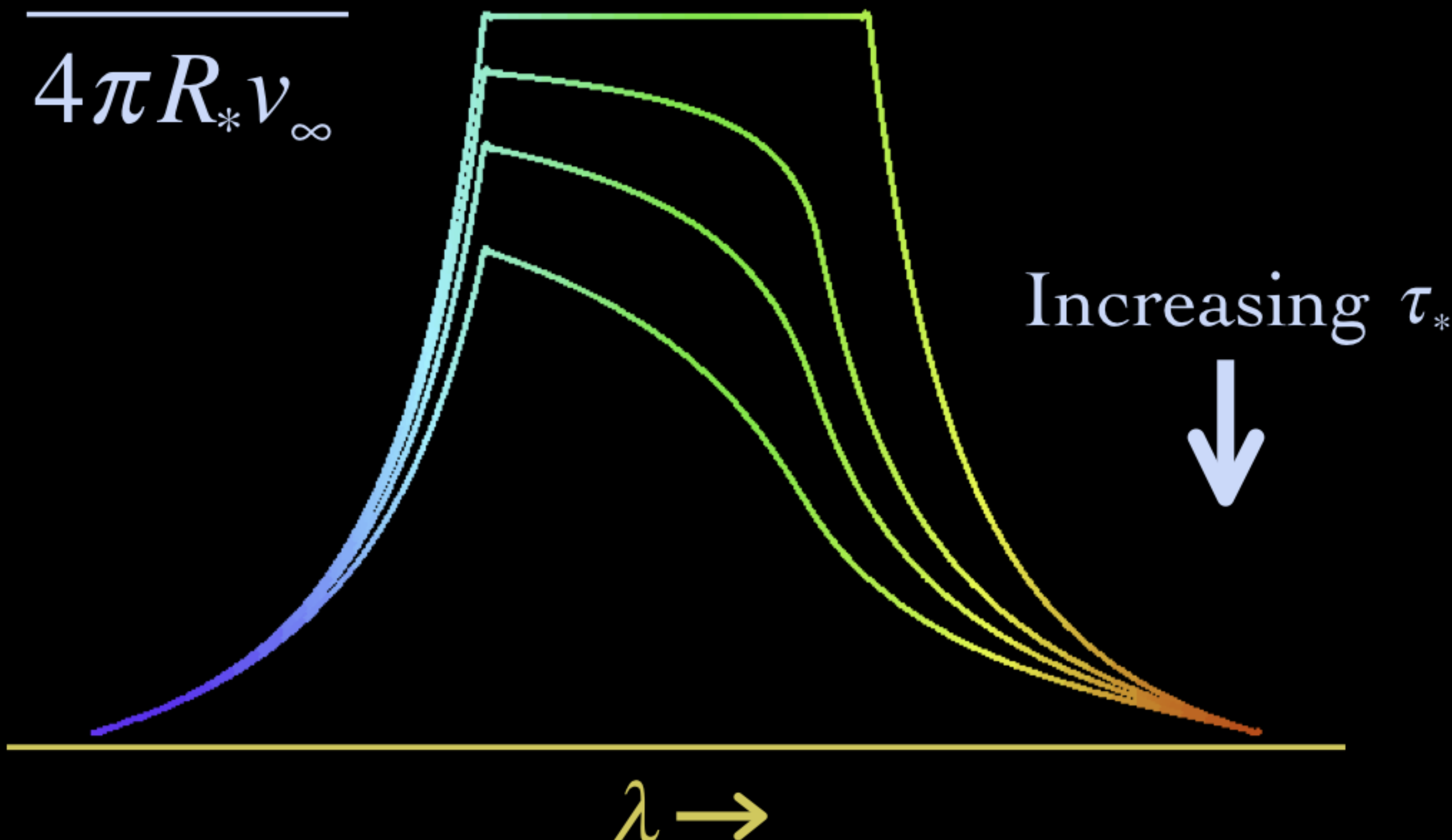

Quantifying the wind optical depth

opacity of the cold wind component (due to bound-free transitions in C, N, O, Ne, Fe)

wind mass-loss rate

$$\dot{M} = 4\pi r^2 v \rho$$

$$\tau_* \equiv \frac{\kappa \dot{M}}{4\pi R_* v_\infty}$$

stellar radius

wind terminal velocity

Line profile shapes

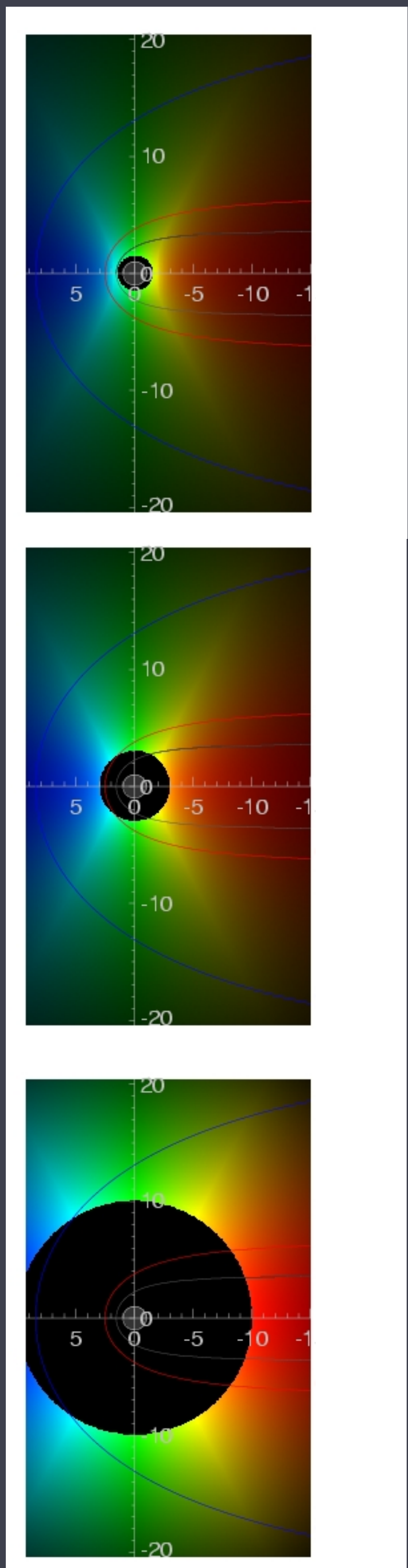

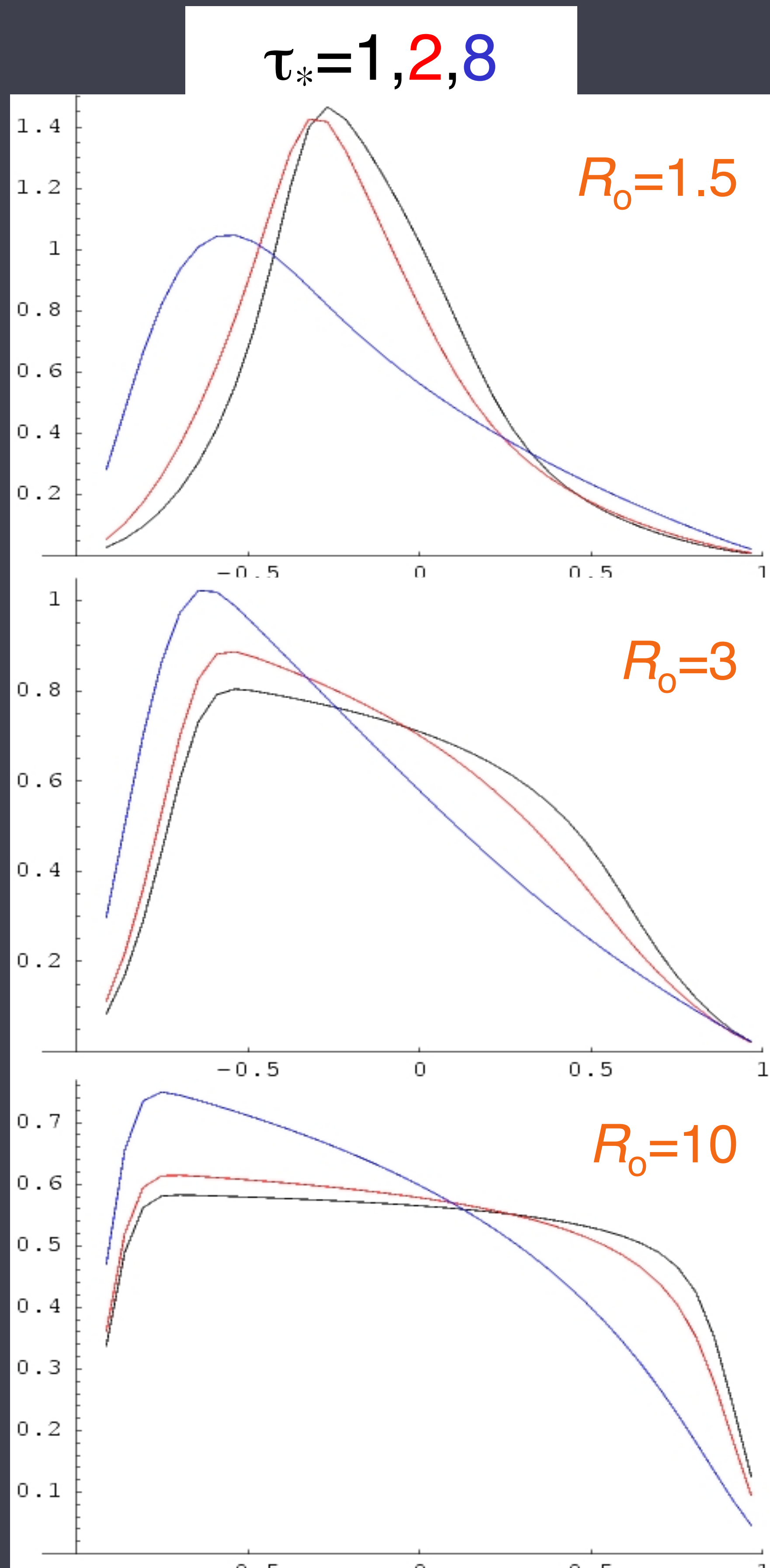

key parameters: R_o & $\tau_\star$

$j \sim \rho^2$ for $r/R_* > R_o$,
$= 0$ otherwise

$$\tau = \tau_* \int_z^\infty \frac{R_* dz'}{r'^2 (1 - R_*/r')^\beta}$$

$$\tau_* \equiv \frac{\kappa \dot{M}}{4\pi R_* v_\infty}$$

Measurements of $\tau_\star$ from line profiles

ζ Ori (Cohen et al. 2006)

ζ Pup (Cohen et al. 2010)

HD 93129A (Cohen et al. 2011)

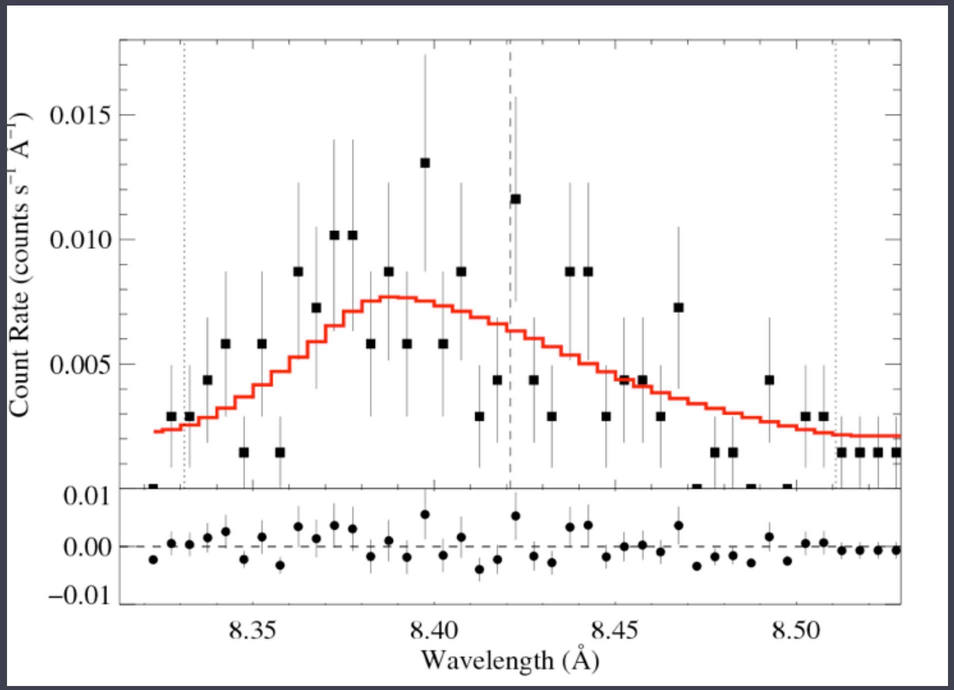

HD 155806 (Naze et al. 2010)

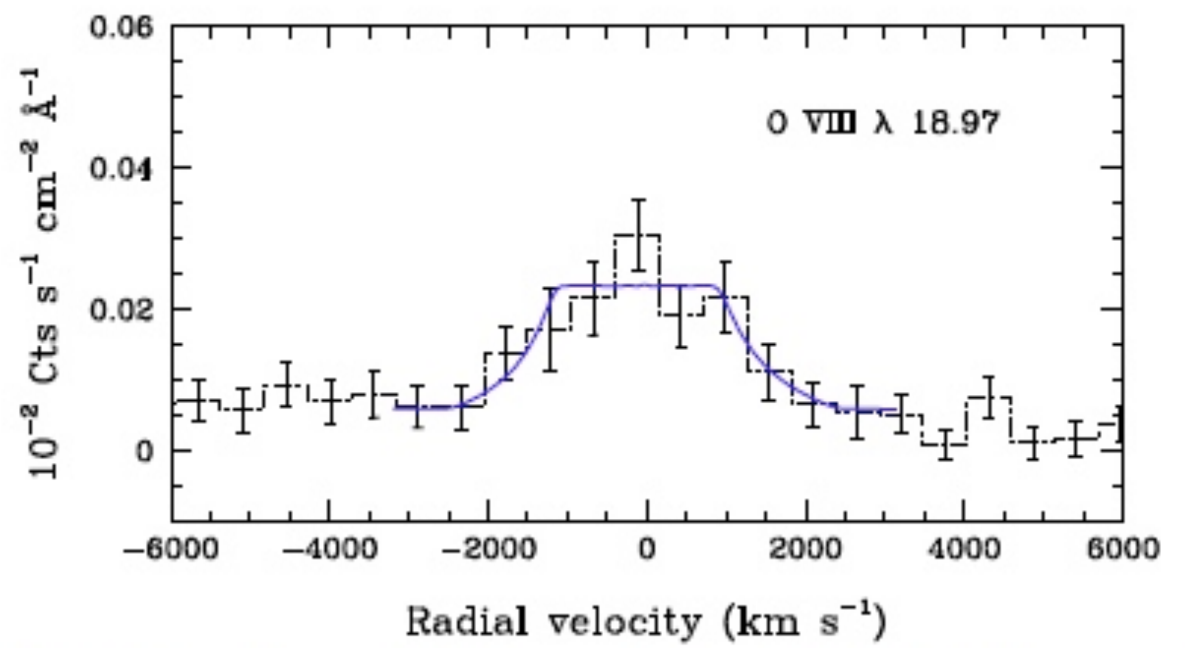

Fig. 2. The best-fit exospheric line-profile model (with the X-rays emitted above $R_0 = 1.85\ R_*$ and a wind opacity of $\tau_{\lambda,*} = 0.0$) overplotted on the RGS data of the O VIII Lyα line (binned to get 1000 bins for the entire wavelength range).

Line profile shapes

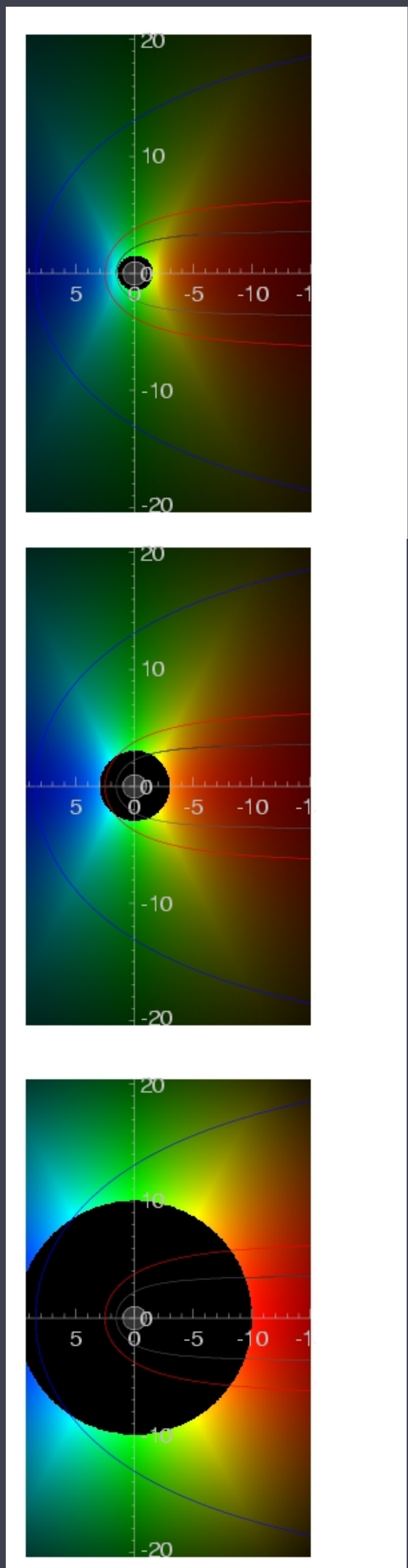

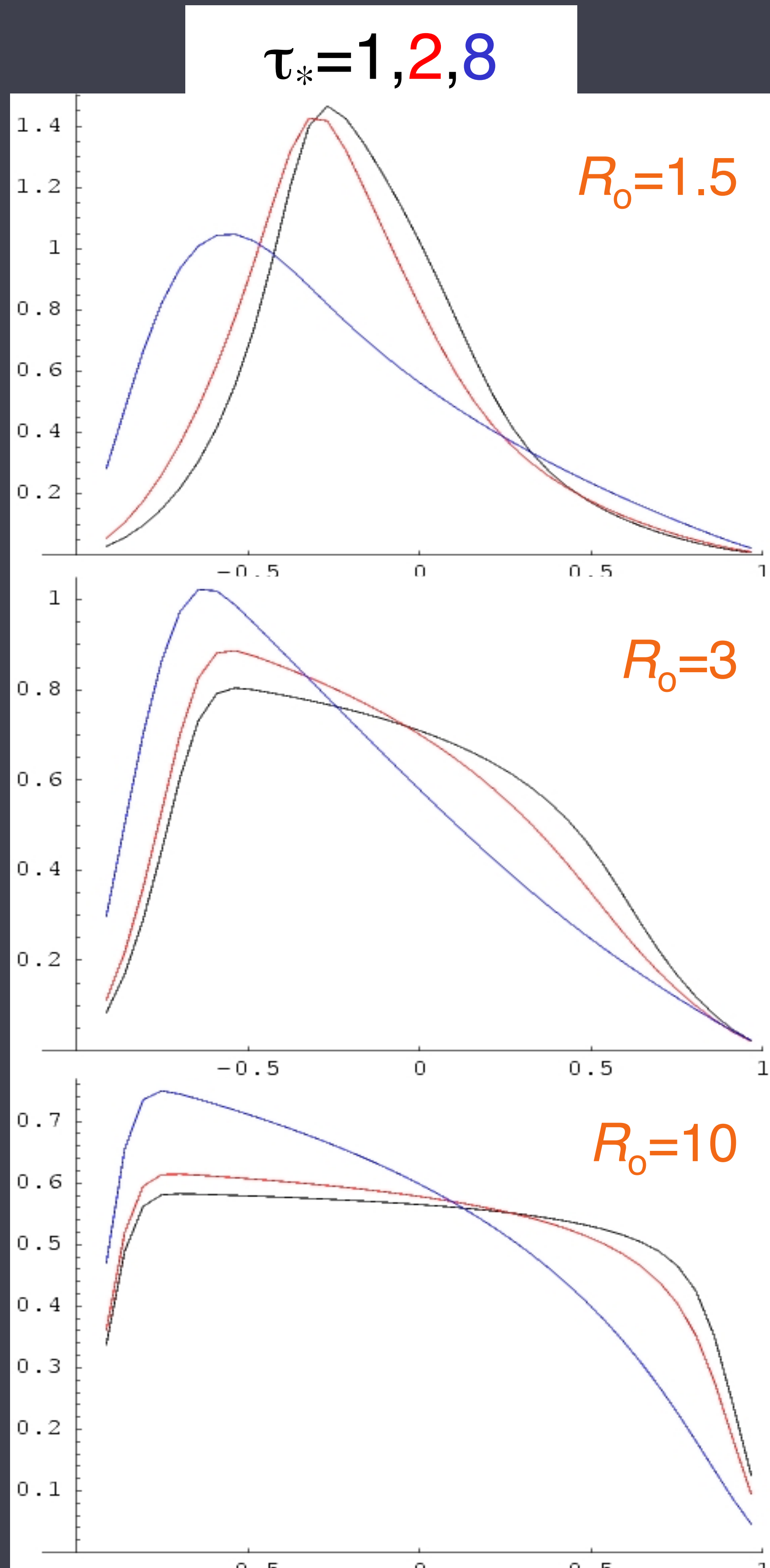

key parameters: R_o & $\tau_\star$

$j \sim \rho^2$ for $r/R_* > R_o$,

$= 0$ otherwise

$$\tau = \tau_* \int_z^\infty \frac{R_* \, dz'}{r'^2 (1 - R_*/r')^\beta}$$

$$\tau_* \equiv \frac{\kappa \dot{M}}{4\pi R_* v_\infty}$$

Line profile shapes: with porosity

key parameters: R_o & $\tau_\star$

$j \sim \rho^2$ for $r/R_* > R_o$,

$= 0$ otherwise

$$\tau = \tau_* \int_z^\infty \frac{R_* dz'}{r'^2 (1 - R_*/r')^\beta}$$

simply replace κ with

$\kappa_{eff} \propto \kappa/(1+h)$

$$\tau_* \equiv \frac{\kappa \dot{M}}{4\pi R_* v_\infty}$$

remember: clumping does not affect X-ray line shapes; only porosity does

Line profiles with porosity

h has to be big for porosity to have an effect

porosity makes lines more symmetric, mimicking lower optical depths

$h = 0\ R_\star$

$h = 0.5\ R_\star$

$h = 1\ R_\star$

$h = 5\ R_\star$

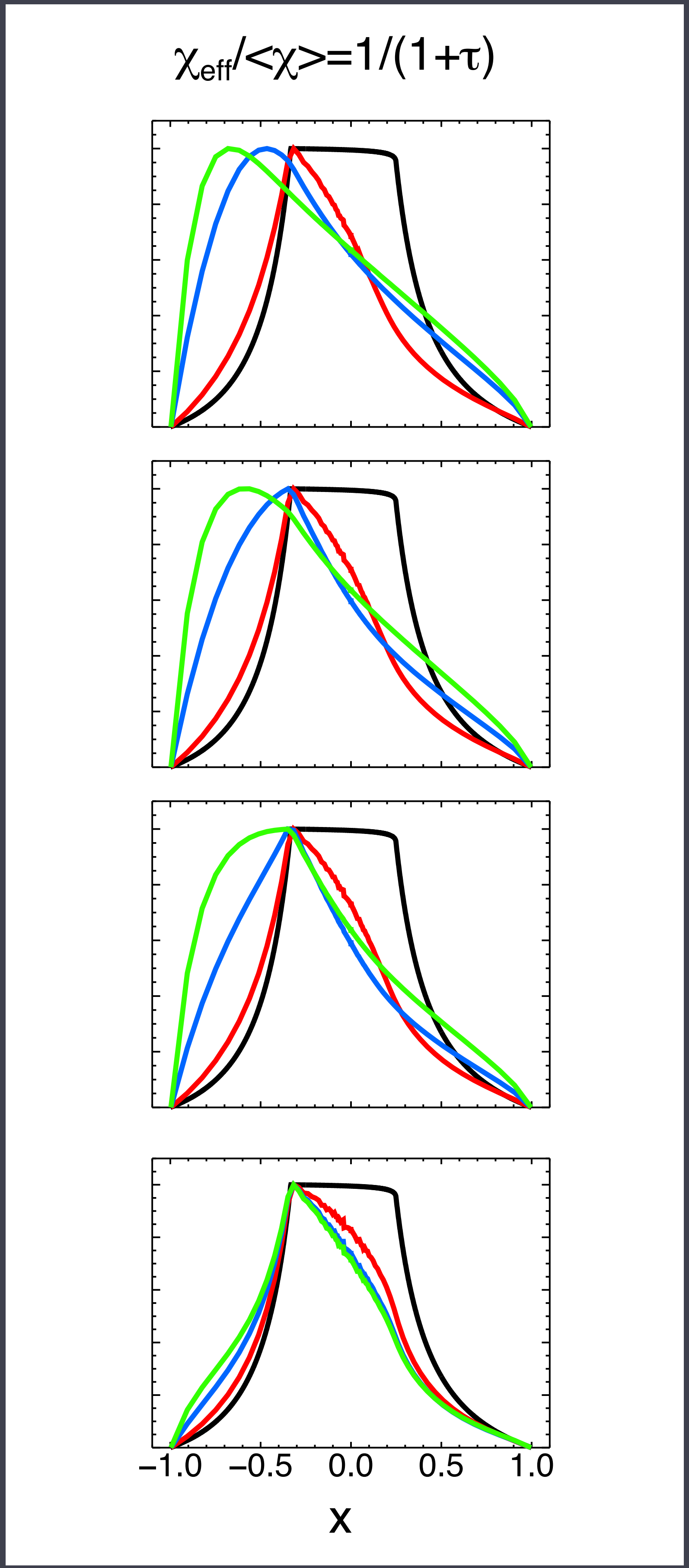

Testing models of clumping and porosity with data

...or, measuring f_{cl} and h

Measuring $\tau_\star$ along with h gives the mass-loss rate, but the two parameters are degenerate

Hα, IR & radio free-free, measures $\dot{M} f_{cl}^{0.5}$.

Testing models of clumping and porosity with data

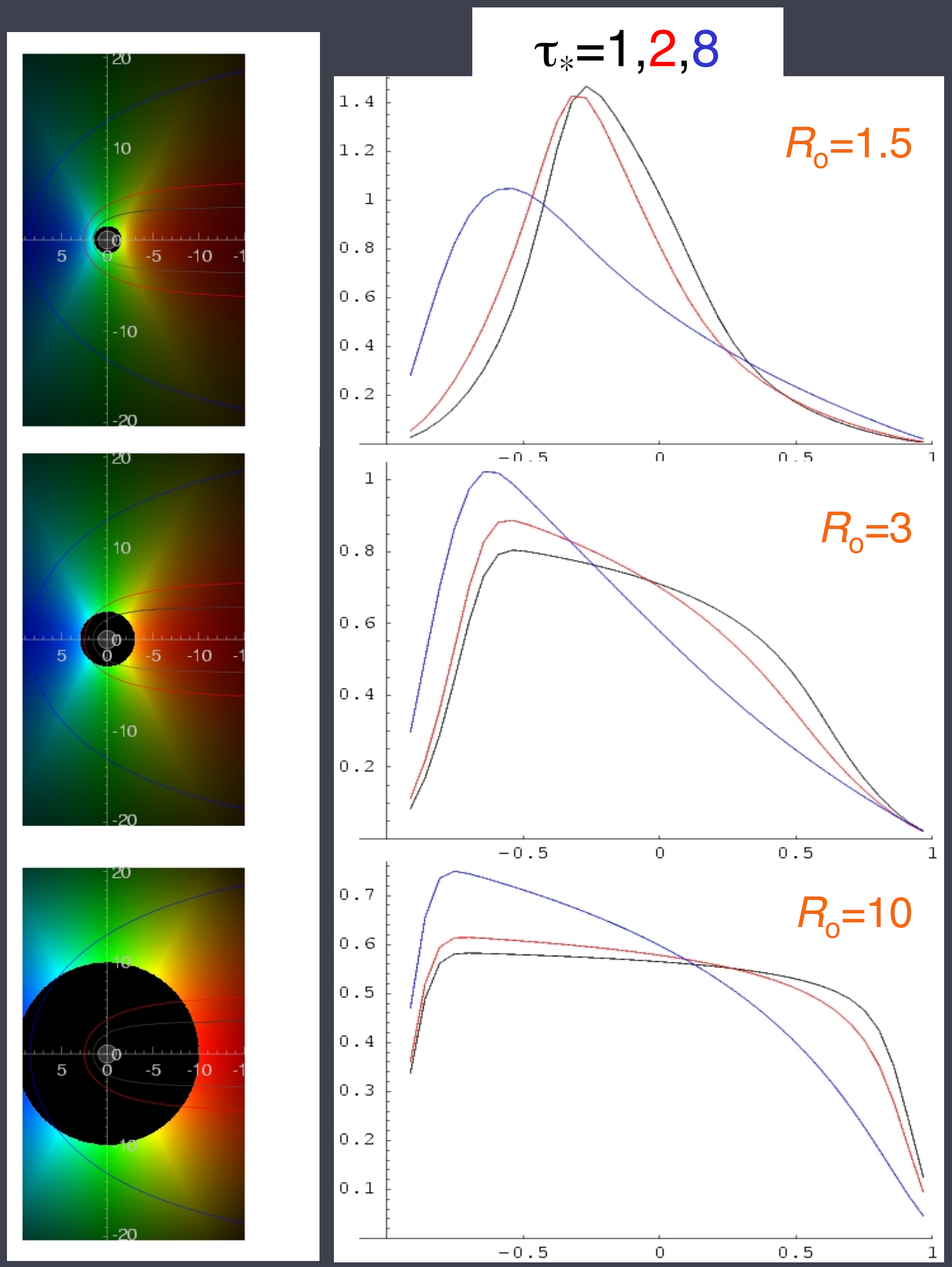

ζ Pup: Chandra MEG

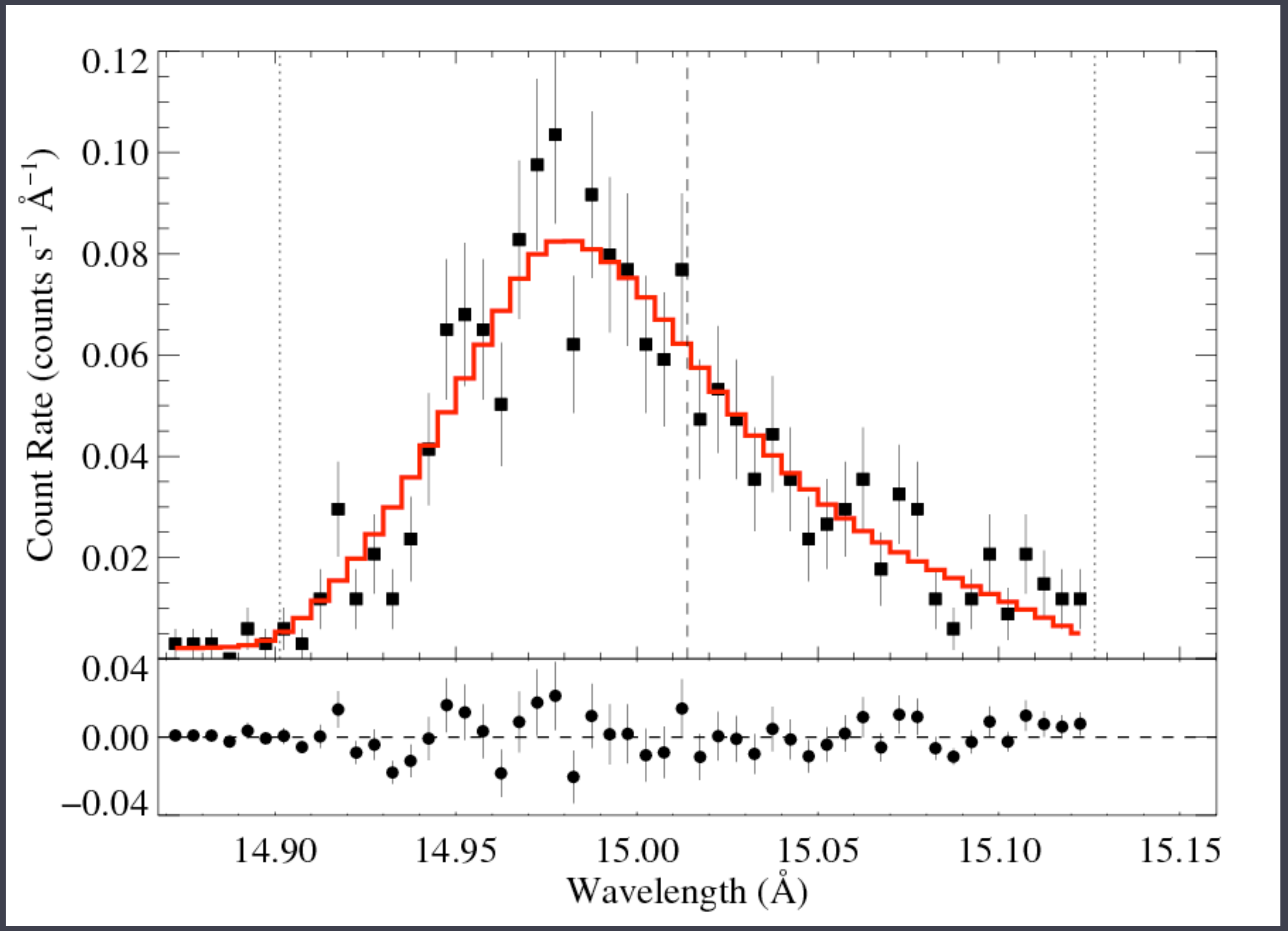

ζ Pup: Chandra MEG

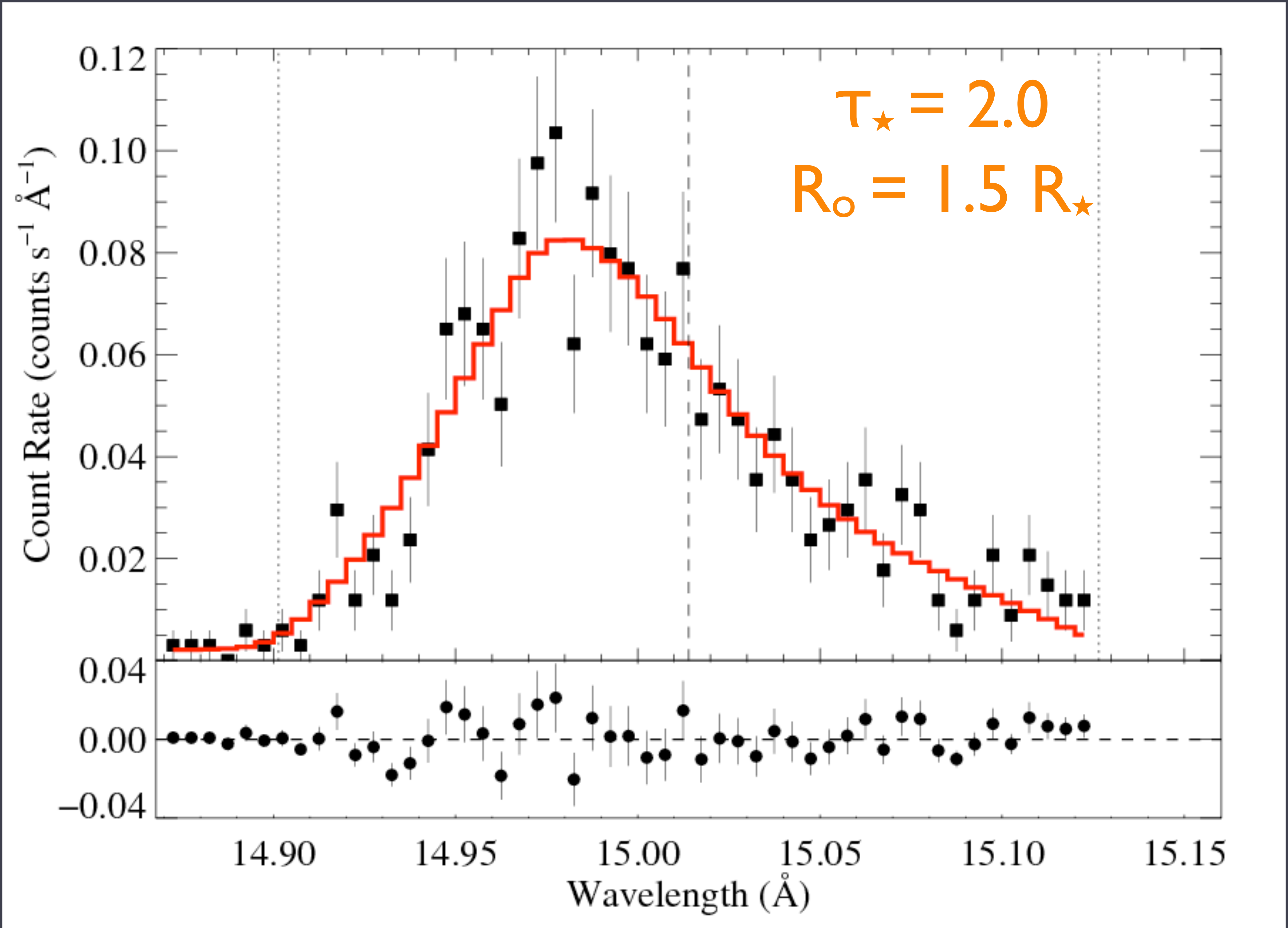

What about with porosity?

Use a model of a radially varying porosity length

$$h(r) = h_\infty(1 - R_\star/r)^\beta$$

note the resemblance:

$$v(r) = v_\infty(1 - R_\star/r)^\beta$$

ζ Pup: Chandra MEG
$h_\infty = 0.5\ R_\star$

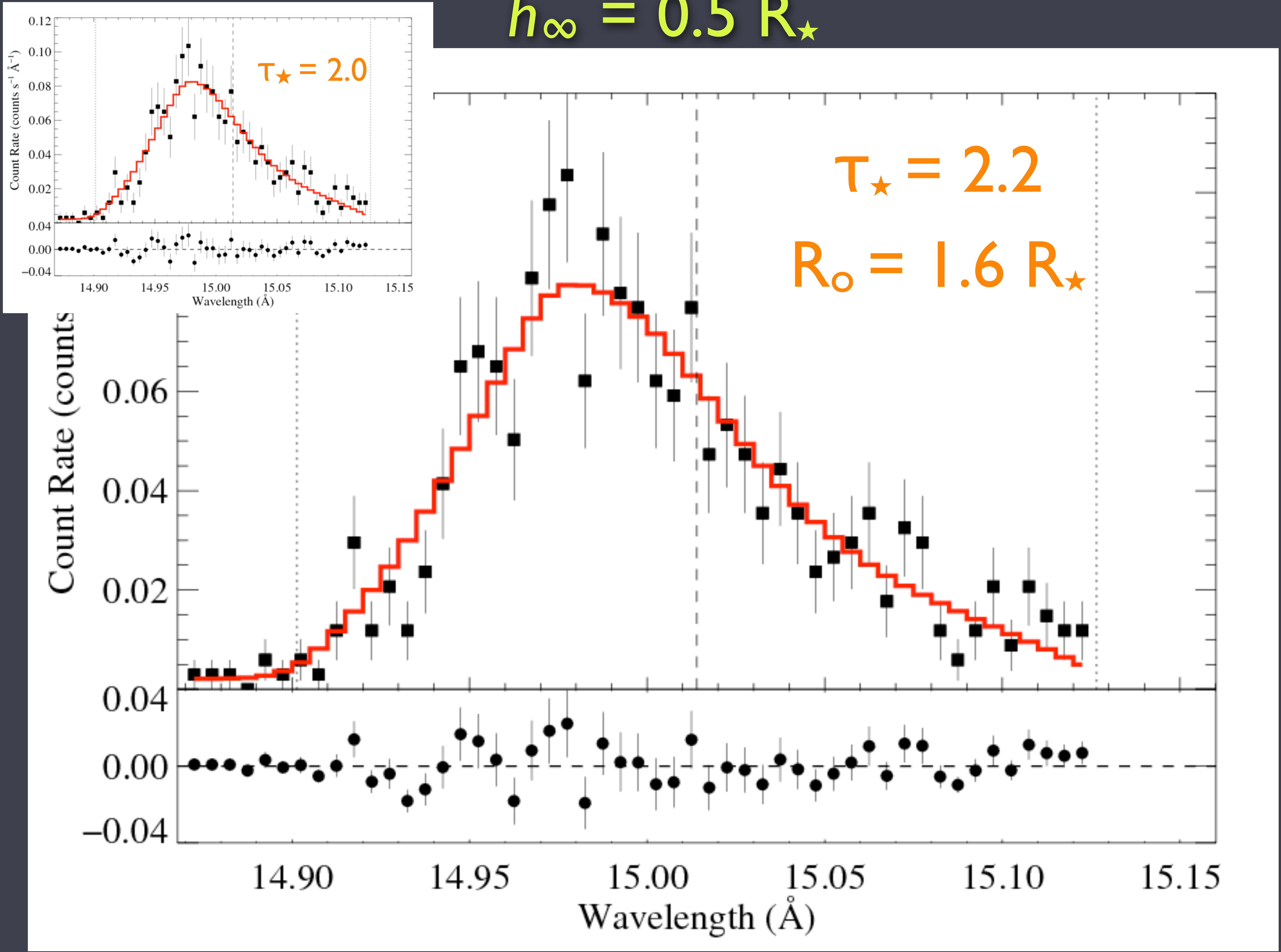

ζ Pup: Chandra MEG
h_∞ = 1 $R_\star$

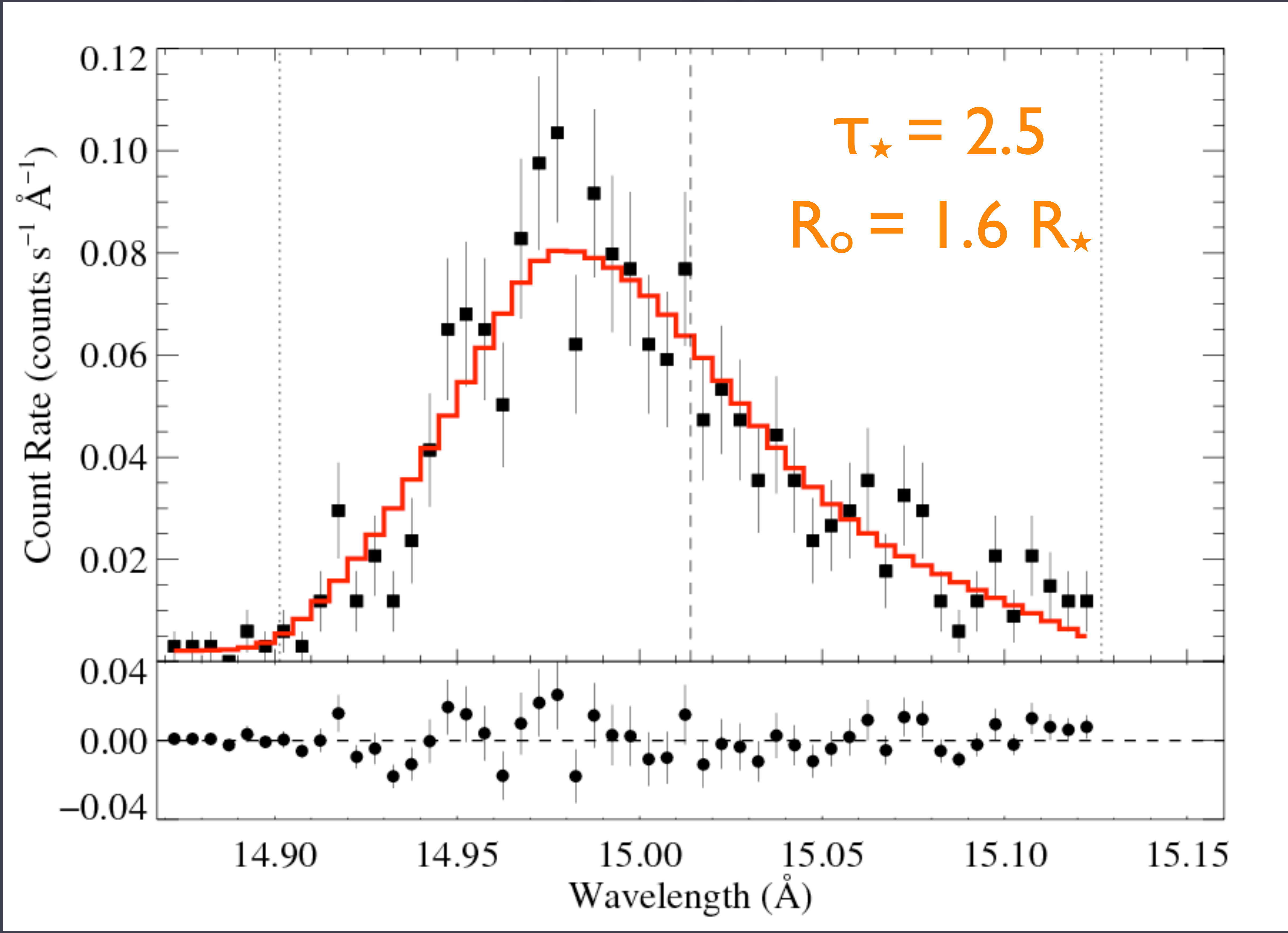

ζ Pup: Chandra MEG
$h_\infty = 5\ R_\star$

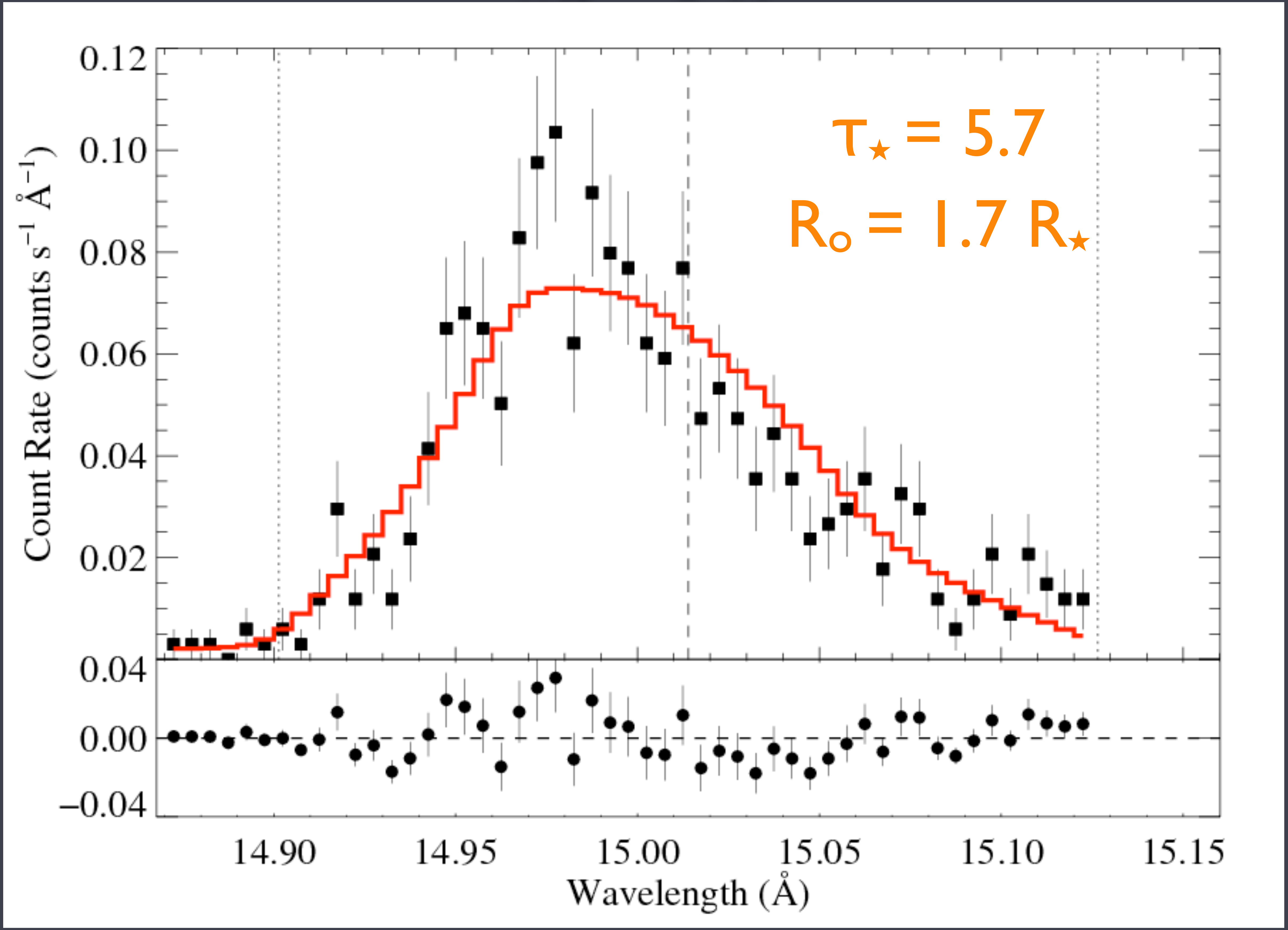

poor fit (P > 99.9%) and large $\tau_\star$

$h_\infty = 5\ R_\star$

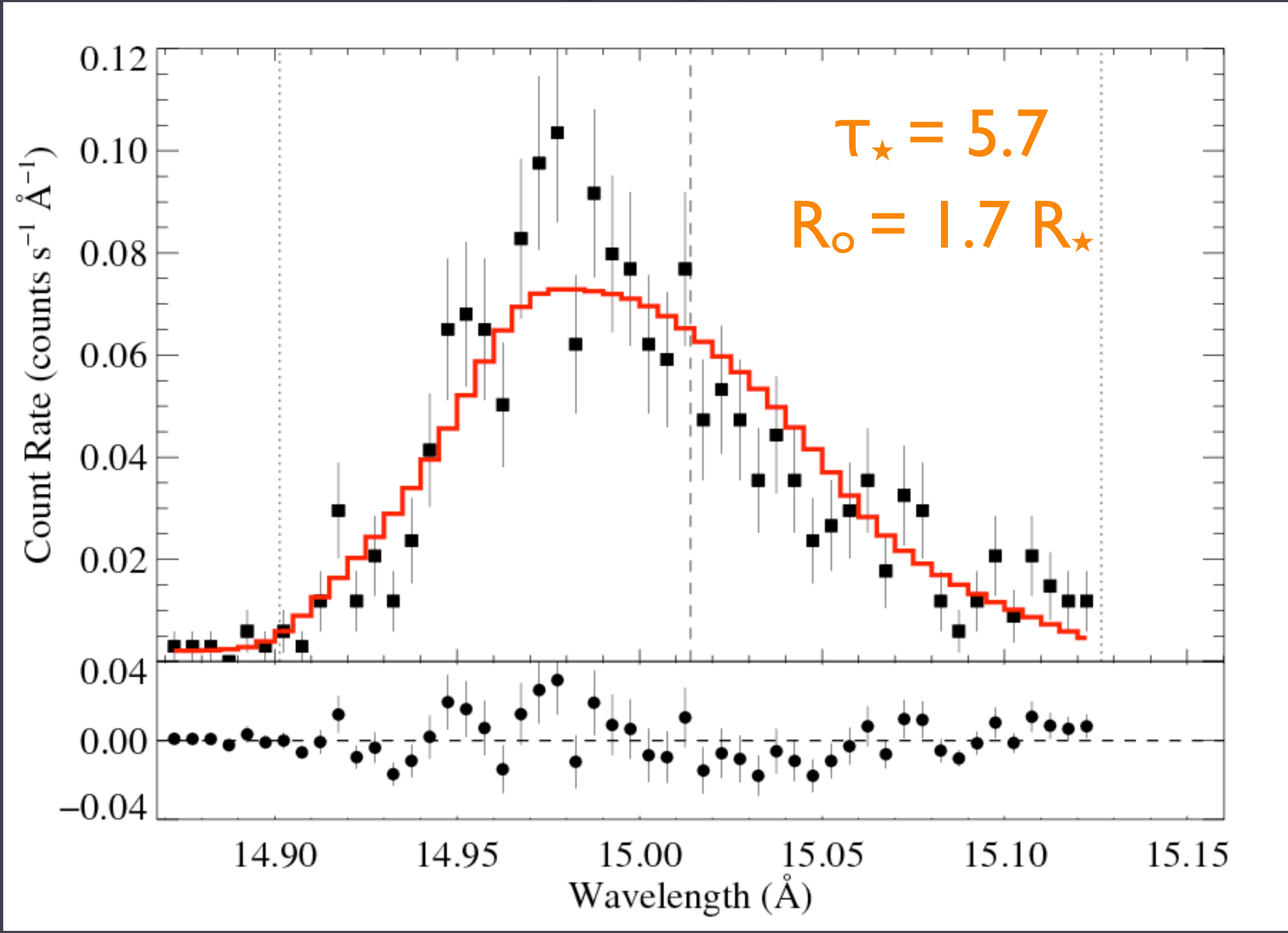

Confidence limits on h_∞ and $\tau_\star$

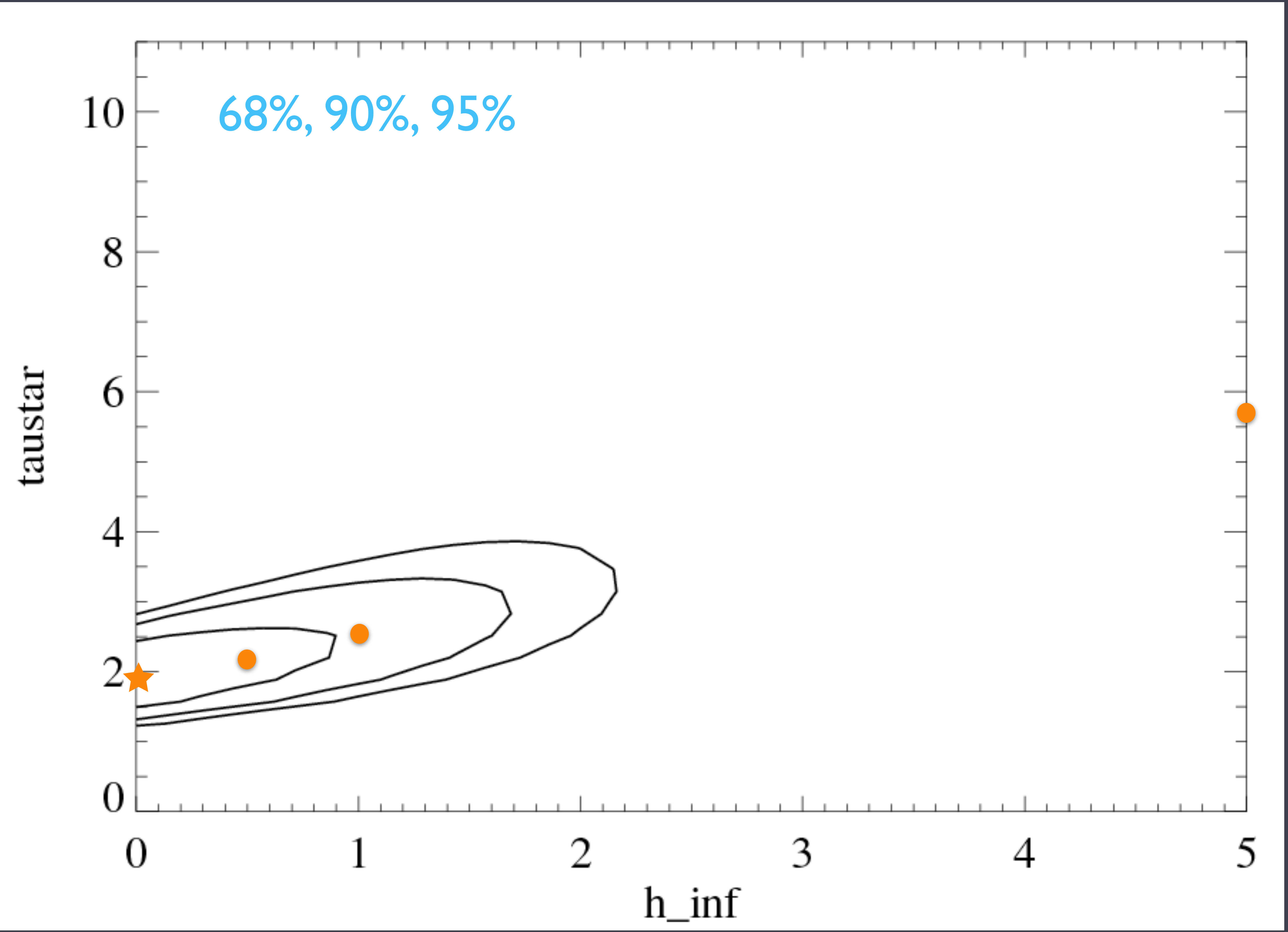

XMM RGS spectrum

$h_\infty = 0$

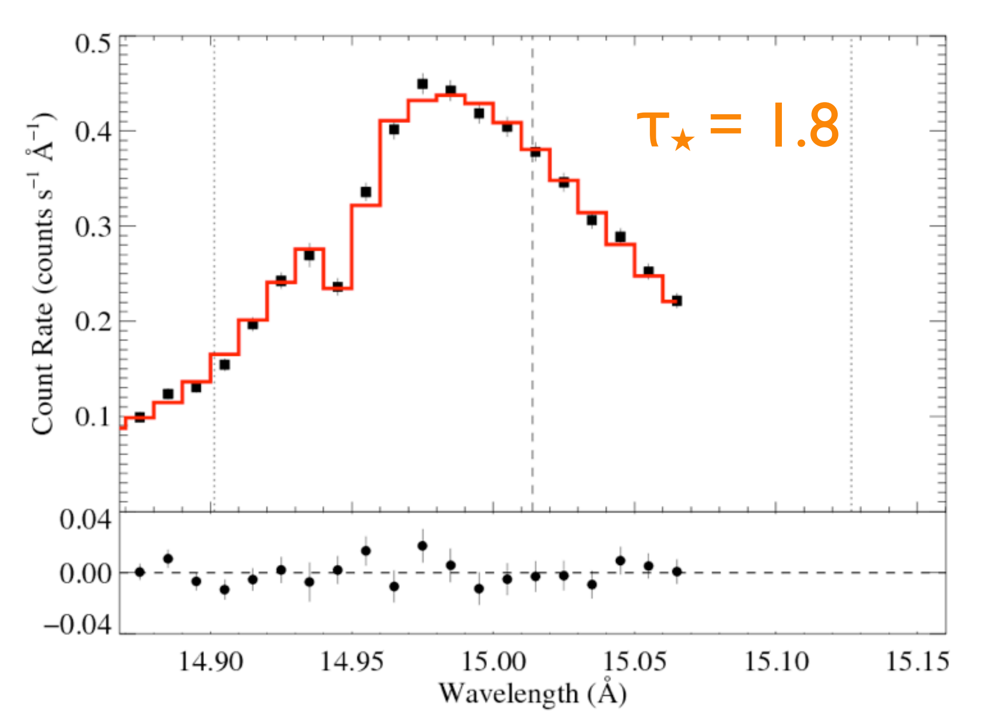

$h_\infty = 0.5$

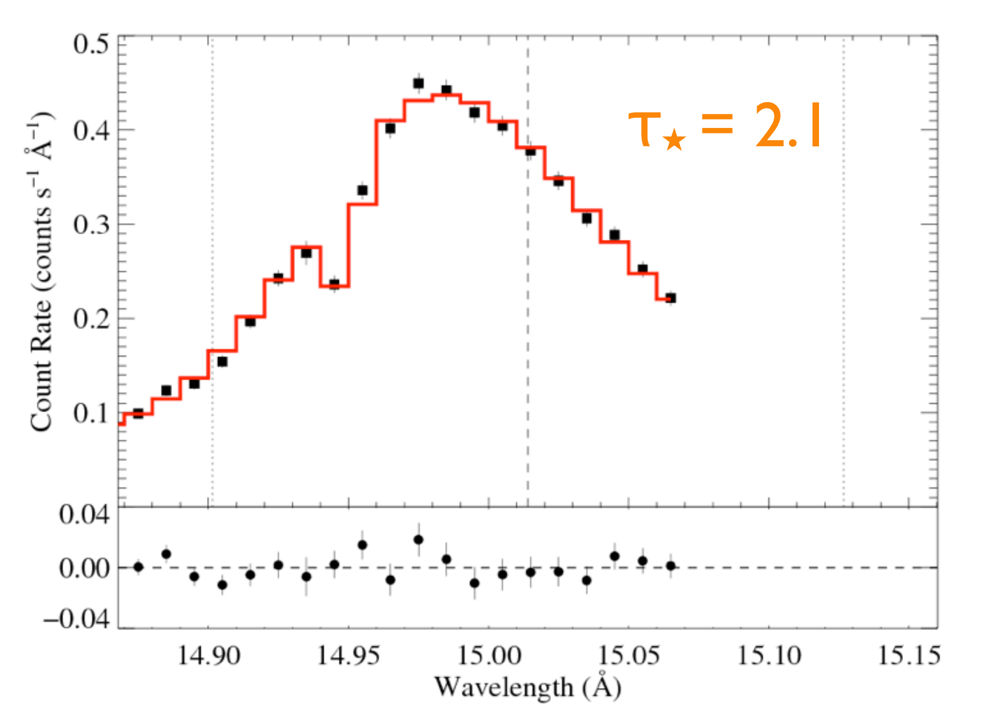

$h_\infty = 1$

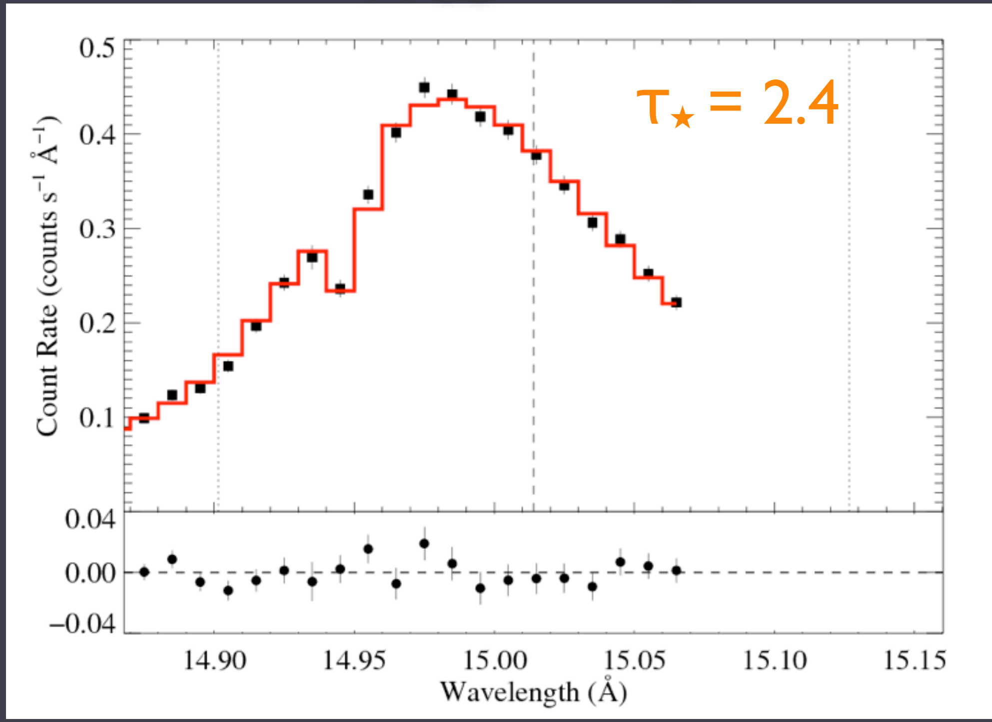

$h_\infty = 5$

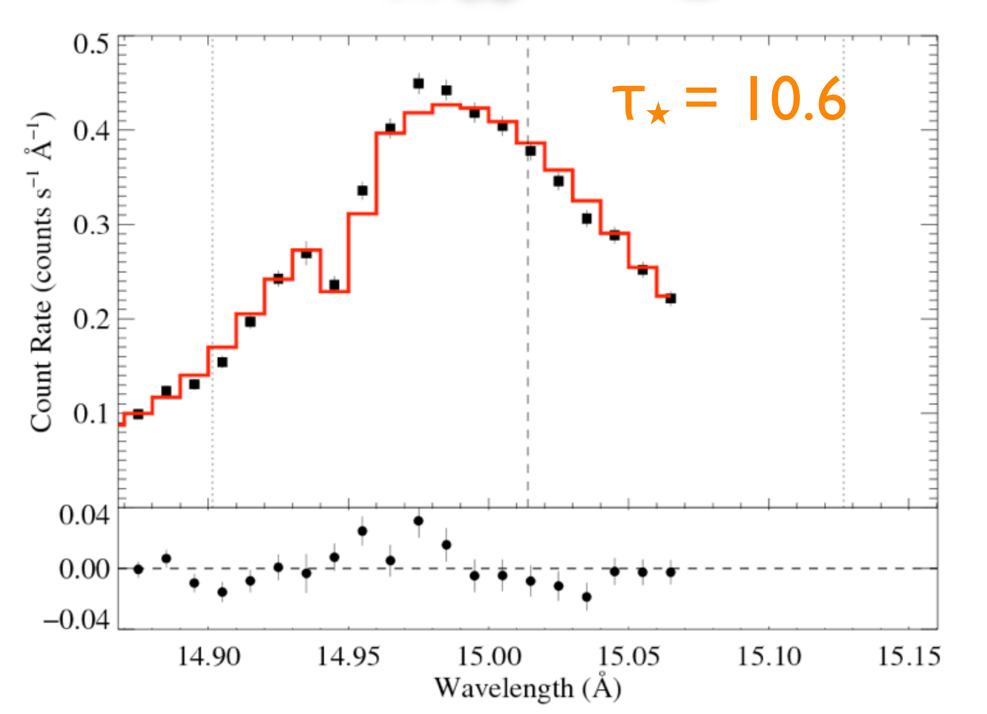

RGS Confidence limits on h_∞ and $\tau_\star$

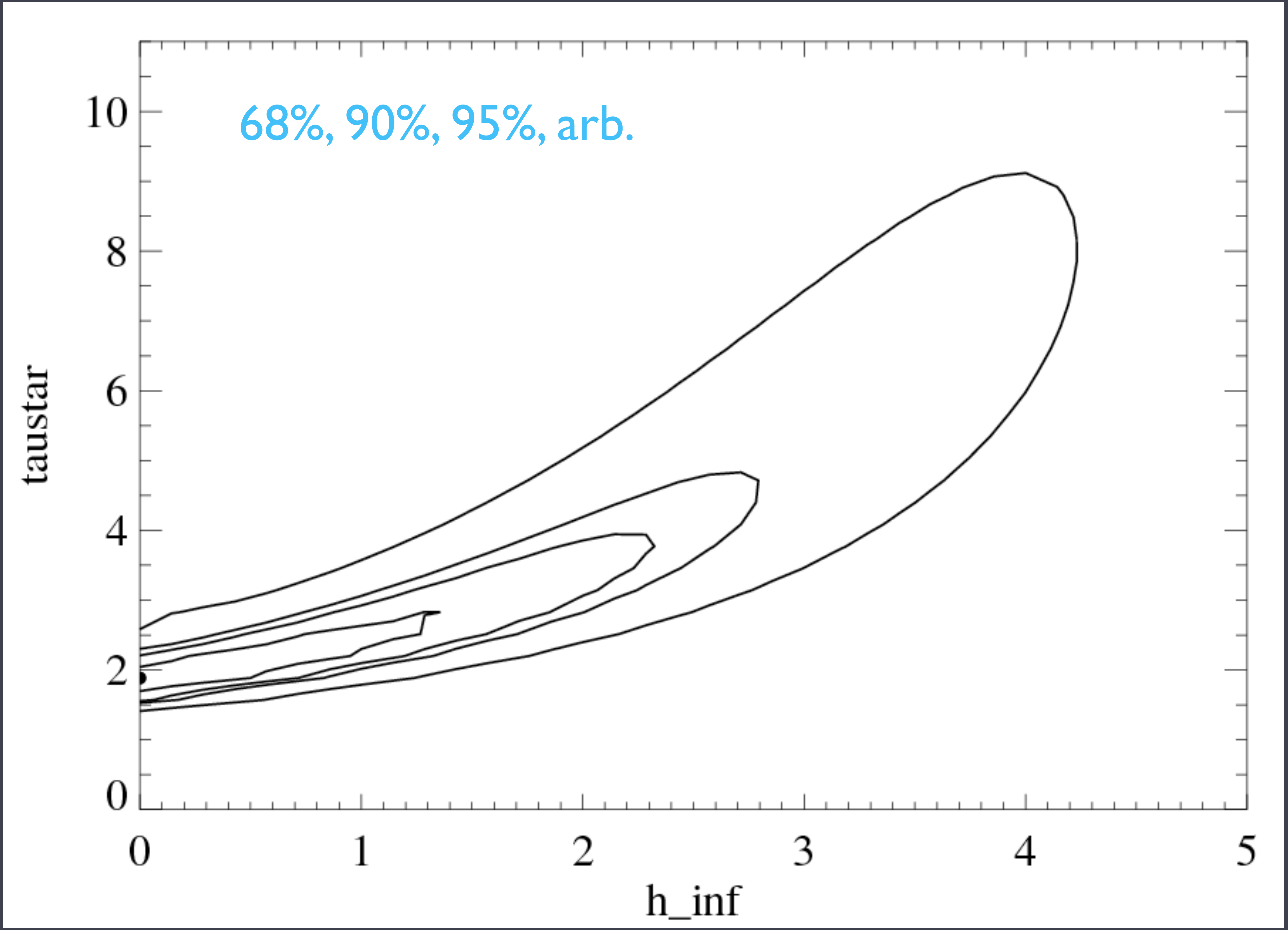

What about other spectral lines?

O VIII Lyα 18.969 Å

$h_\infty = 0$

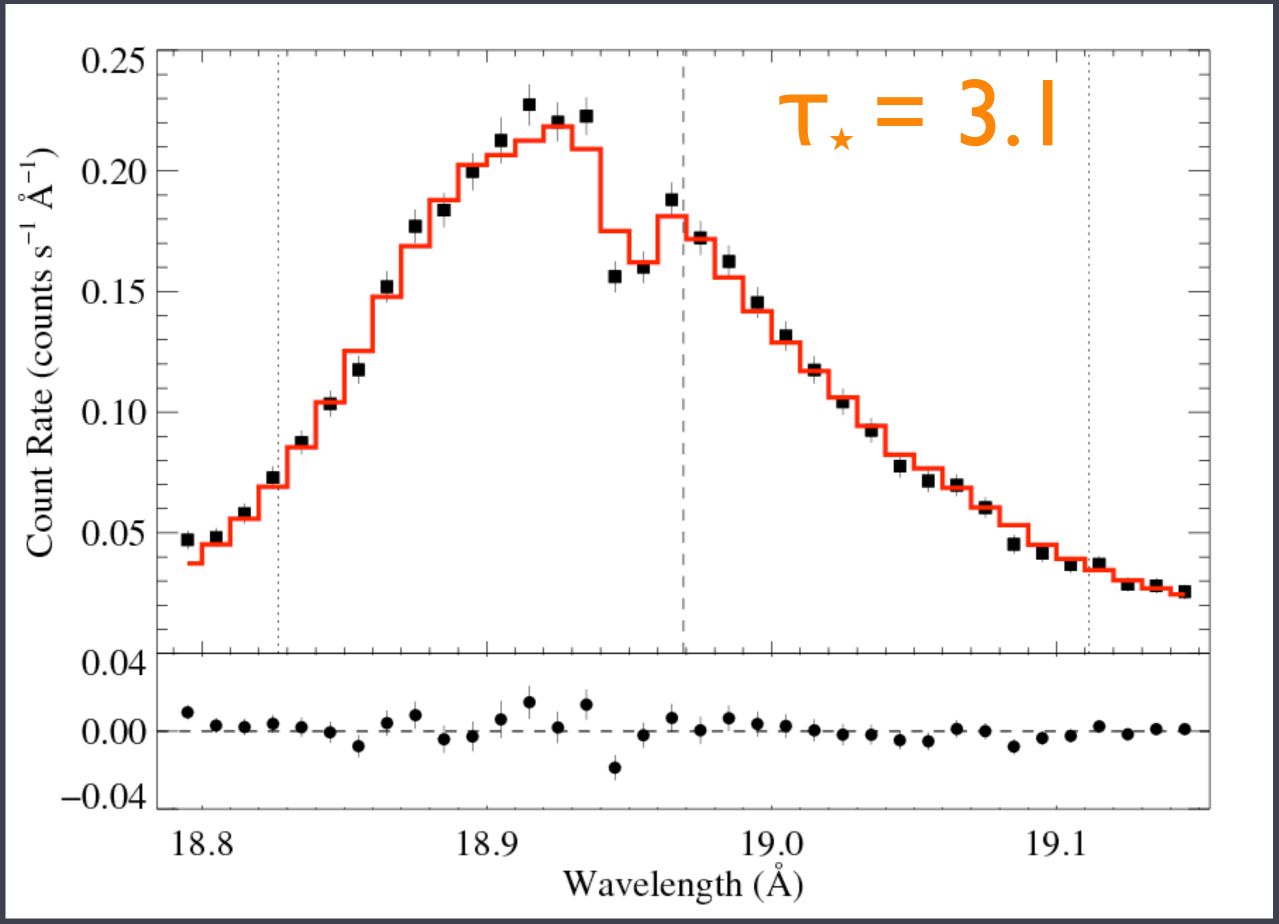

$h_\infty = 0$

Fe XVII 15.014 Å

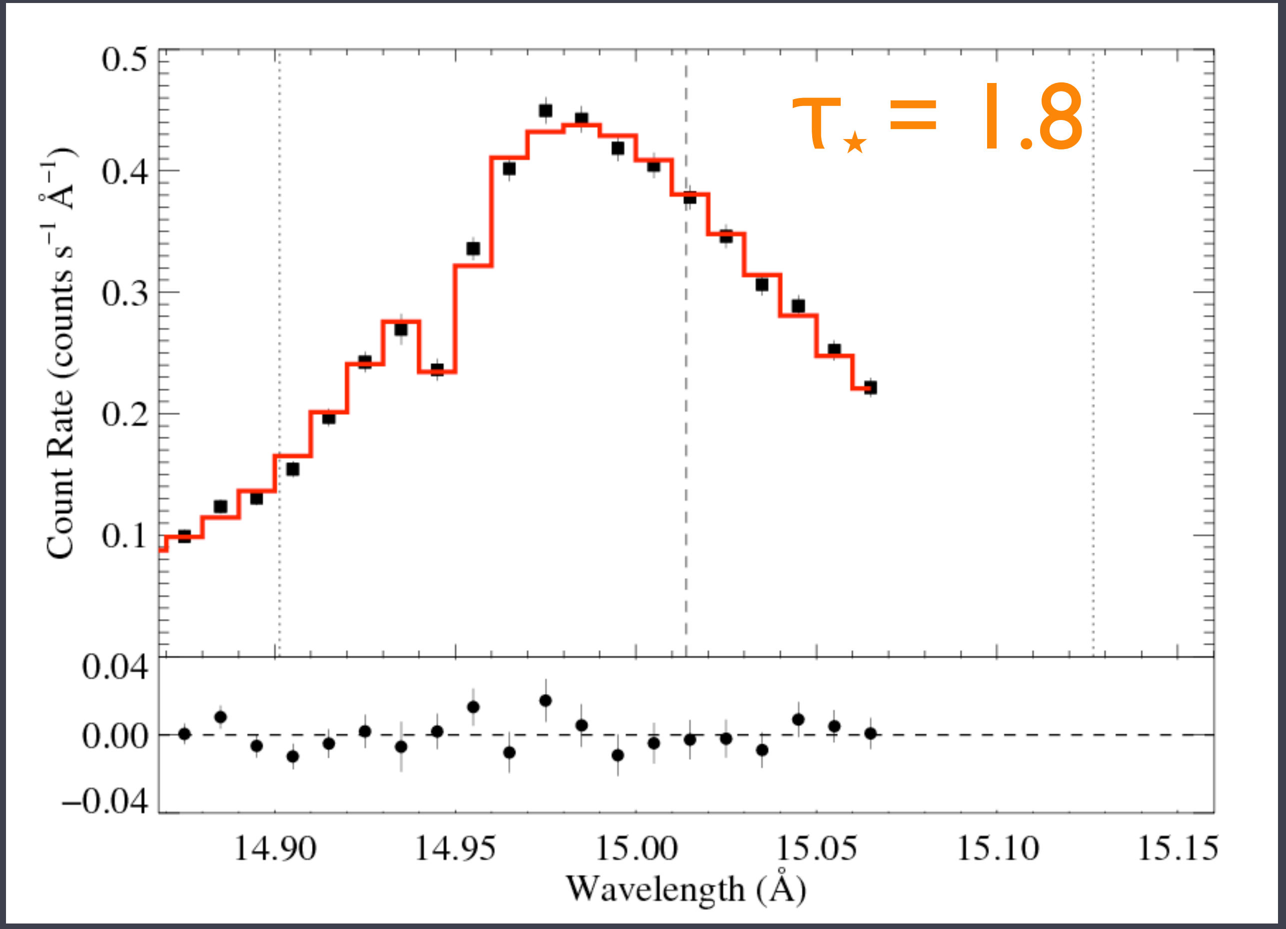

What about other spectral lines?

O VIII Lyα 18.969 Å

$h_\infty = 0$ $h_\infty = 5$

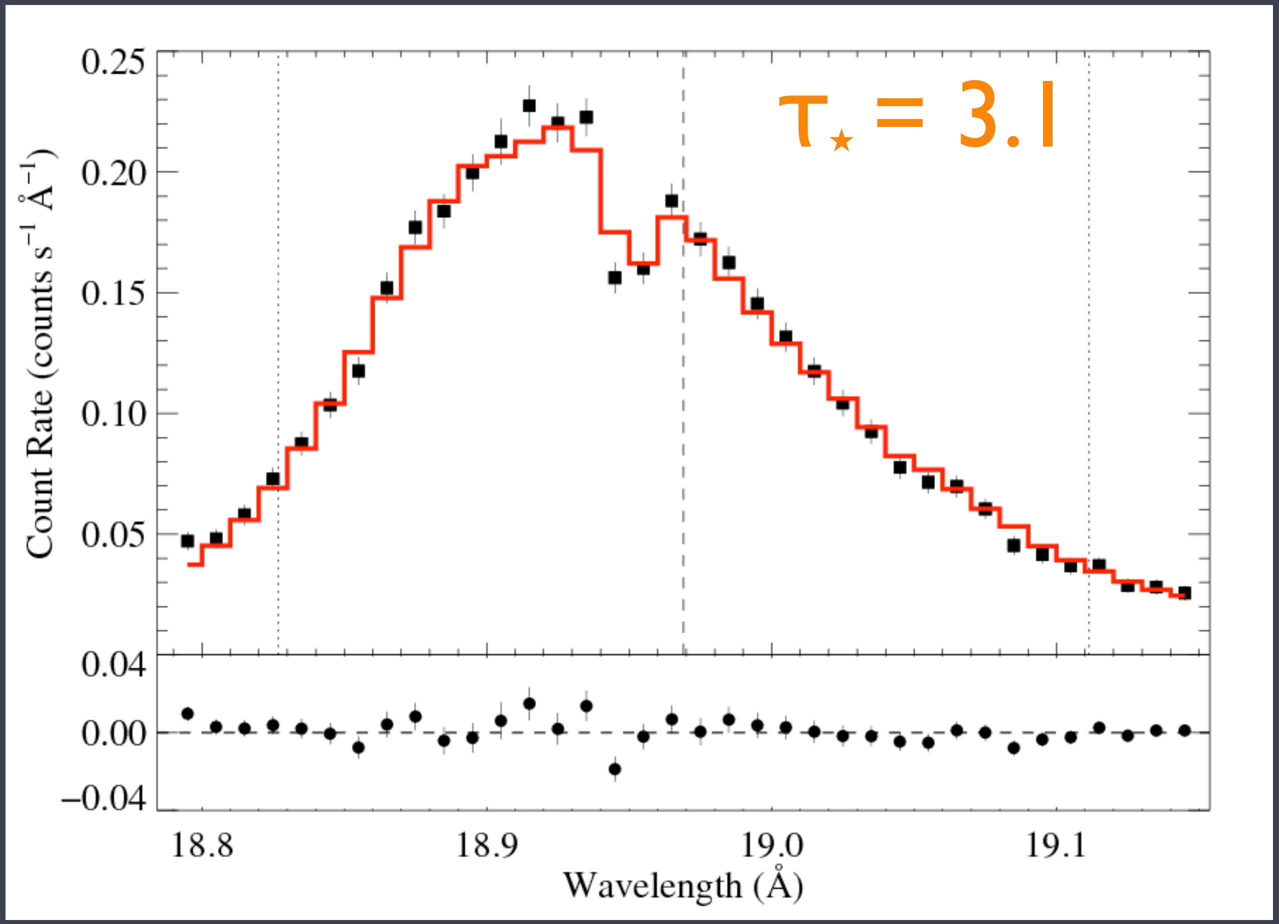

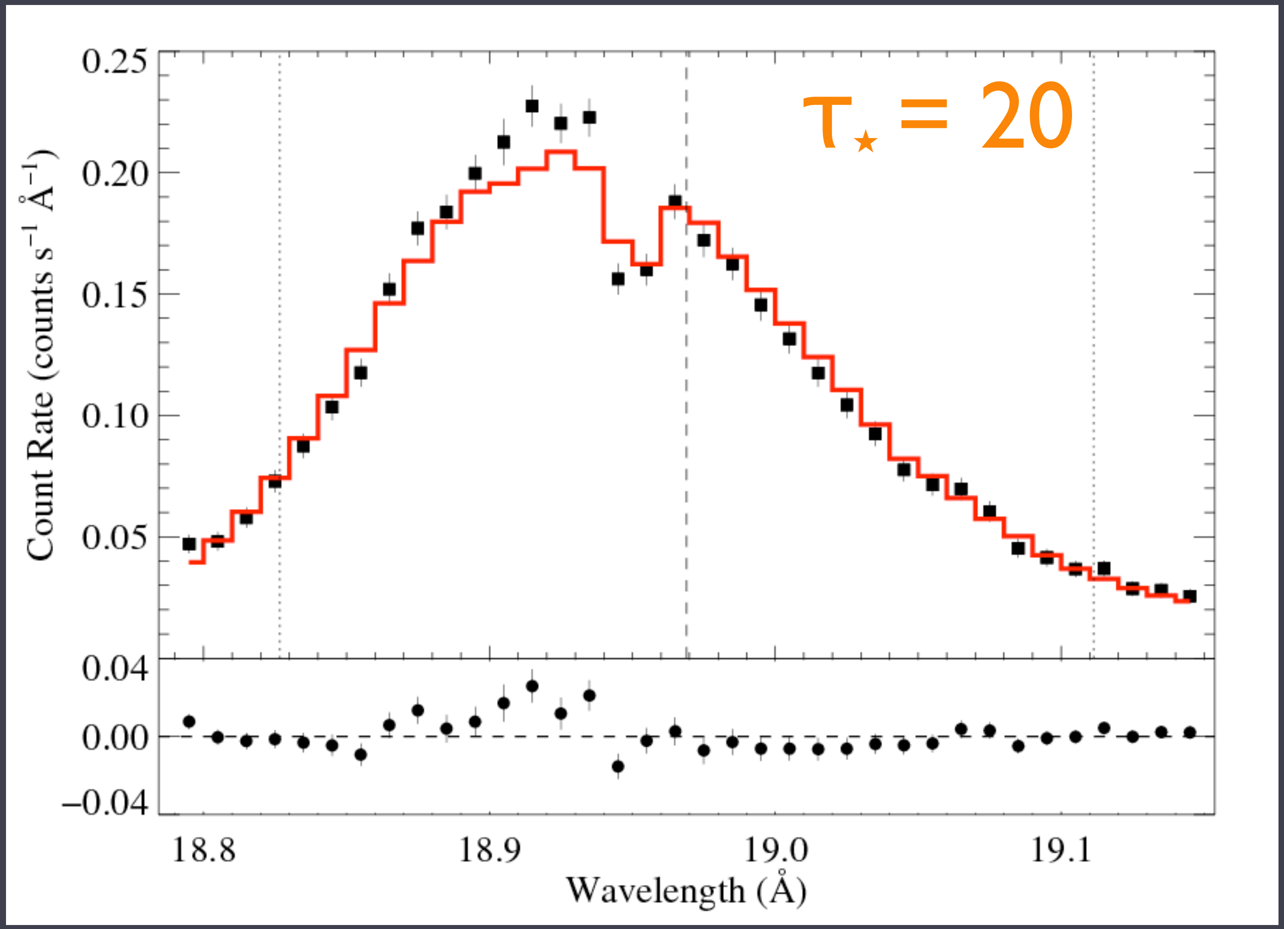

RGS: Confidence limits on h_∞ and $\tau_\star$

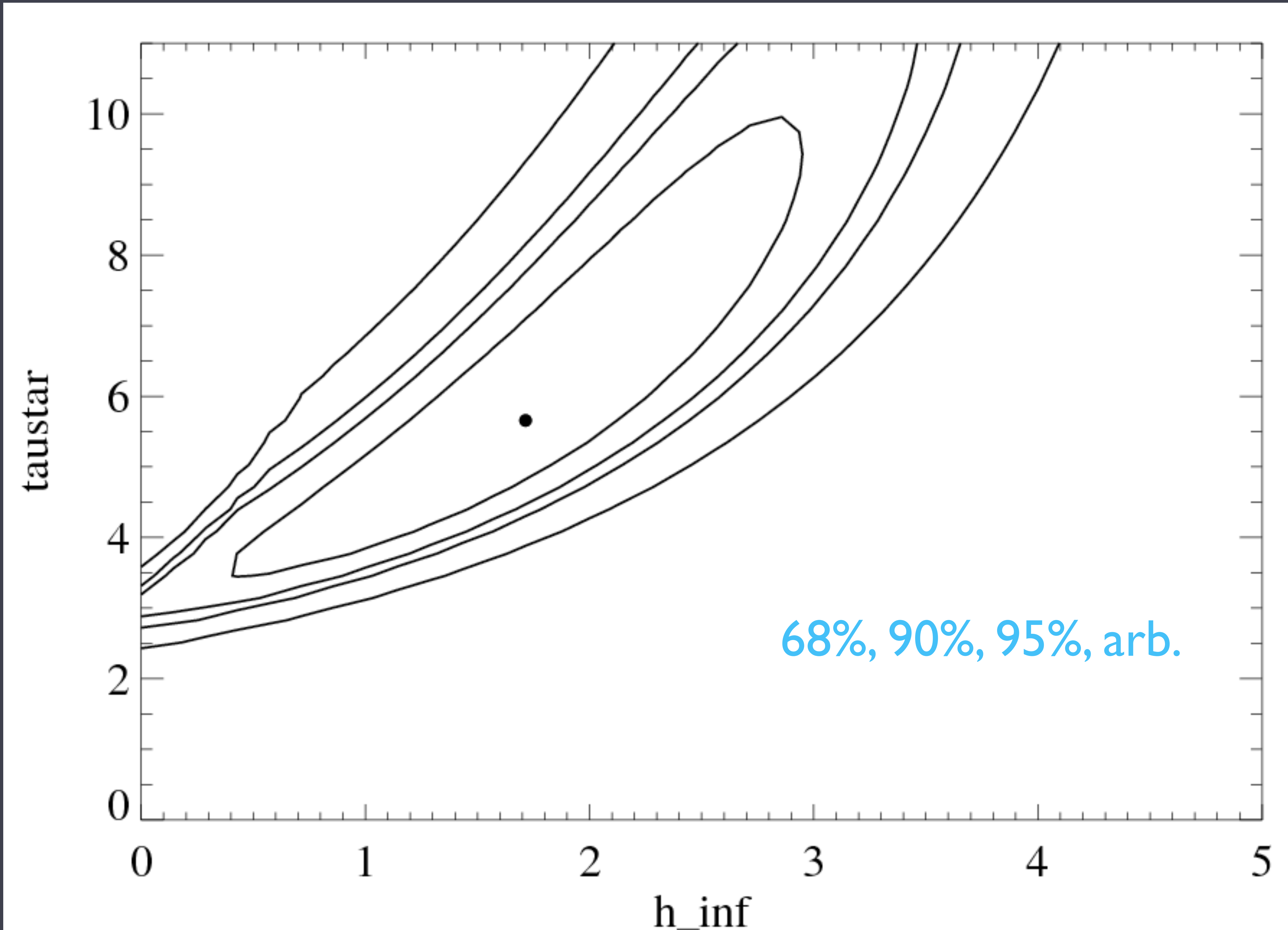

Chandra: Confidence limits on h_∞ and $\tau_\star$

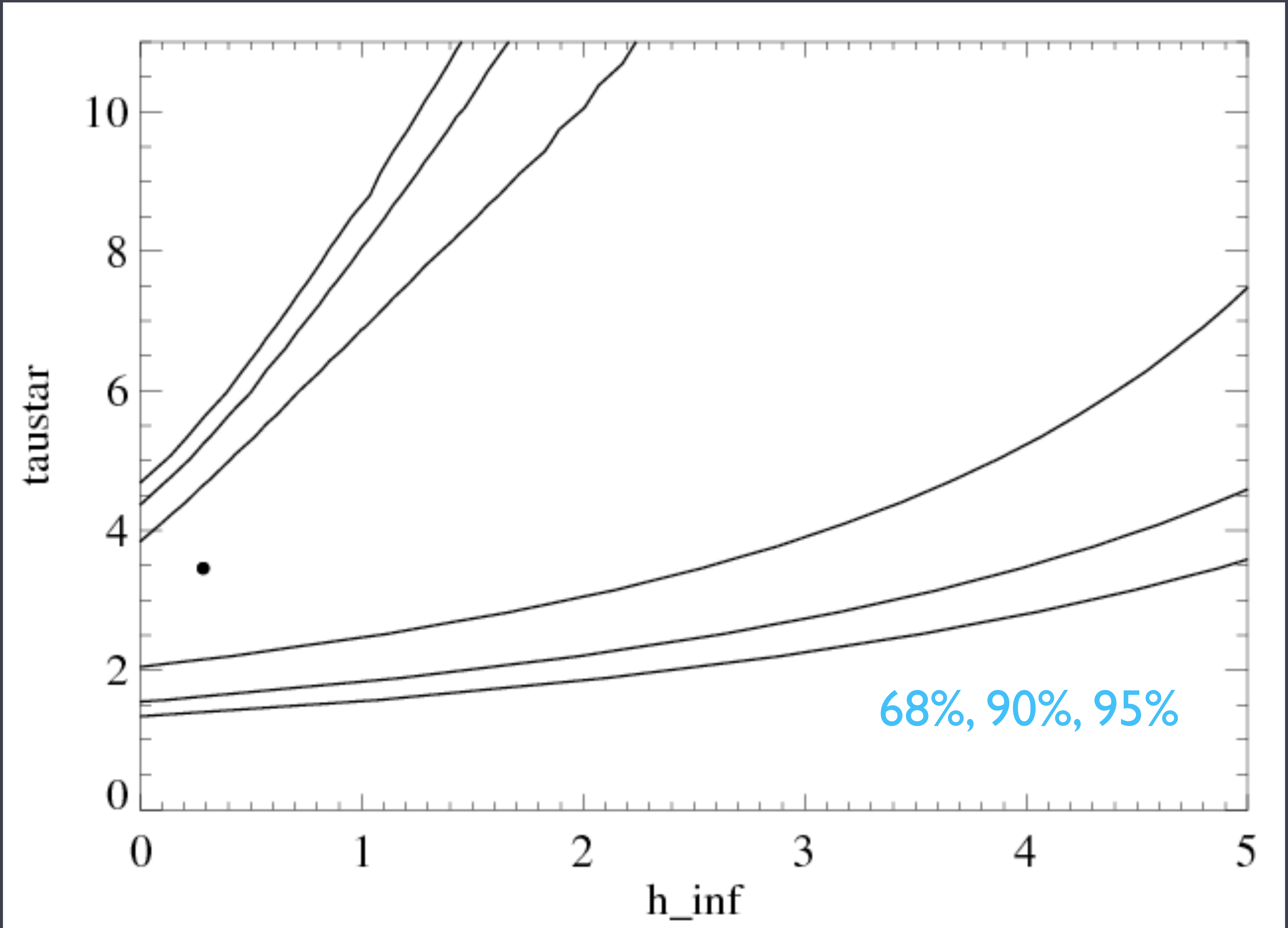

What about other spectral lines?

Ne X Lyα 12.134 Å : *XMM* RGS

$h_\infty = 0$ $h_\infty = 5$

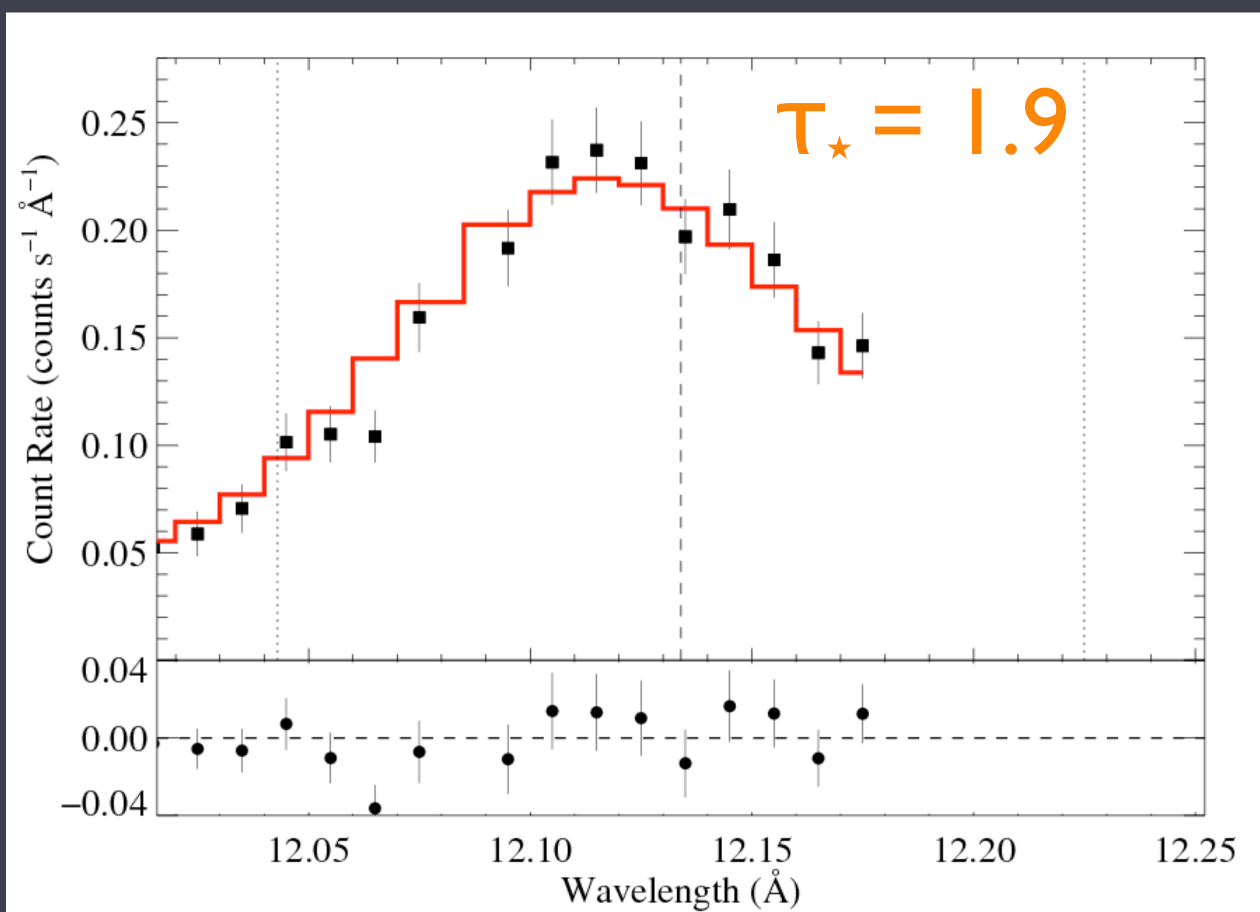

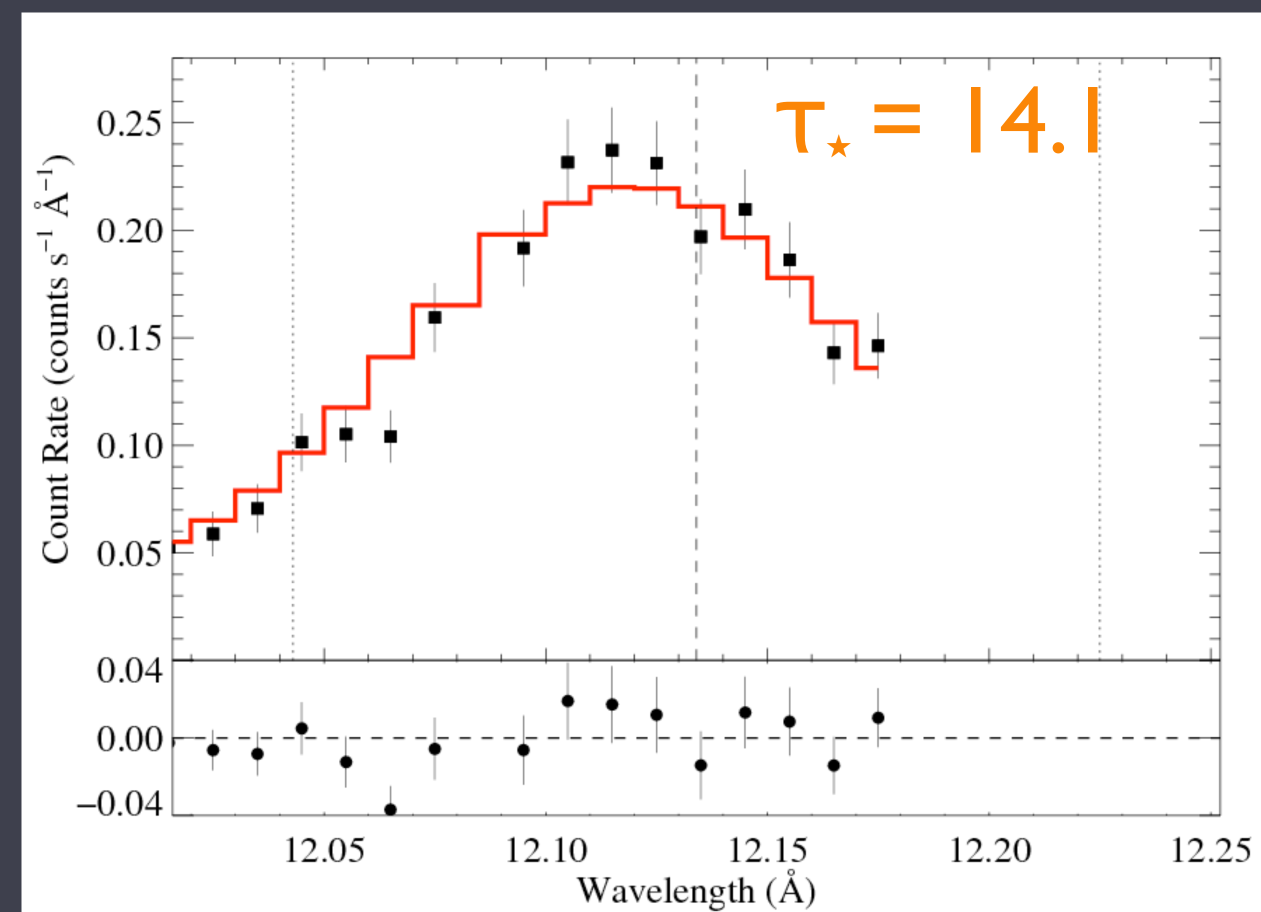

lower S/N, high porosity fit is only moderately disfavored

Conclusion 1

High porosity can be rejected

Conclusion 2

Moderate porosity ($h_\infty \leq 1$) increases $\tau_\star$ by only 20% to 30%

What about non-spherical clumps?

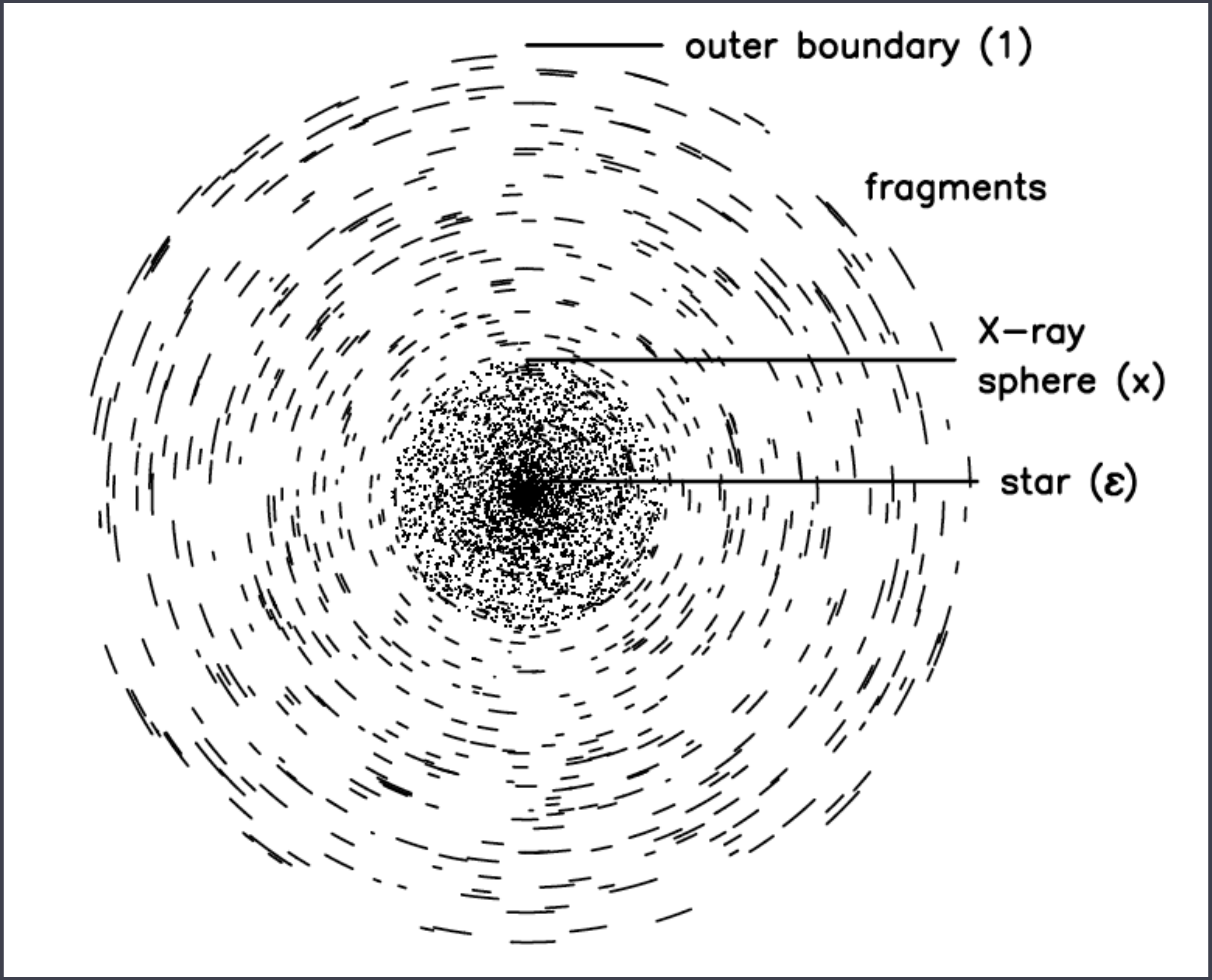

Feldmeier, Oskinova, & Hamann 2003

Flattened clumps (pancakes - shell fragments)

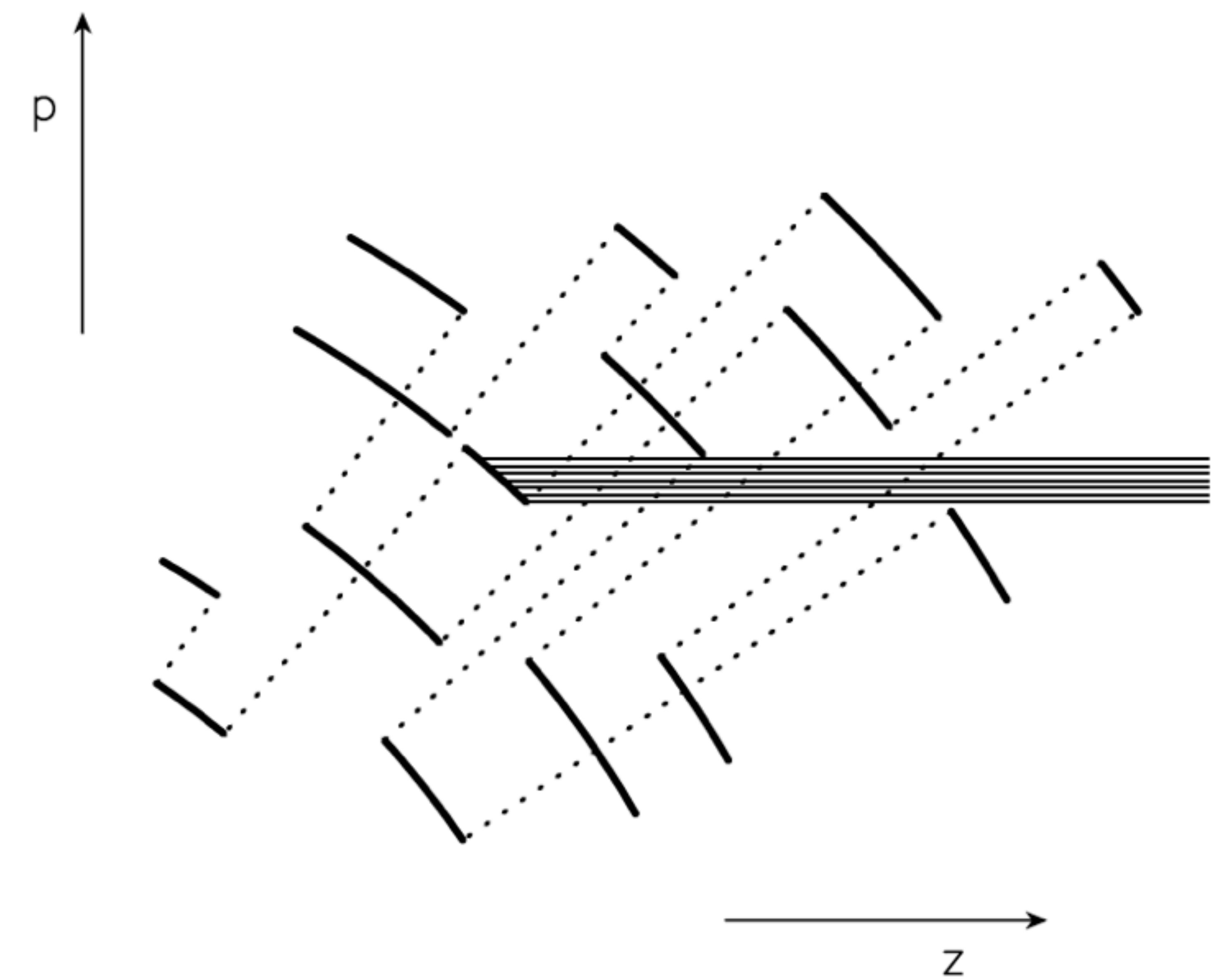

Fig. 2. Photon escape chanels for $N = 3$. The dotted lines indicate where dense shells got fragmented. The lines drawn parallel to the z axis indicate photon escape chanels towards the observer.

Flattened clumps: lateral escape is enhanced

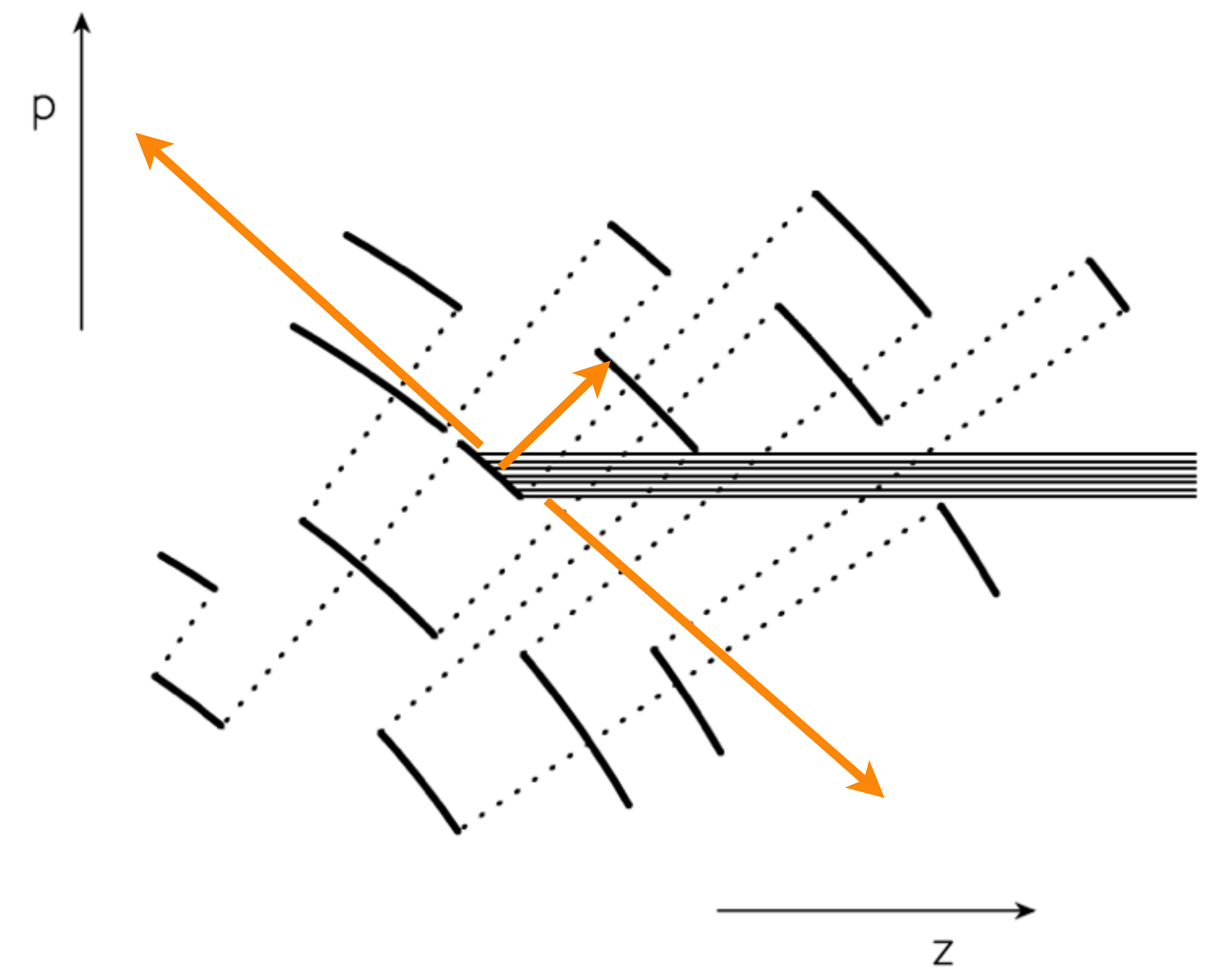

Fig. 2. Photon escape chanels for $N = 3$. The dotted lines indicate where dense shells got fragmented. The lines drawn parallel to the z axis indicate photon escape chanels towards the observer.

Radial fragments = *anisotropic* porosity

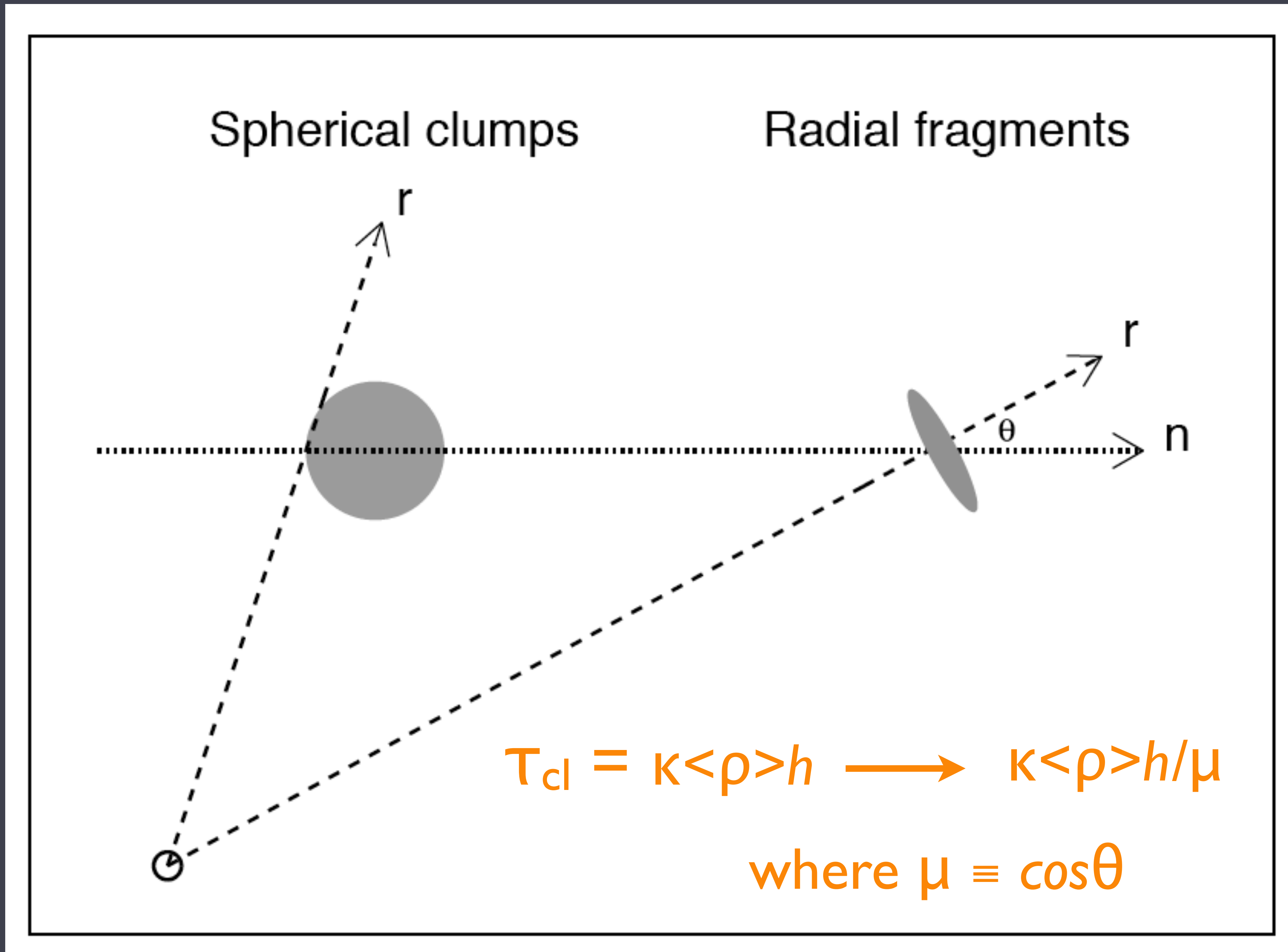

$$\tau_{cl} = \kappa \langle \rho \rangle h \longrightarrow \kappa \langle \rho \rangle h / \mu$$

where $\mu \equiv \cos\theta$

Radial fragments = *anisotropic* porosity

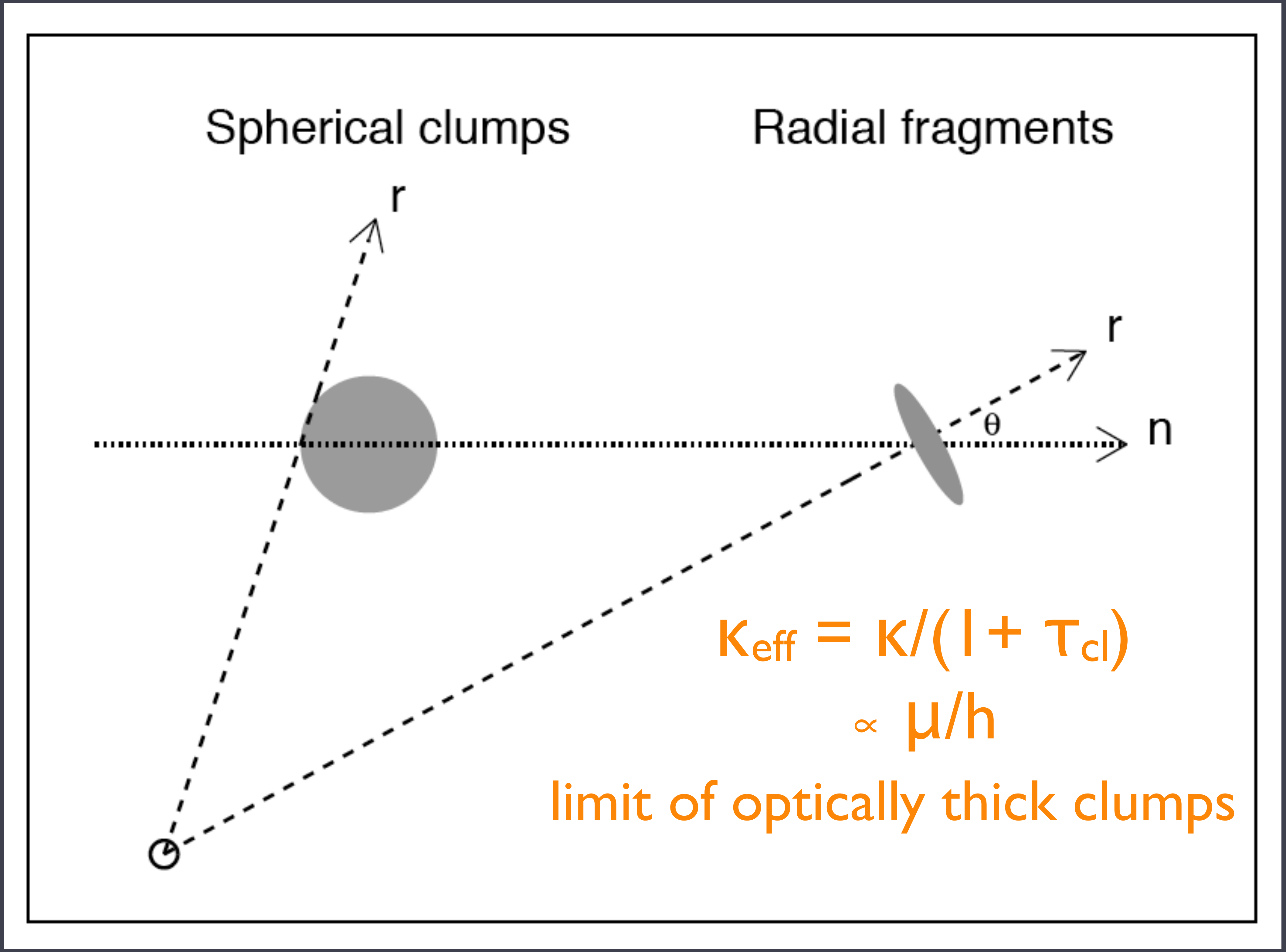

$$\kappa_{eff} = \kappa/(1+\tau_{cl})$$
$$\propto \mu/h$$

limit of optically thick clumps

The Venetian blind effect

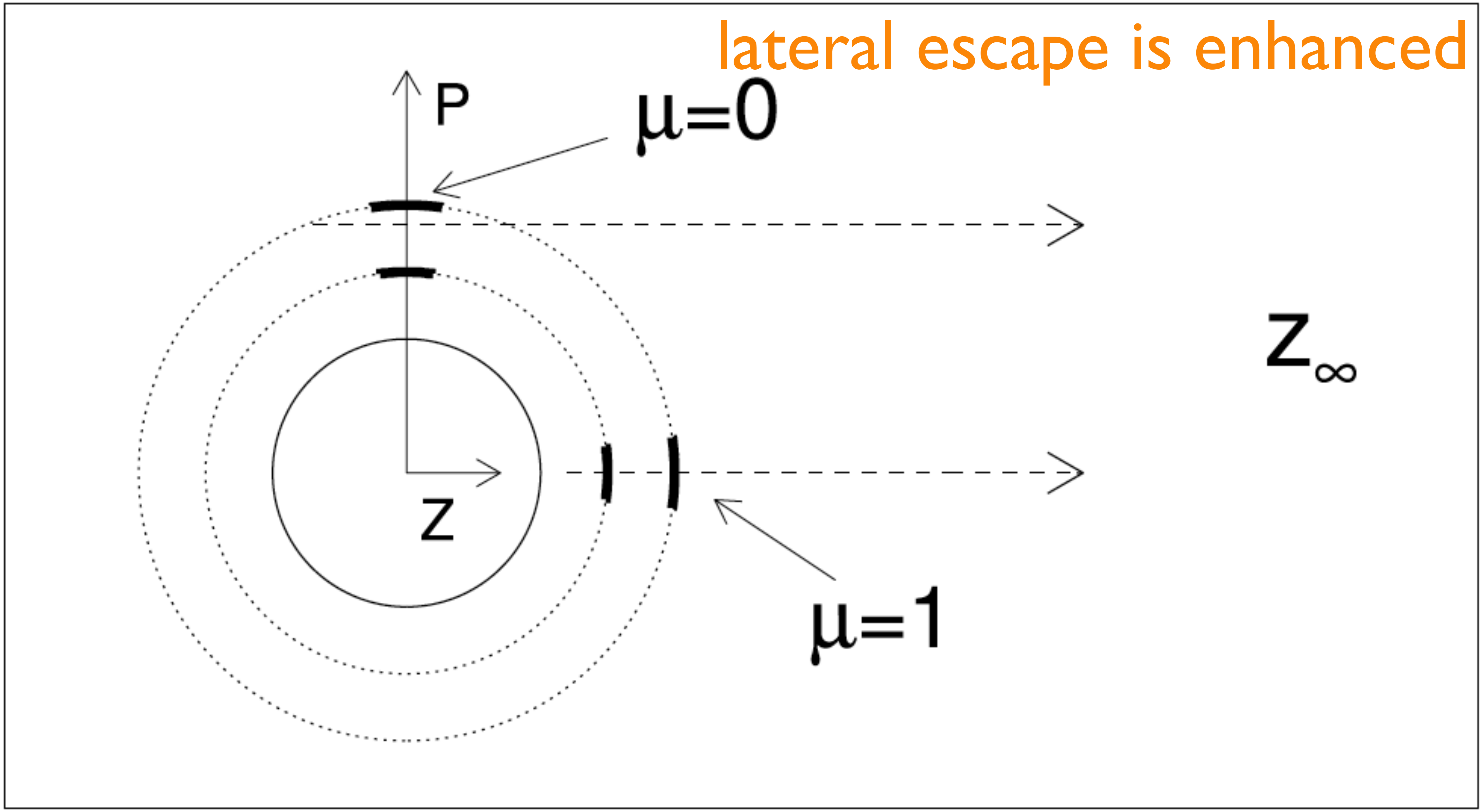

Figure 4. Illustration of the 'venetian blind' effect seen in porosity models using an anisotropic effective opacity. The dashed arrowed lines represent two different p-rays and the observer is assumed to be located at z_∞.

Visualizations of porous wind models

all clumps have $\ell = 0.1r$

$h_\infty = 4$

isotropic porosity

anisotropic porosity

open Venetian blinds

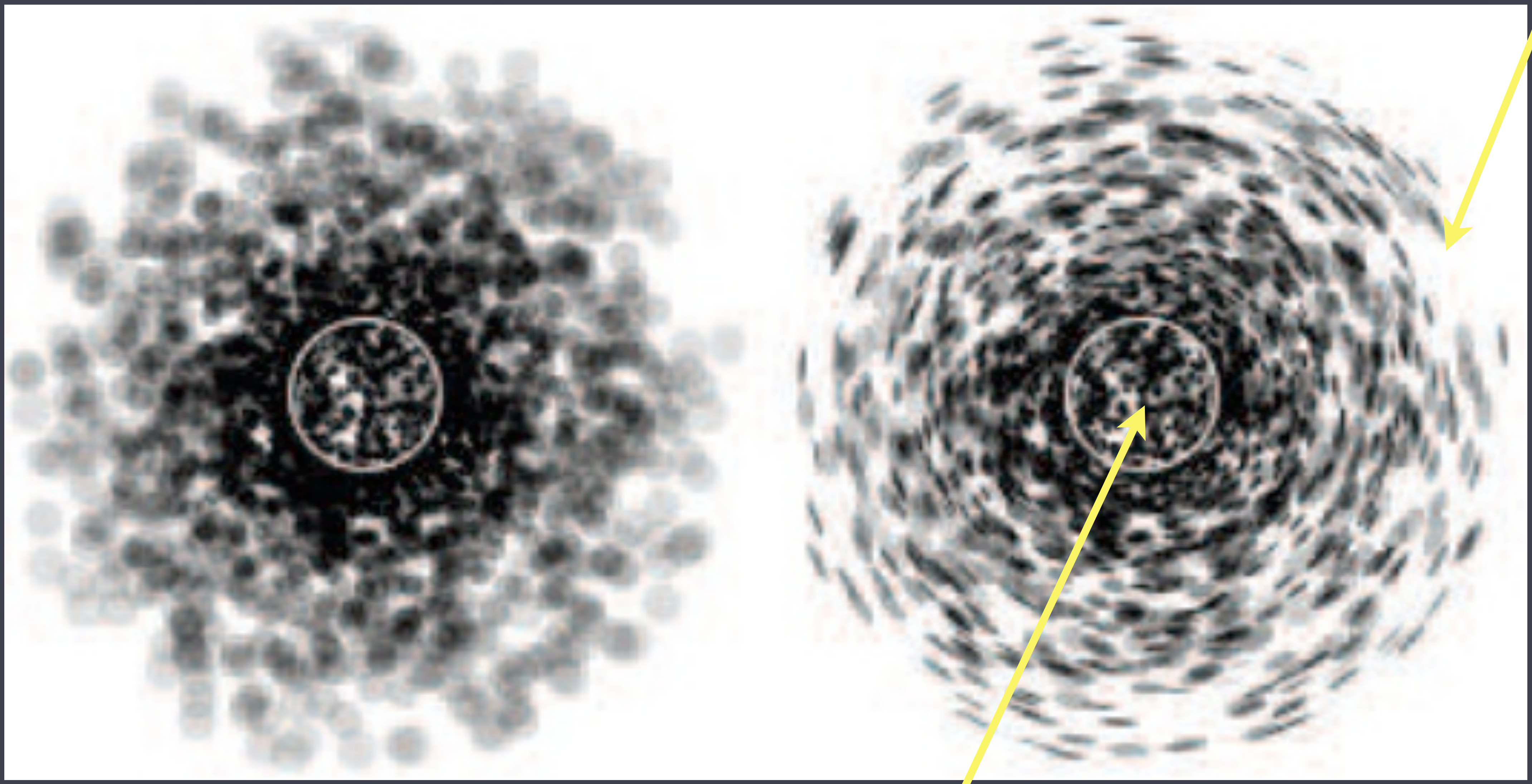

closed Venetian blinds

Visualizations of porous wind models

all clumps have $\ell = 0.1r$

isotropic porosity

$h_\infty = 0$ $h_\infty = 0.25$ $h_\infty = 0.5$ $h_\infty = 1$ $h_\infty = 2$ $h_\infty = 4$ $h_\infty = 8$

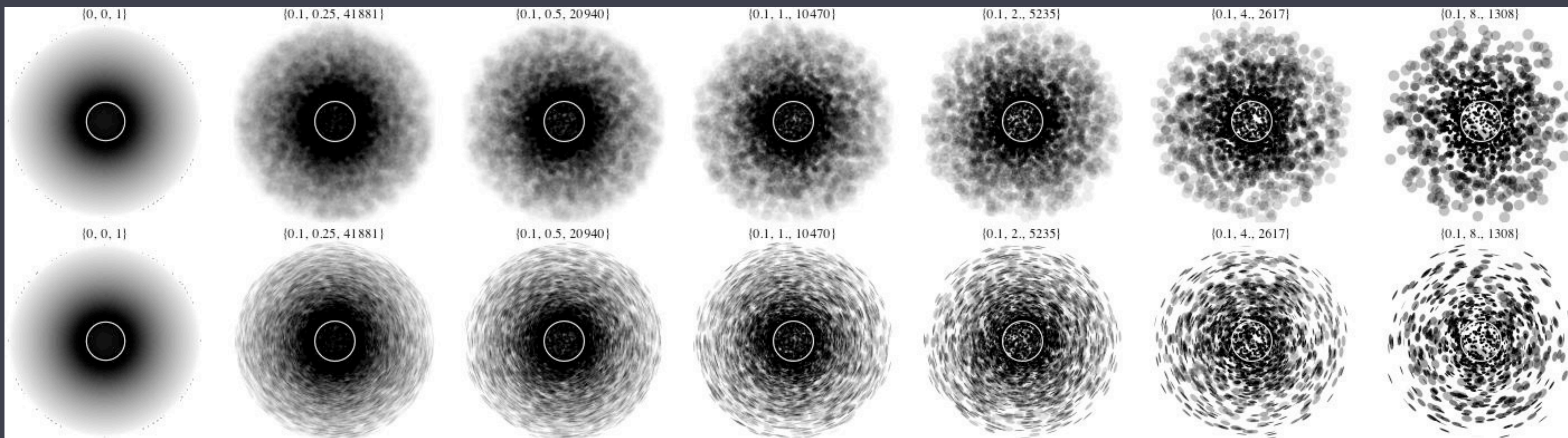

anisotropic porosity

Venetian blind *bump*

lateral escape is enhanced

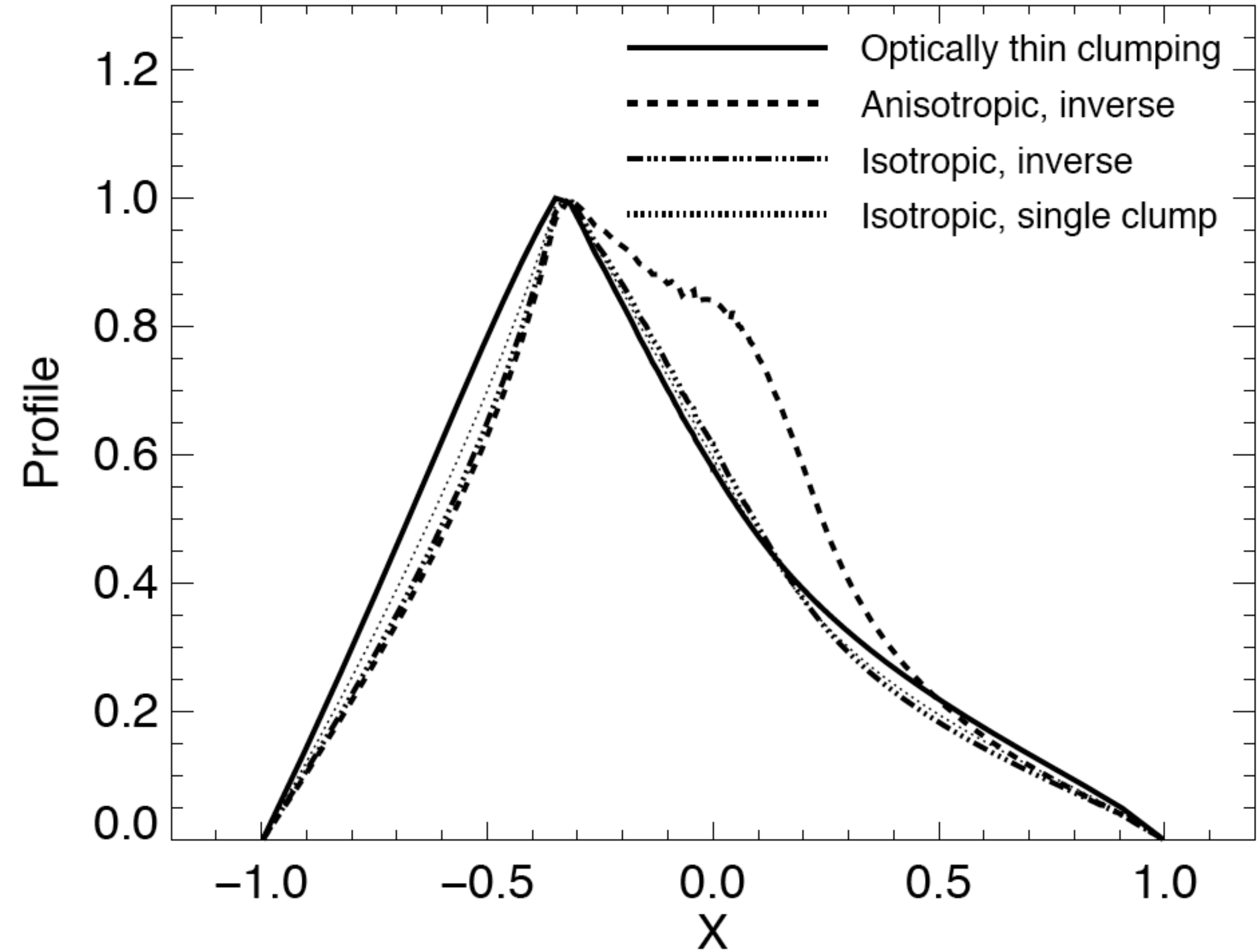

Figure 5. Line profiles for $h_\infty/R_\star = 1.0$ and $\tau_\star = 2.5$, using different effective opacity laws, as labelled.

Venetian blind *bump*

lateral escape is enhanced

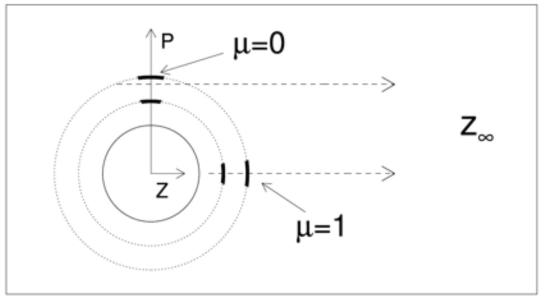

Figure 4. Illustration of the 'venetian blind' effect seen in porosity models using an anisotropic effective opacity. The dashed arrowed lines represent two different p-rays and the observer is assumed to be located at z_∞.

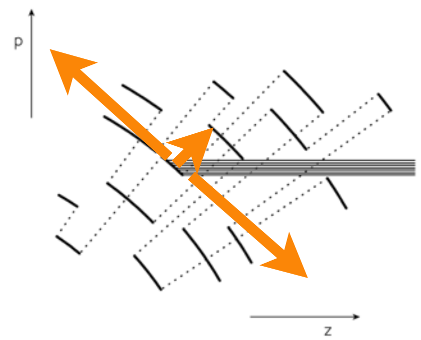

Fig. 2. Photon escape chanels for $N = 3$. The dotted lines indicate where dense shells got fragmented. The lines drawn parallel to the z axis indicate photon escape chanels towards the observer.

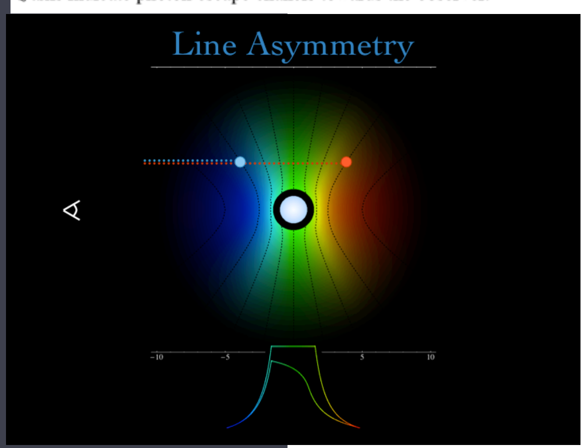

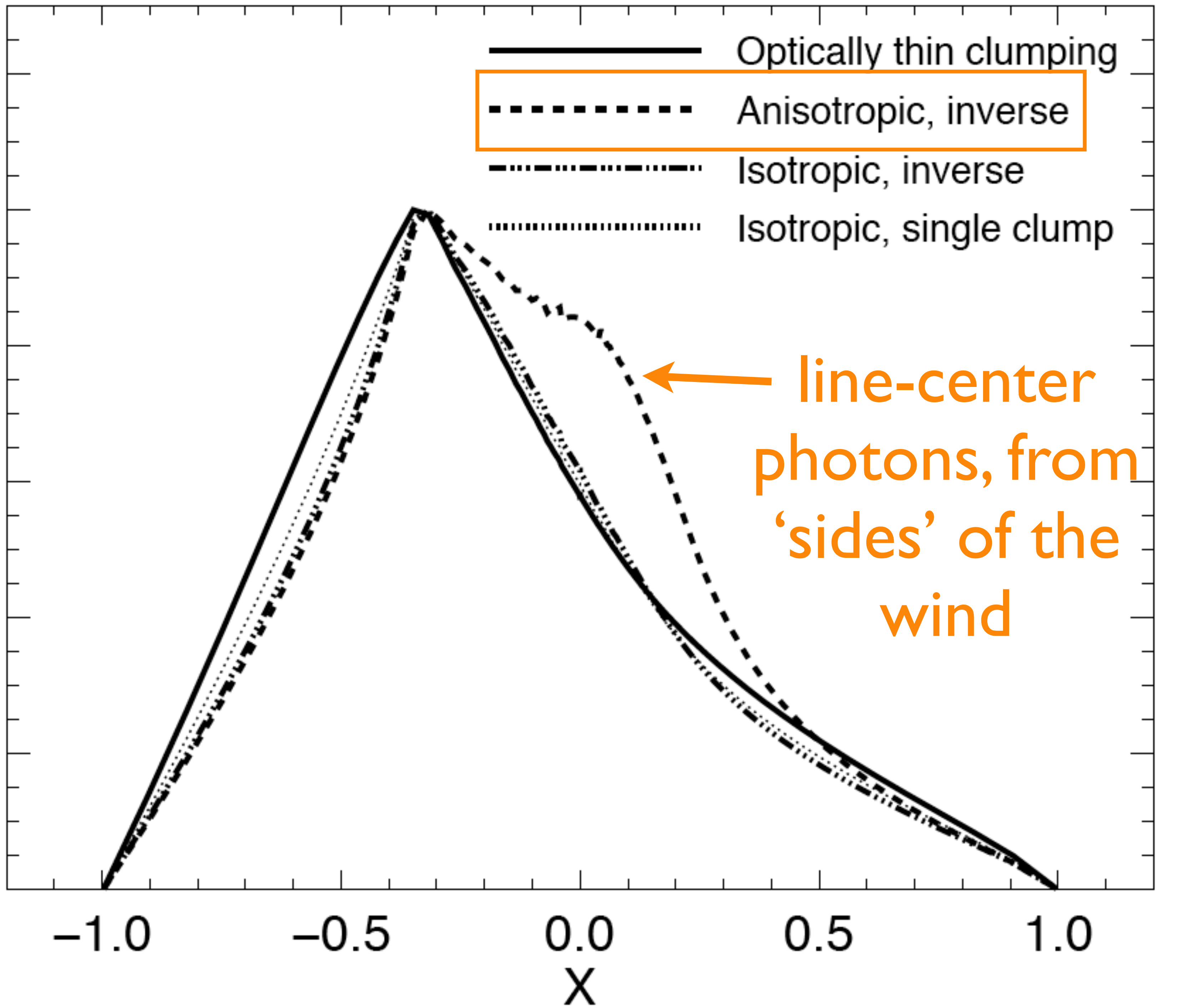

Figure 5. Line profiles for $h_\infty/R_\star = 1.0$ and $\tau_\star = 2.5$, using different effective opacity laws, as labelled.

ζ Pup: Chandra

$h_\infty = 5$

Fe XVII 15.014 Å

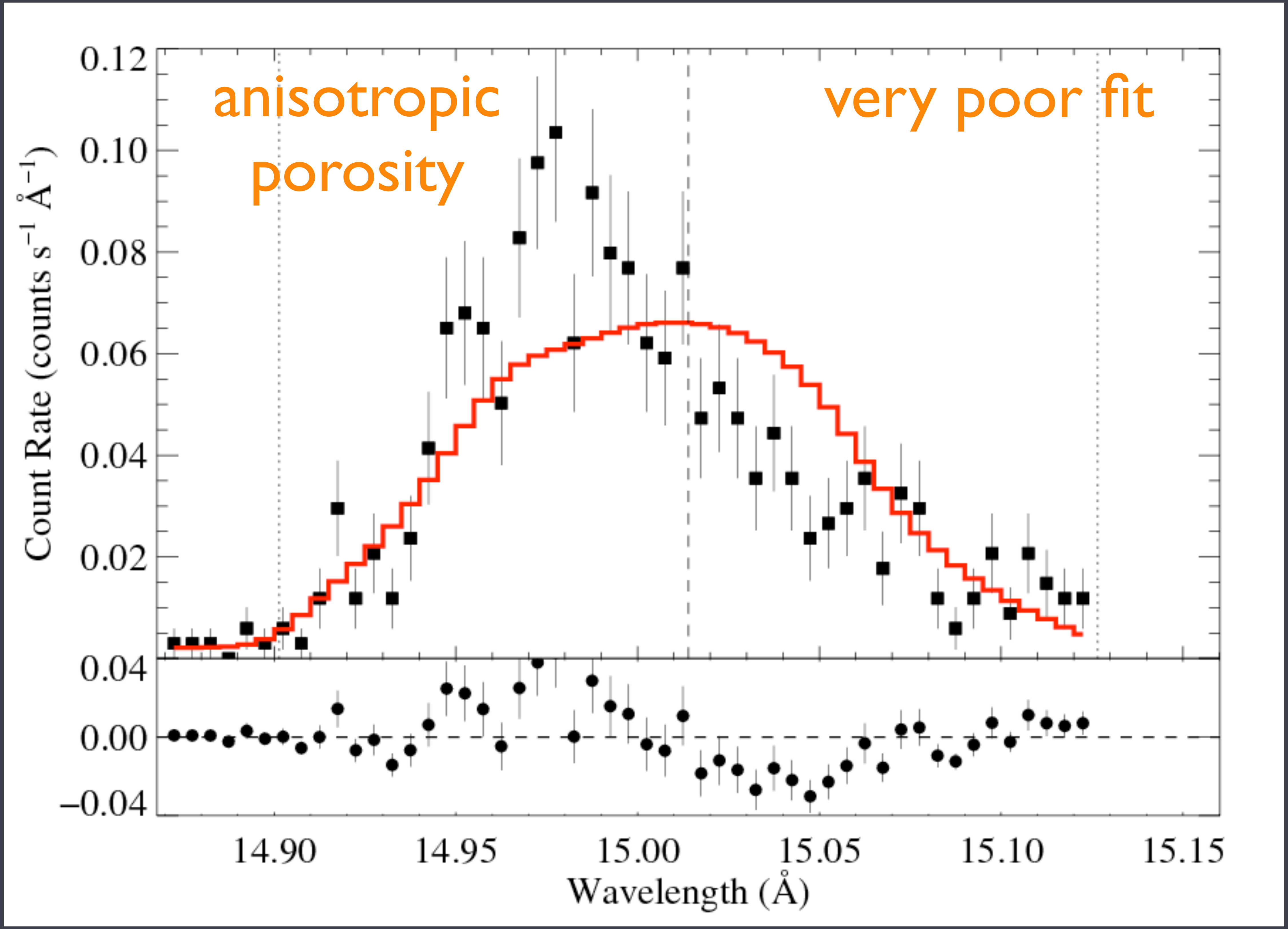

ζ Pup: Chandra

$h_\infty = 5$

Fe XVII 15.014 Å

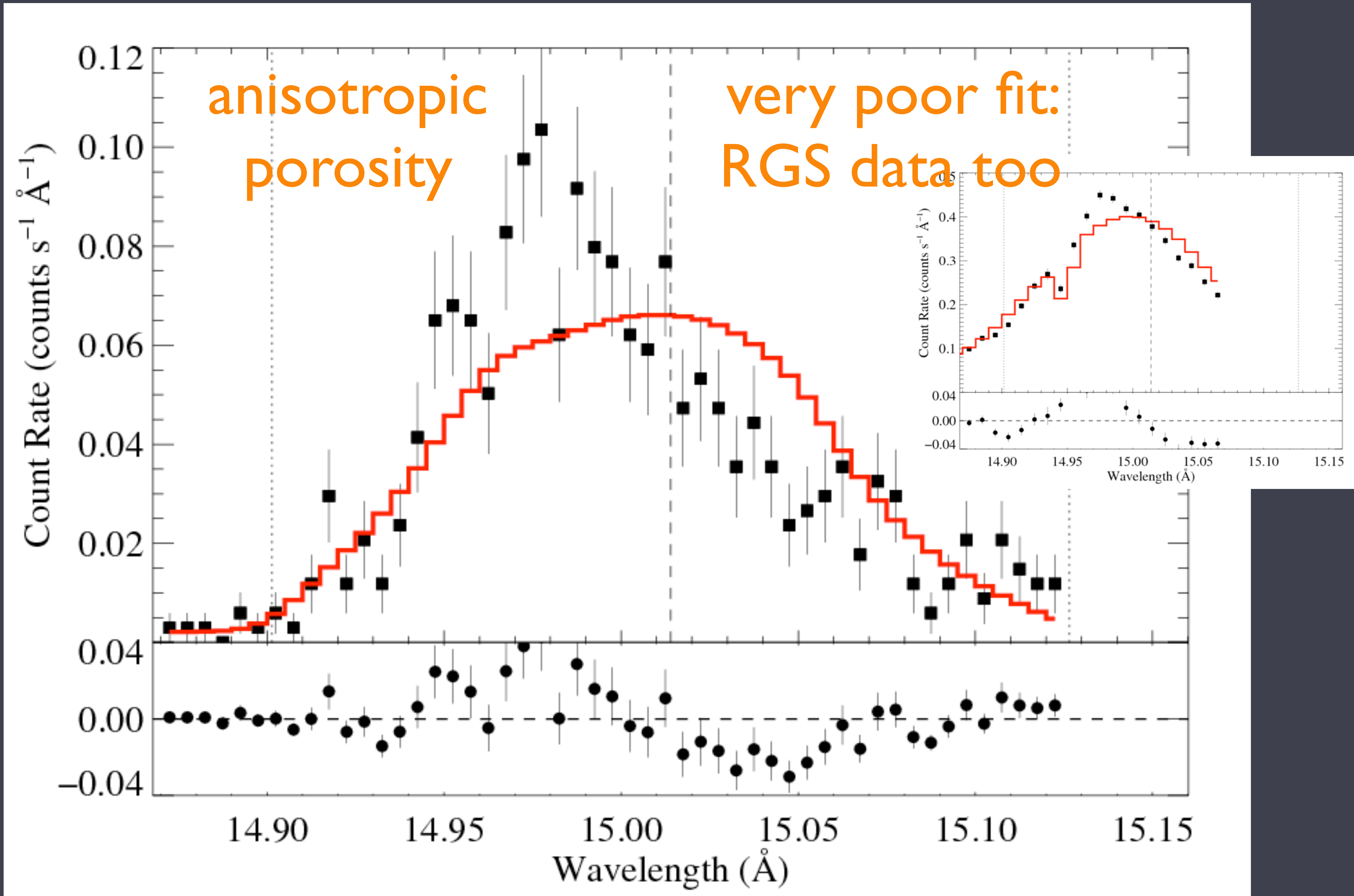

ζ Pup: Chandra $h_\infty = 0.5$ Fe XVII 15.014 Å

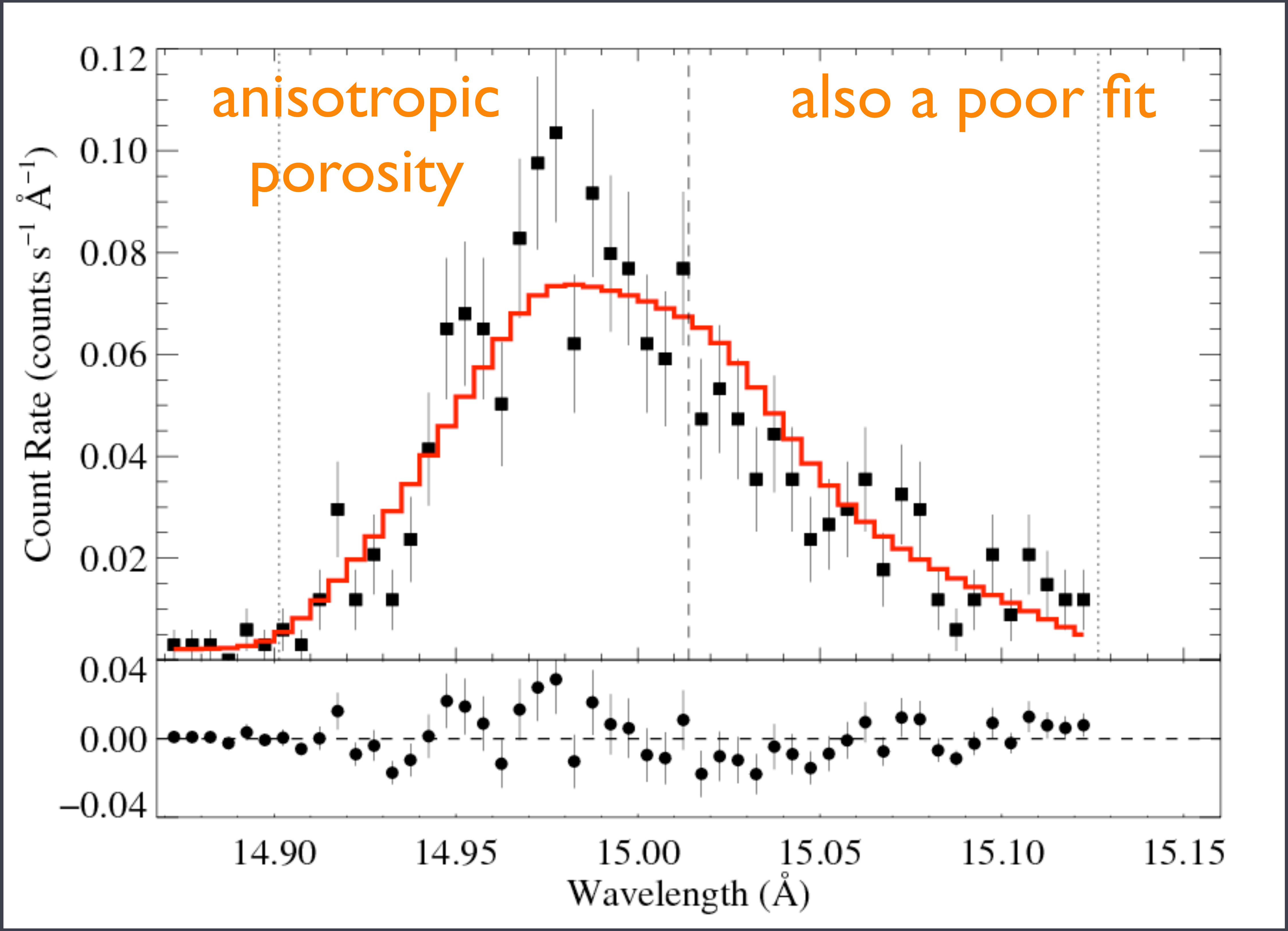

Conclusion 3

Even modest *anisotropic* porosity can be rejected

Global Conclusion

Porosity is *not* important in hot star winds

1. High porosity can be rejected

2. Moderate porosity ($h_\infty \leq 1$) increases $\tau_\star$ by only 20% to 30%

3. Even modest *anisotropic* porosity can be rejected

Theory context: perhaps this is not surprising

1-D numerical simulations

reasons why 1-D simulations overestimate porosity

- geometry: all "clumps" are spherical shells
- inner wind has $h \ll h_\infty$
- grid resolution

clumps

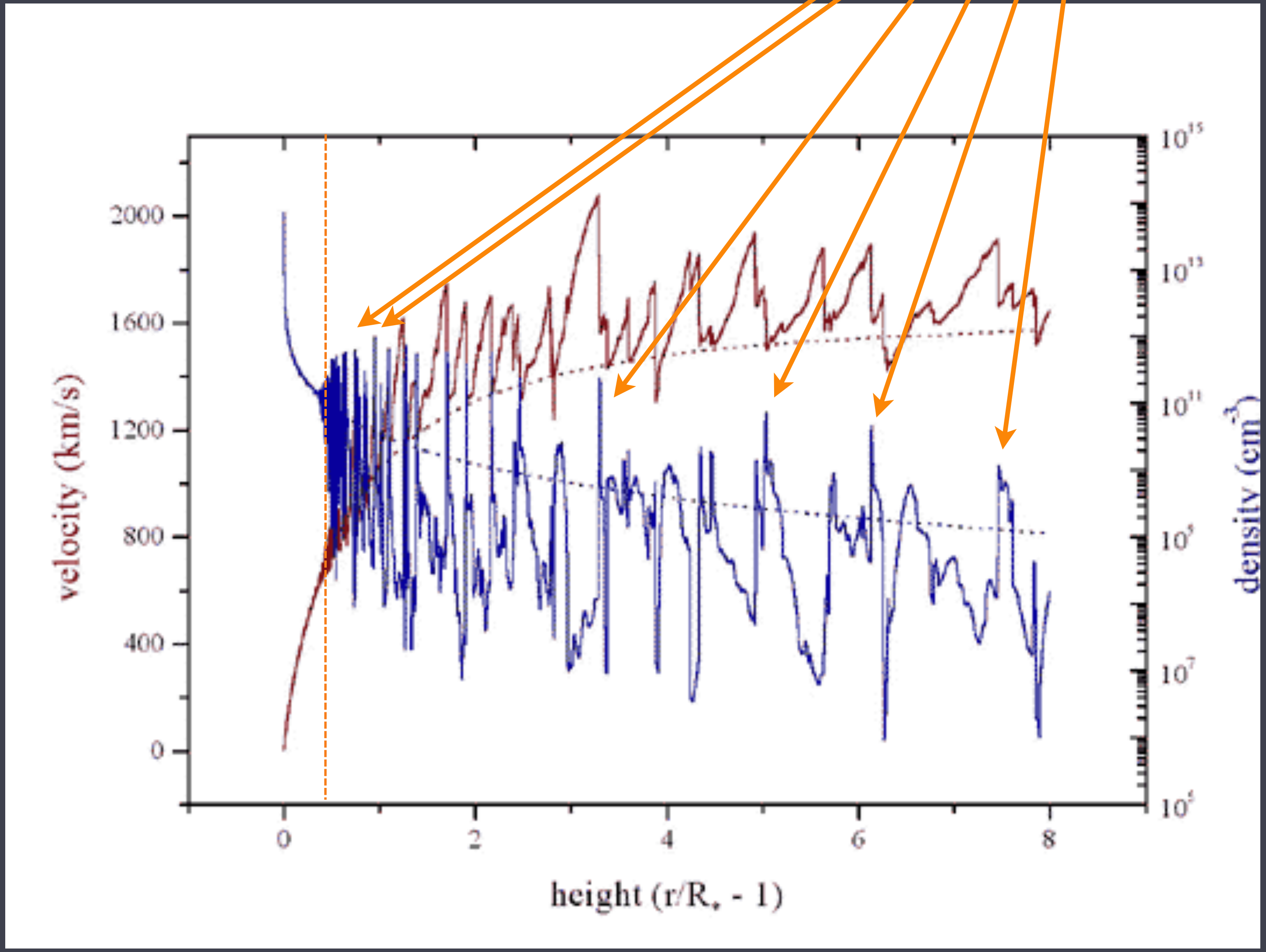

More realistic 2-D simulations: R-T like break-up; structure on quite *small scales*

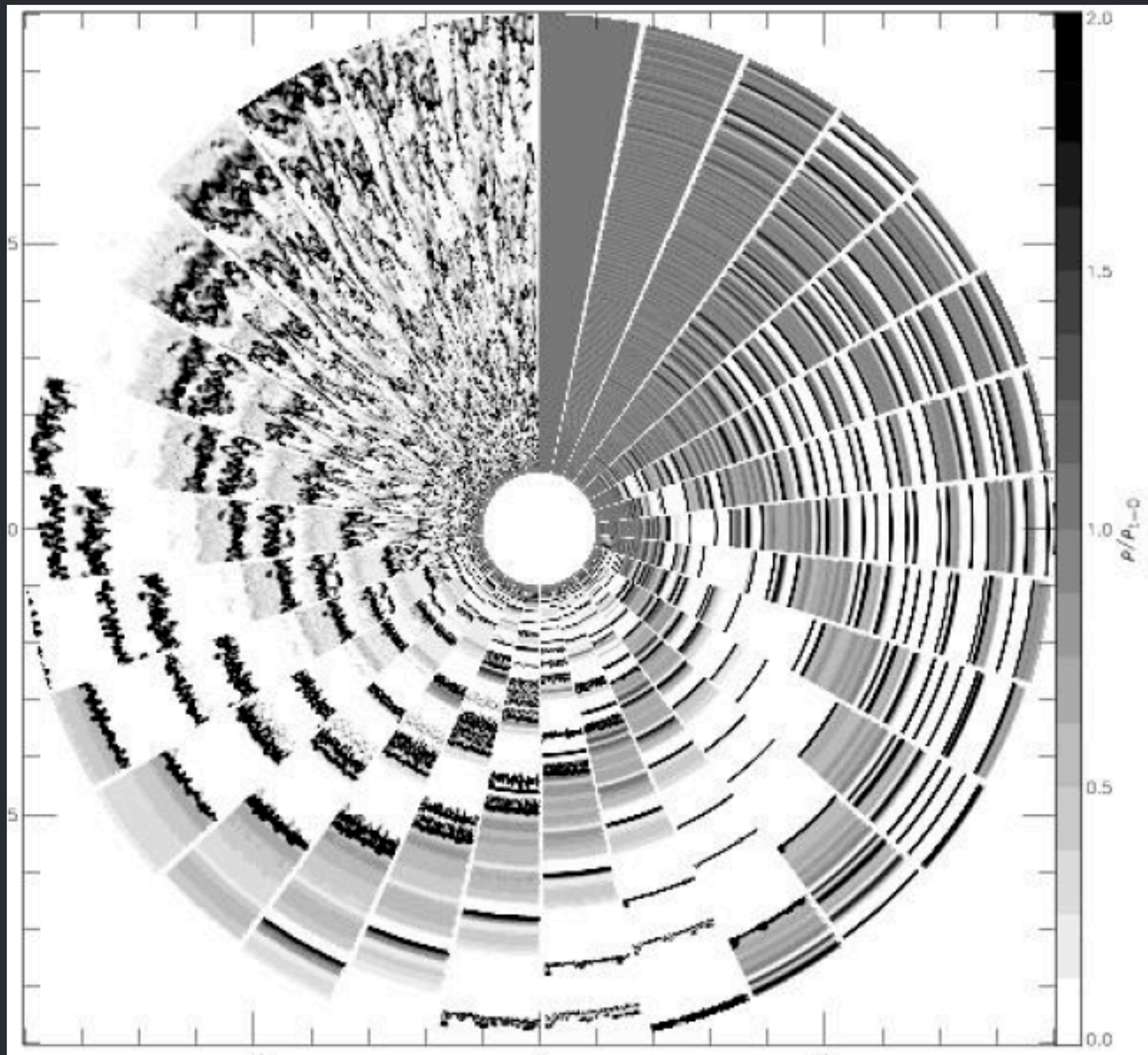

Dessart & Owocki 2005

In some cases, structure approaches the grid scale: clumps are very small; not optically thick

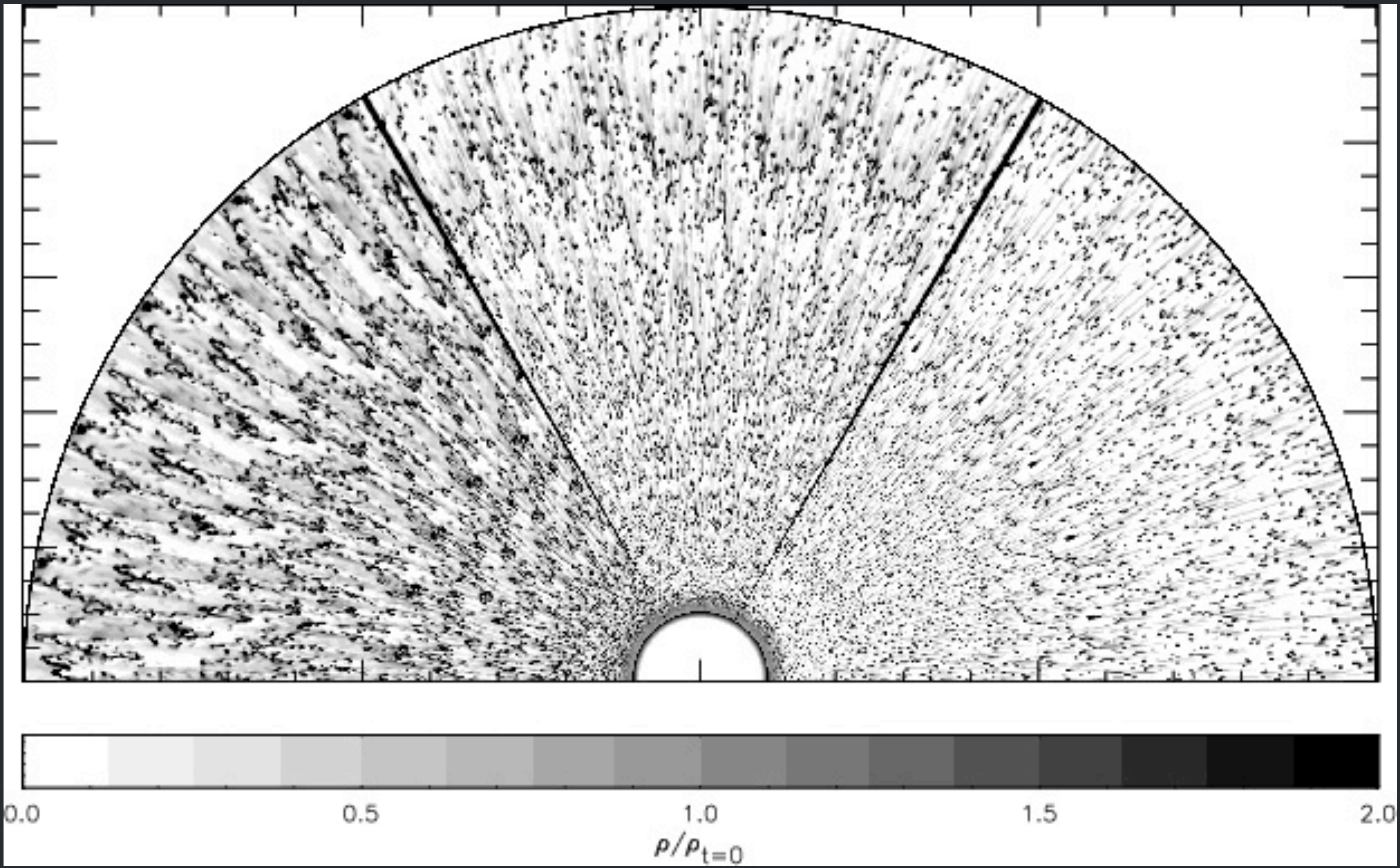

Dessart & Owocki 2003, *A&A*, 406, L1

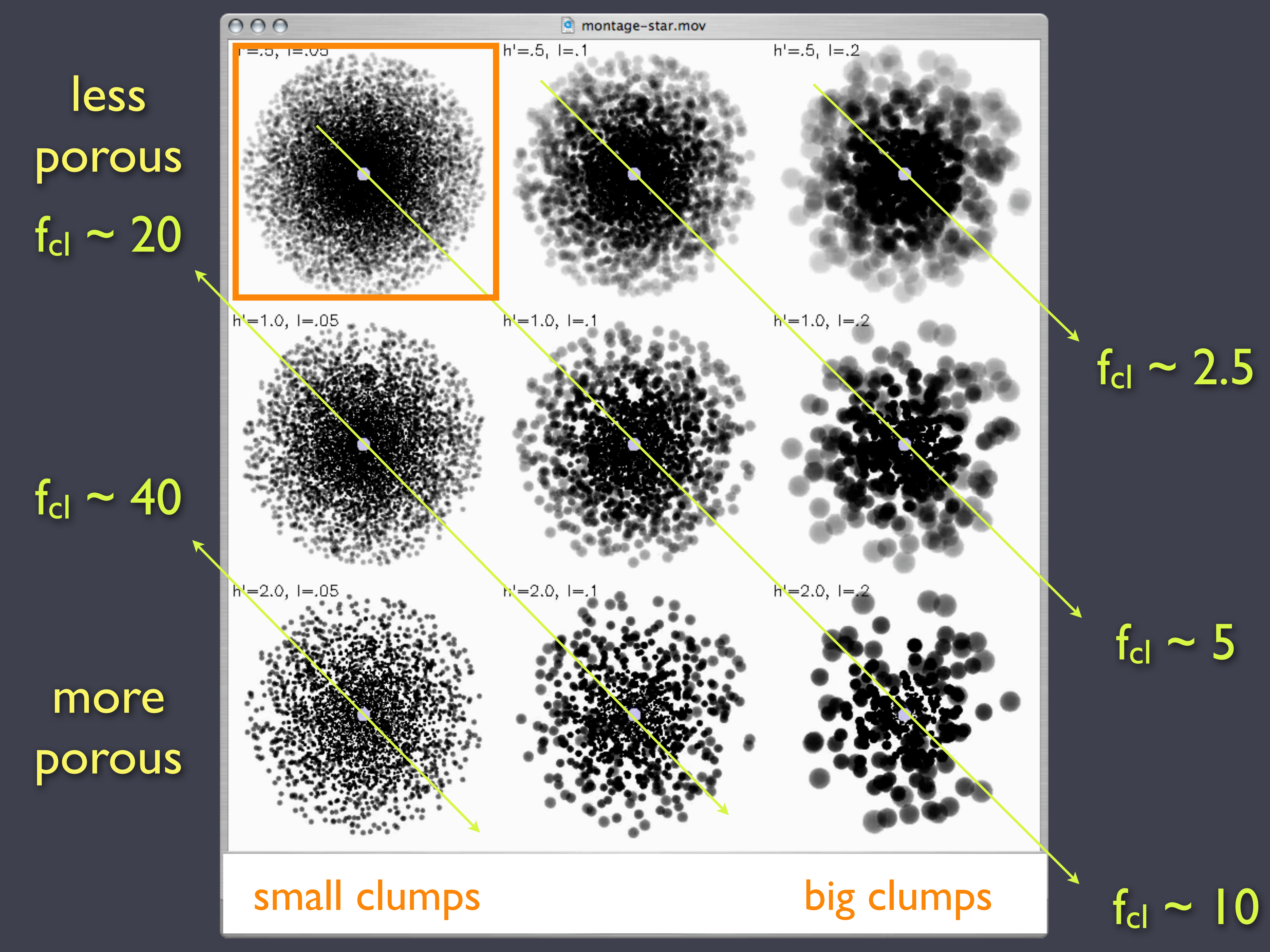

less porous
$f_{cl} \sim 20$
$f_{cl} \sim 40$
more porous
montage-star.mov
h'=.5, l=.1
h'=.5, l=.2
h'=1.0, l=.05
h'=1.0, l=.1
h'=1.0, l=.2
h'=2.0, l=.05
h'=2.0, l=.1
h'=2.0, l=.2
small clumps
big clumps
$f_{cl} \sim 2.5$
$f_{cl} \sim 5$
$f_{cl} \sim 10$

So, clumping *without* porosity.

What observational constraints?

X-ray line profiles to measure the clumping factor and the mass-loss rate

basic definition: $f_{cl} \equiv \langle\rho^2\rangle/\langle\rho\rangle^2$

from density-squared diagnostic like Hα

from (column) density diagnostic like $\tau_\star$ from X-ray profiles

ζ Pup *Chandra*: three emission lines

Mg Lyα: 8.42 Å | Ne Lyα: 12.13 Å | O Lyα: 18.97 Å

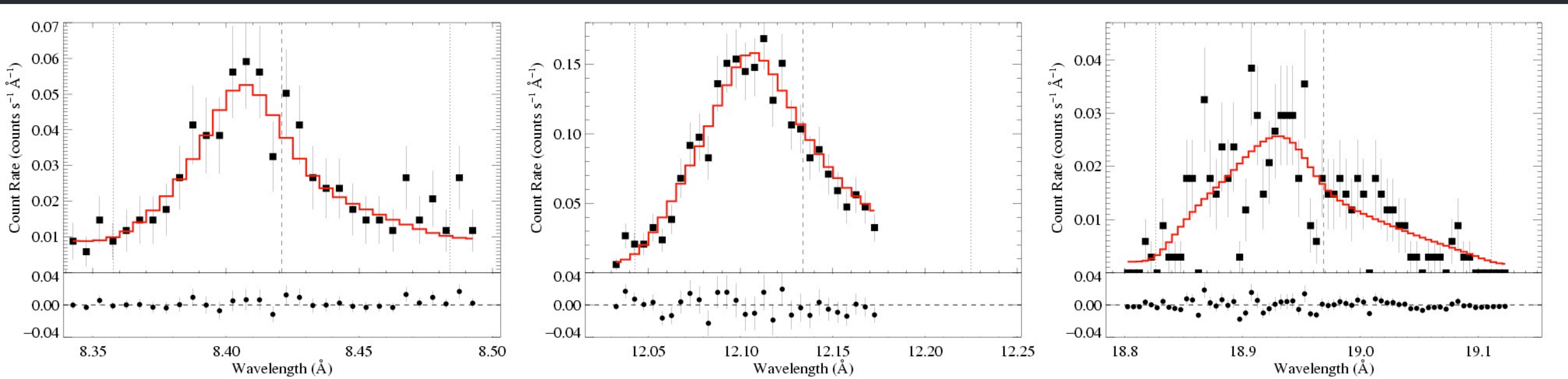

$\tau_* = 1$ | $\tau_* = 2$ | $\tau_* = 3$

Recall:

$$\tau_* \equiv \frac{\kappa \dot{M}}{4\pi R_* v_\infty}$$

Results from the 3 line fits shown previously

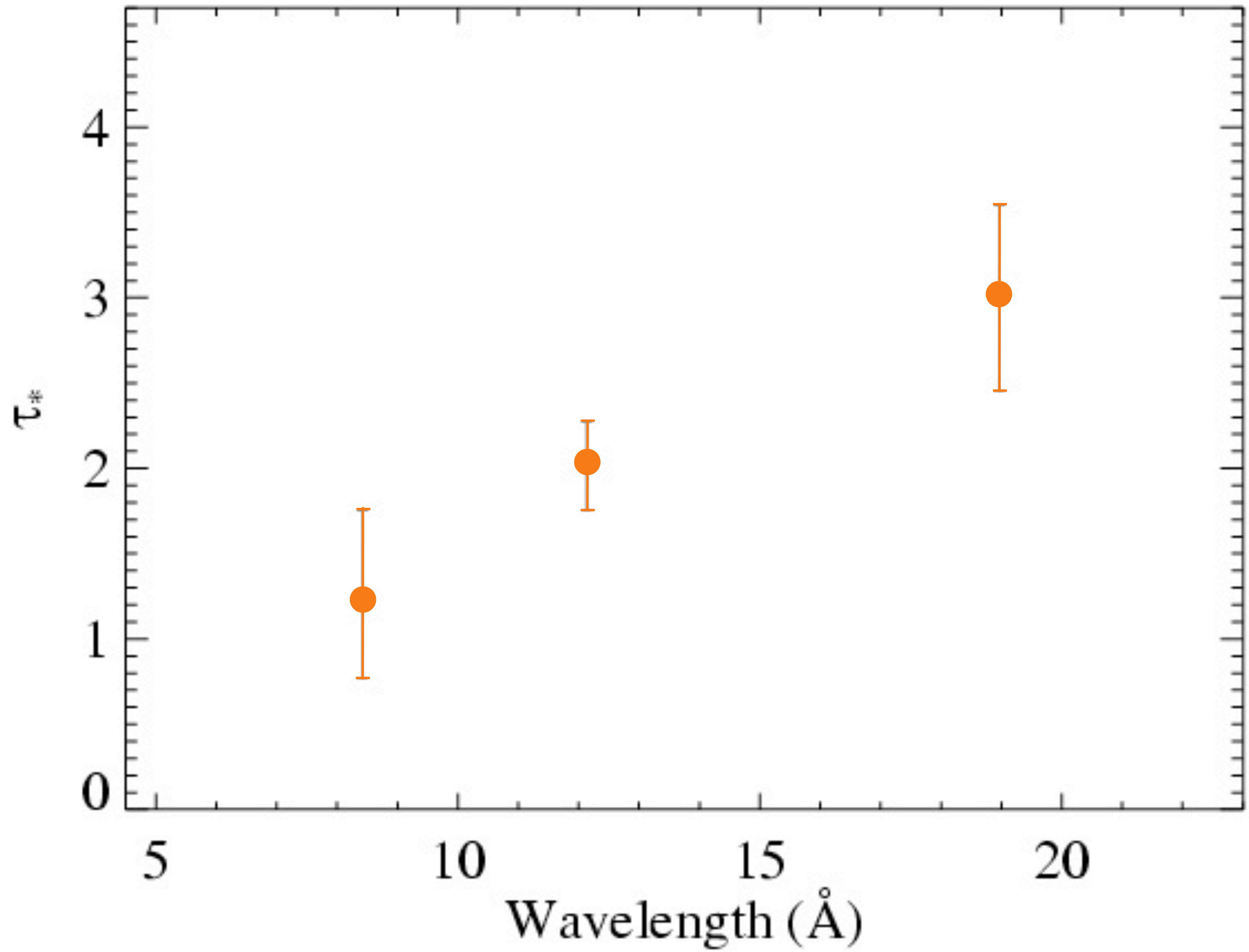

Fits to 16 lines in the *Chandra* spectrum of ζ Pup

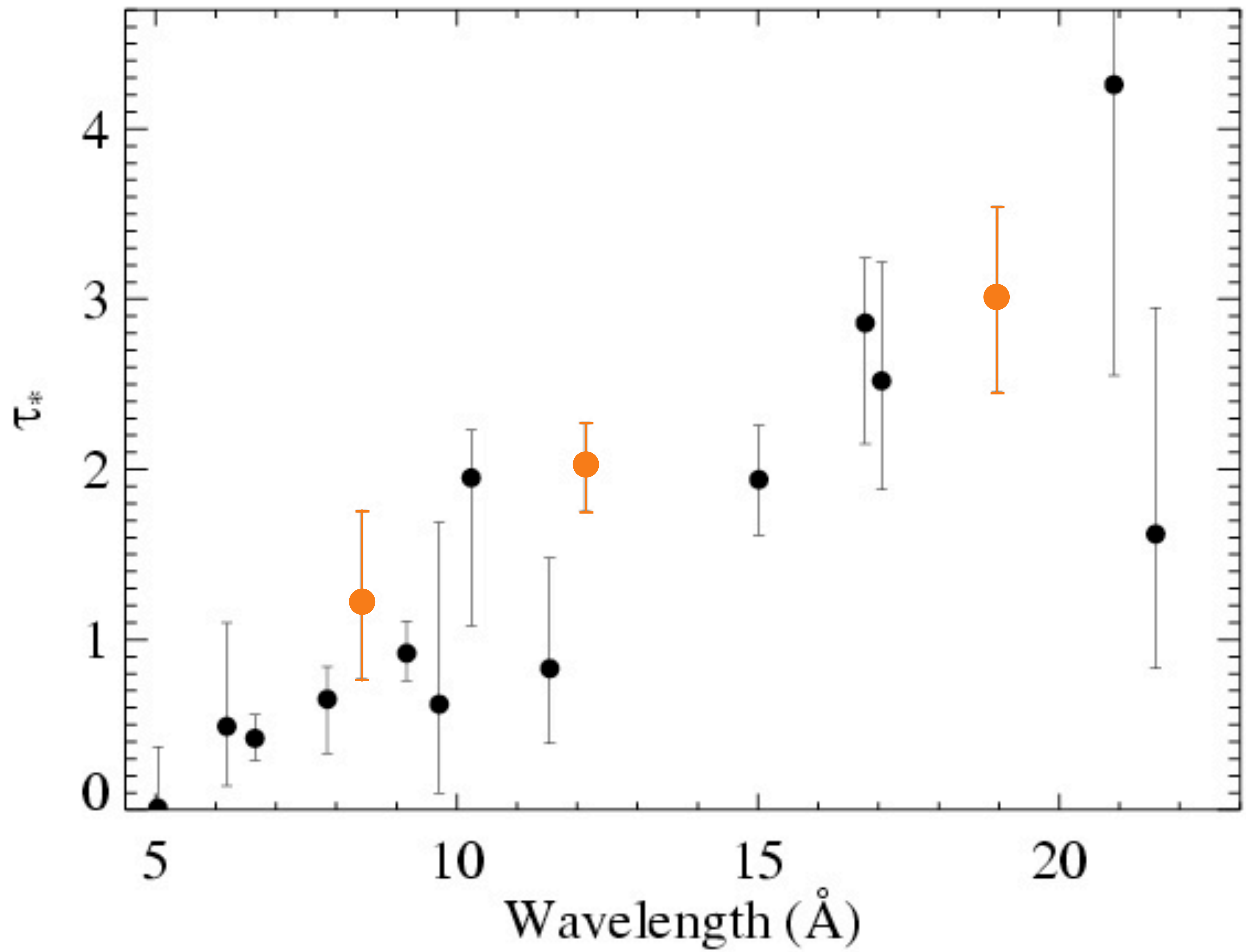

Fits to 16 lines in the *Chandra* spectrum of ζ Pup

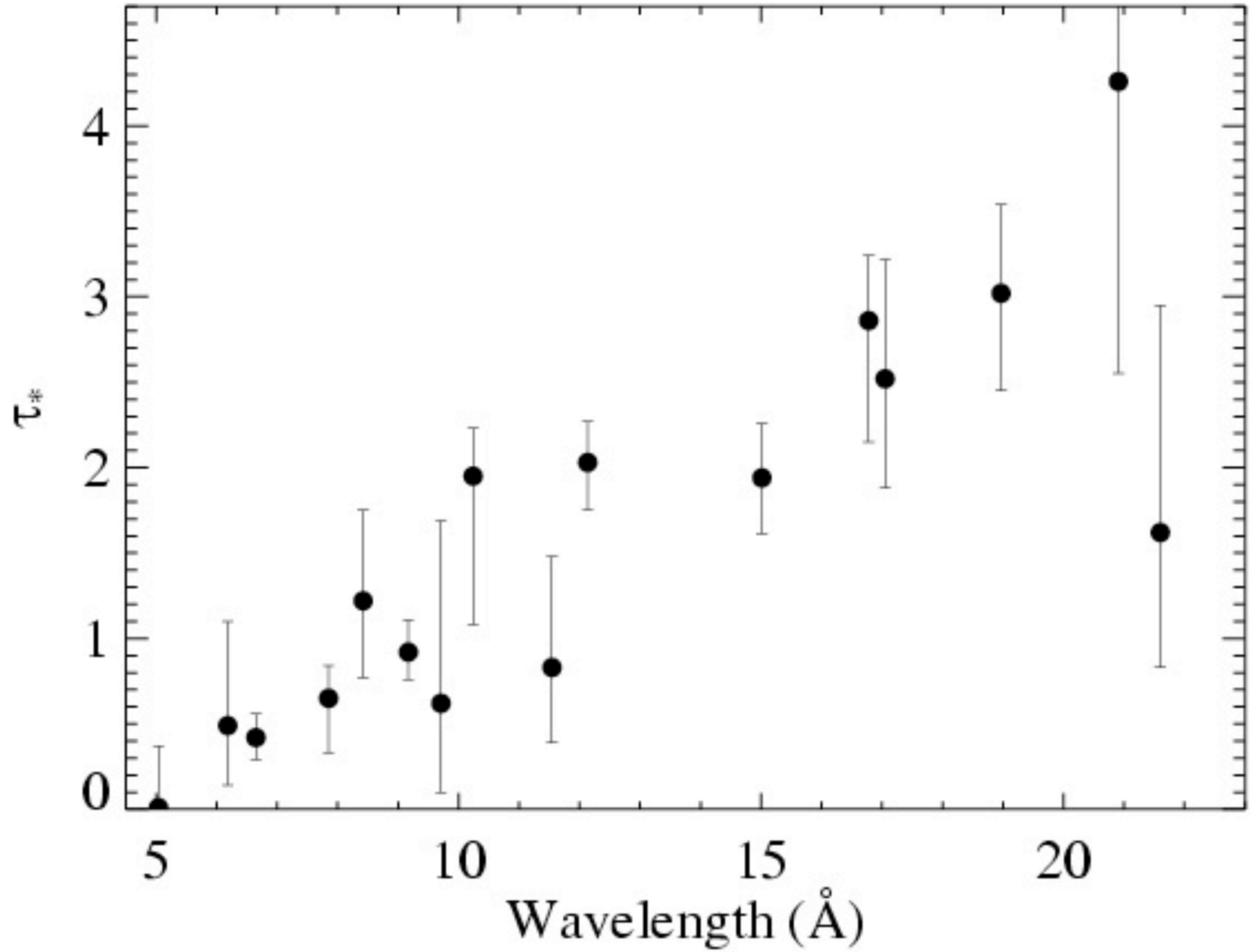

Fits to 16 lines in the *Chandra* spectrum of ζ Pup

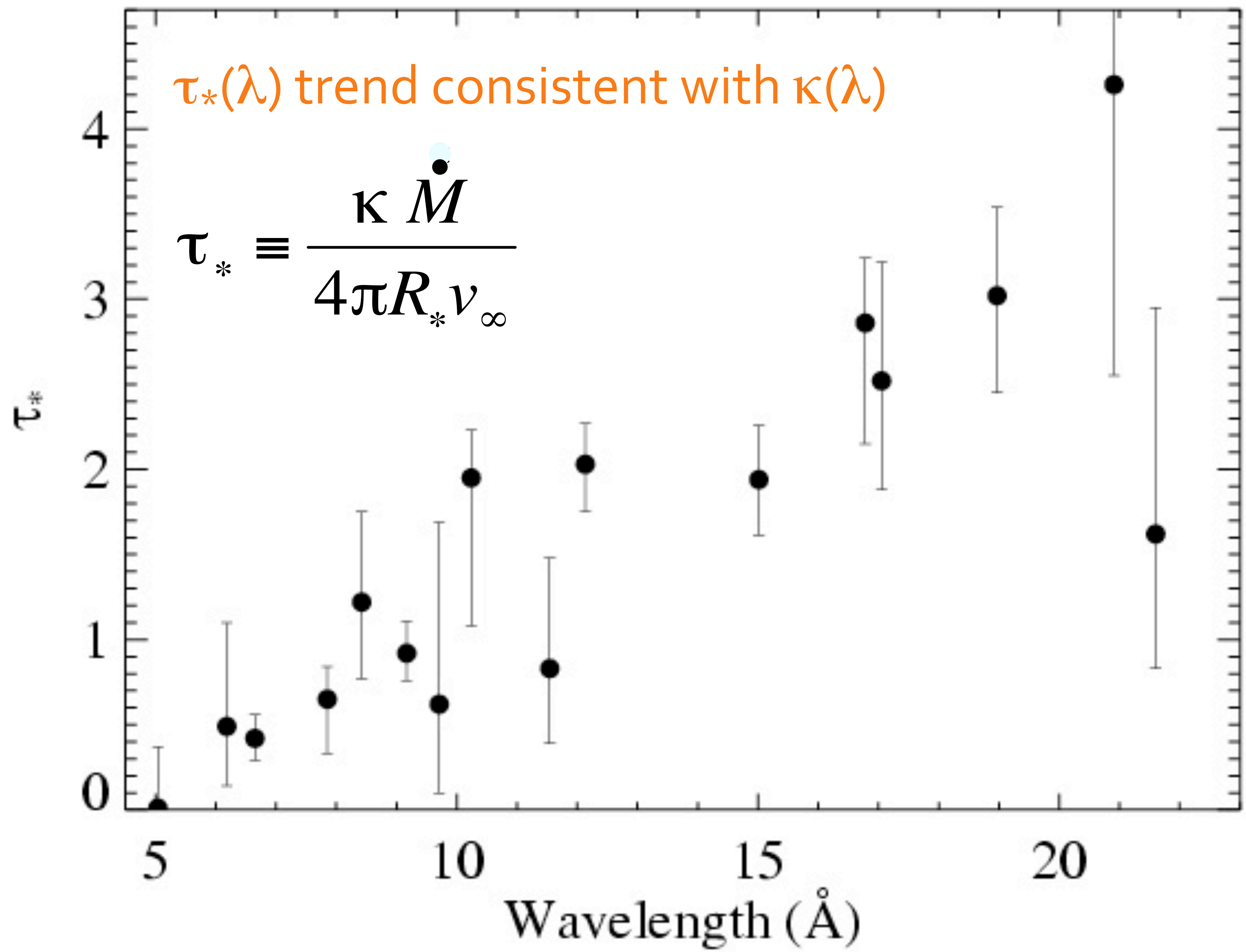

$\tau_*(\lambda)$ trend consistent with $\kappa(\lambda)$

$$\tau_* \equiv \frac{\kappa \dot{M}}{4\pi R_* v_\infty}$$

Fits to 16 lines in the *Chandra* spectrum of ζ Pup

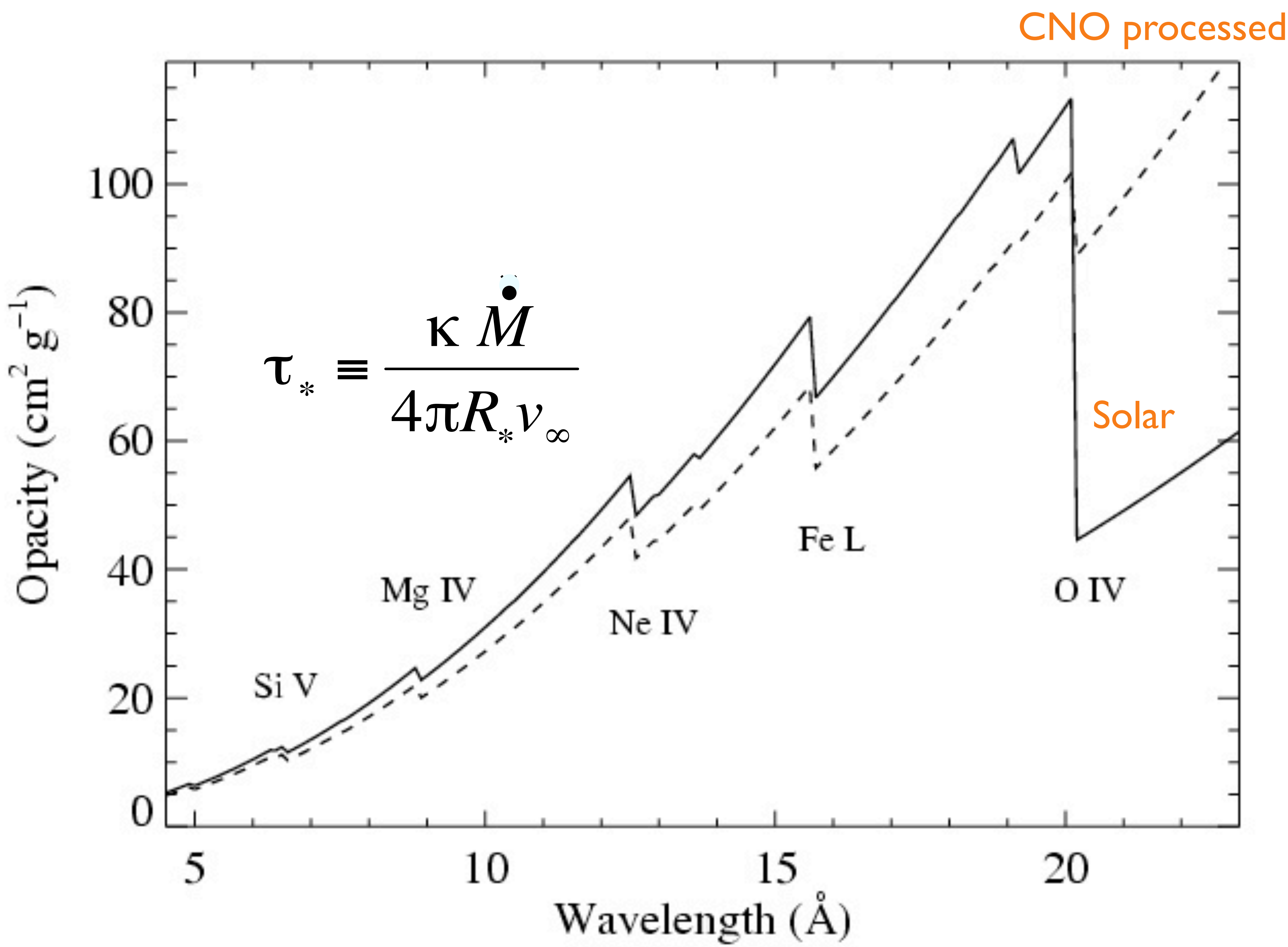

$$\tau_* \equiv \frac{\kappa \dot{M}}{4\pi R_* v_\infty}$$

$$\tau_* \equiv \frac{\kappa \dot{M}}{4\pi R_* v_\infty}$$

$\dot{M}$ becomes the free parameter of the fit to the $\tau_*(\lambda)$ trend

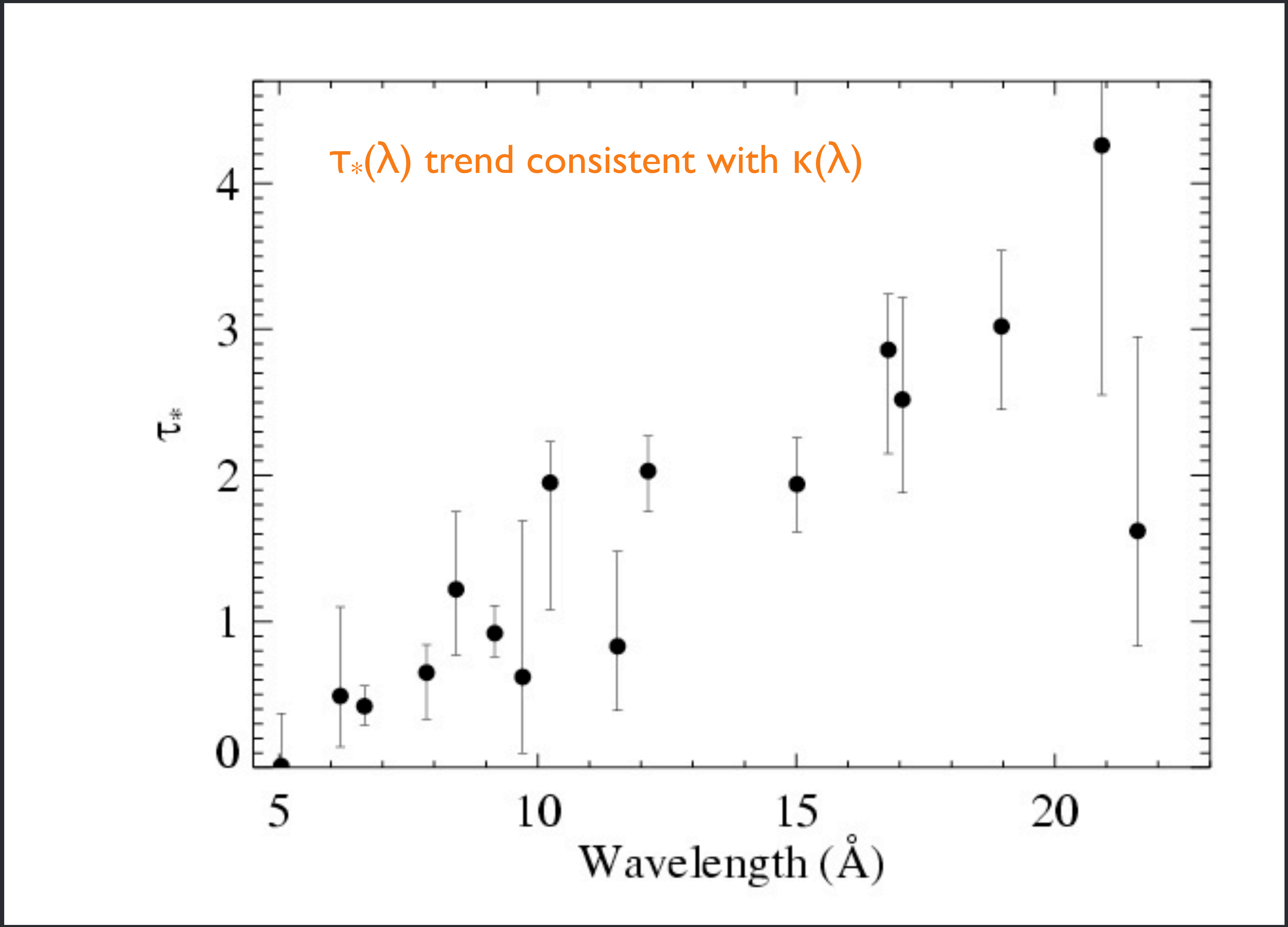

$$\tau_* \equiv \frac{\kappa \dot{M}}{4\pi R_* v_\infty}$$

$\dot{M}$ becomes the free parameter of the fit to the $\tau_*(\lambda)$ trend

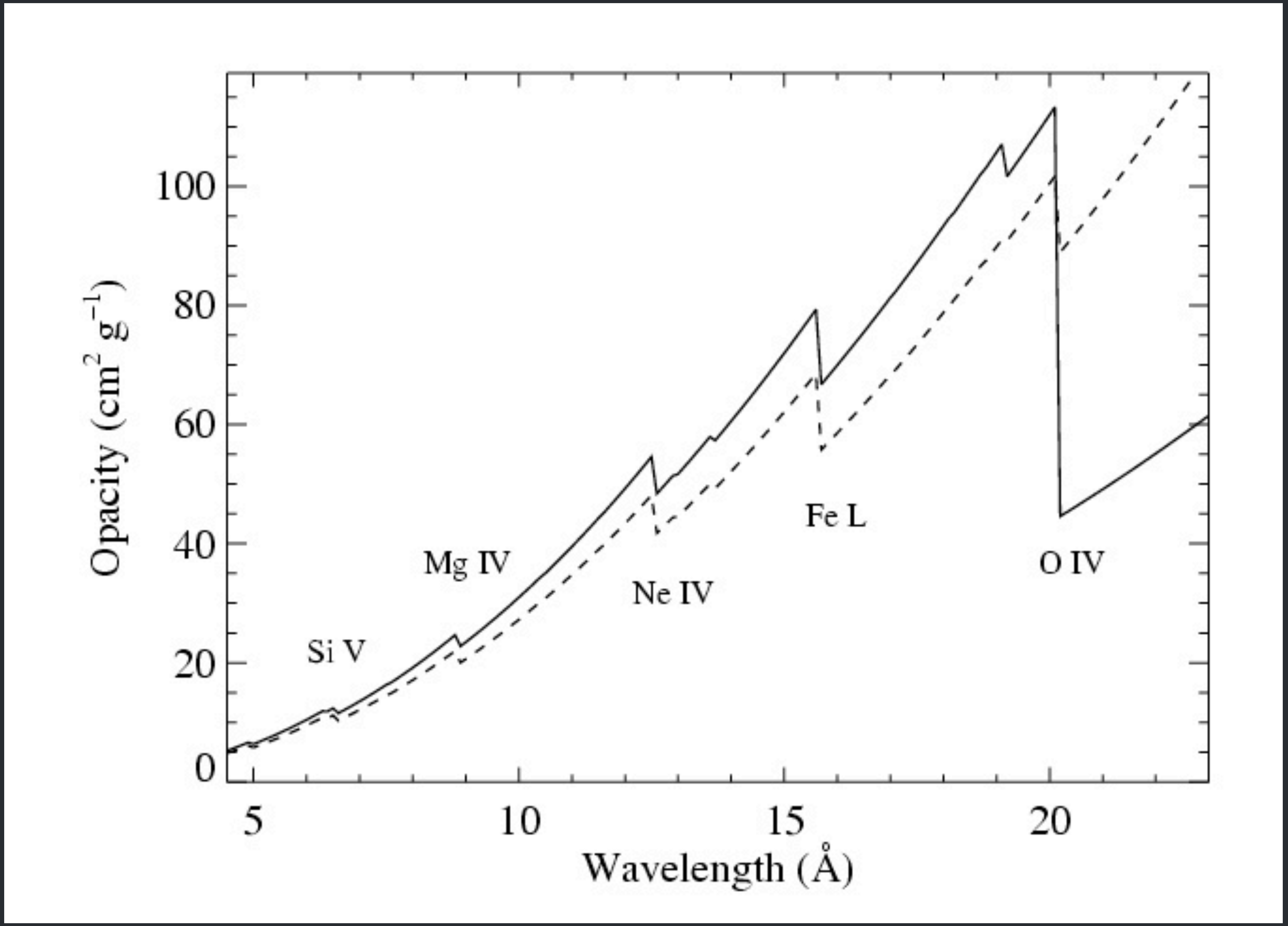

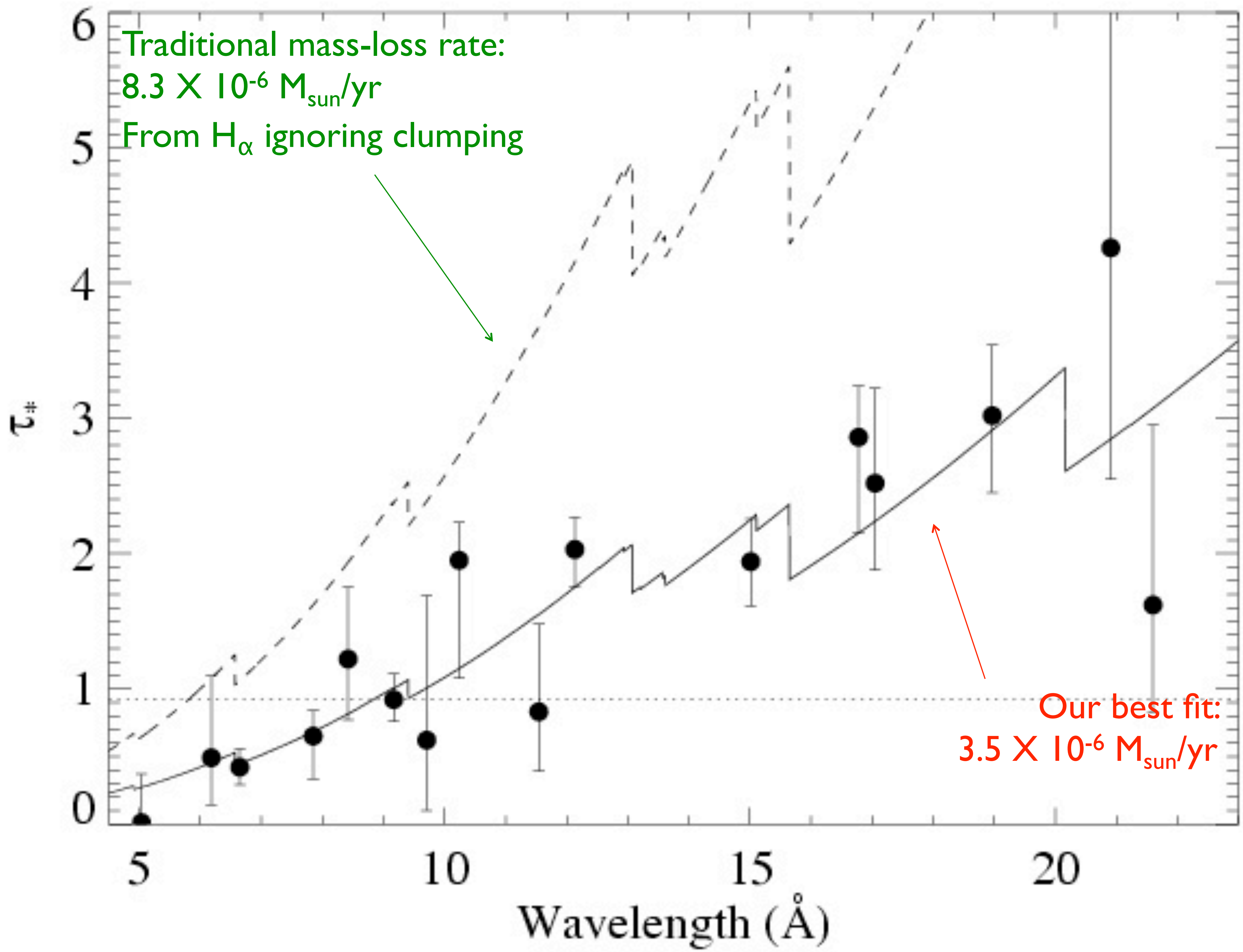

Traditional mass-loss rate:
8.3 X 10^{-6} M$_{sun}$/yr
From H$_{\alpha}$ ignoring clumping
Our best fit:
3.5 X 10^{-6} M$_{sun}$/yr
τ_*
0
1
2
3
4
5
6
5
10
15
20
Wavelength (Å)

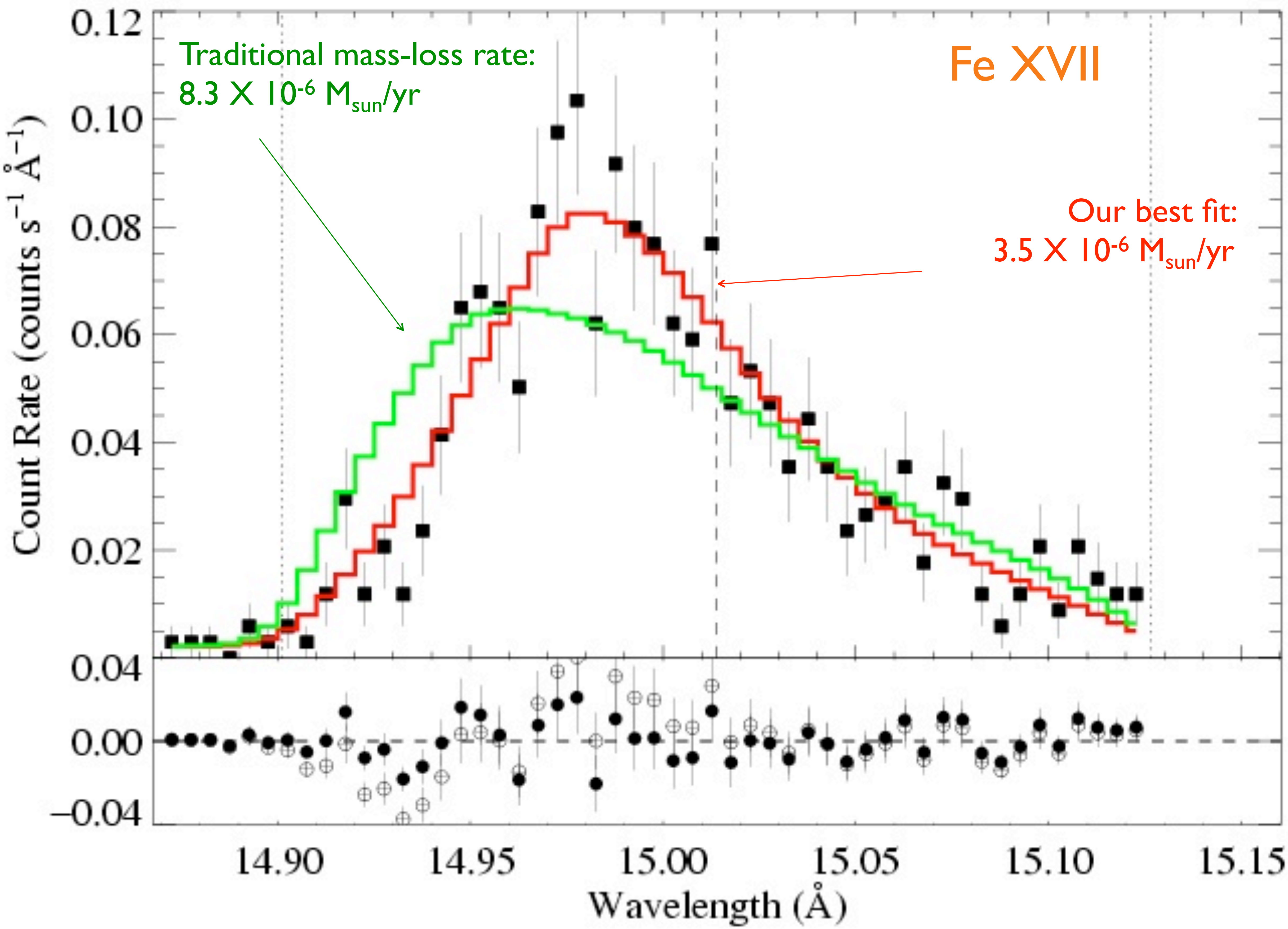
Traditional mass-loss rate:
8.3 X 10^{-6} M_{sun}/yr
Fe XVII
Our best fit:
3.5 X 10^{-6} M_{sun}/yr
Count Rate (counts s^{-1} Å^{-1})
Wavelength (Å)
0.12
0.10
0.08
0.06
0.04
0.02
0.04
0.00
–0.04
14.90
14.95
15.00
15.05
15.10
15.15

ζ Pup mass-loss rate < 4.2 x 10^{-6} M_{sun}/yr

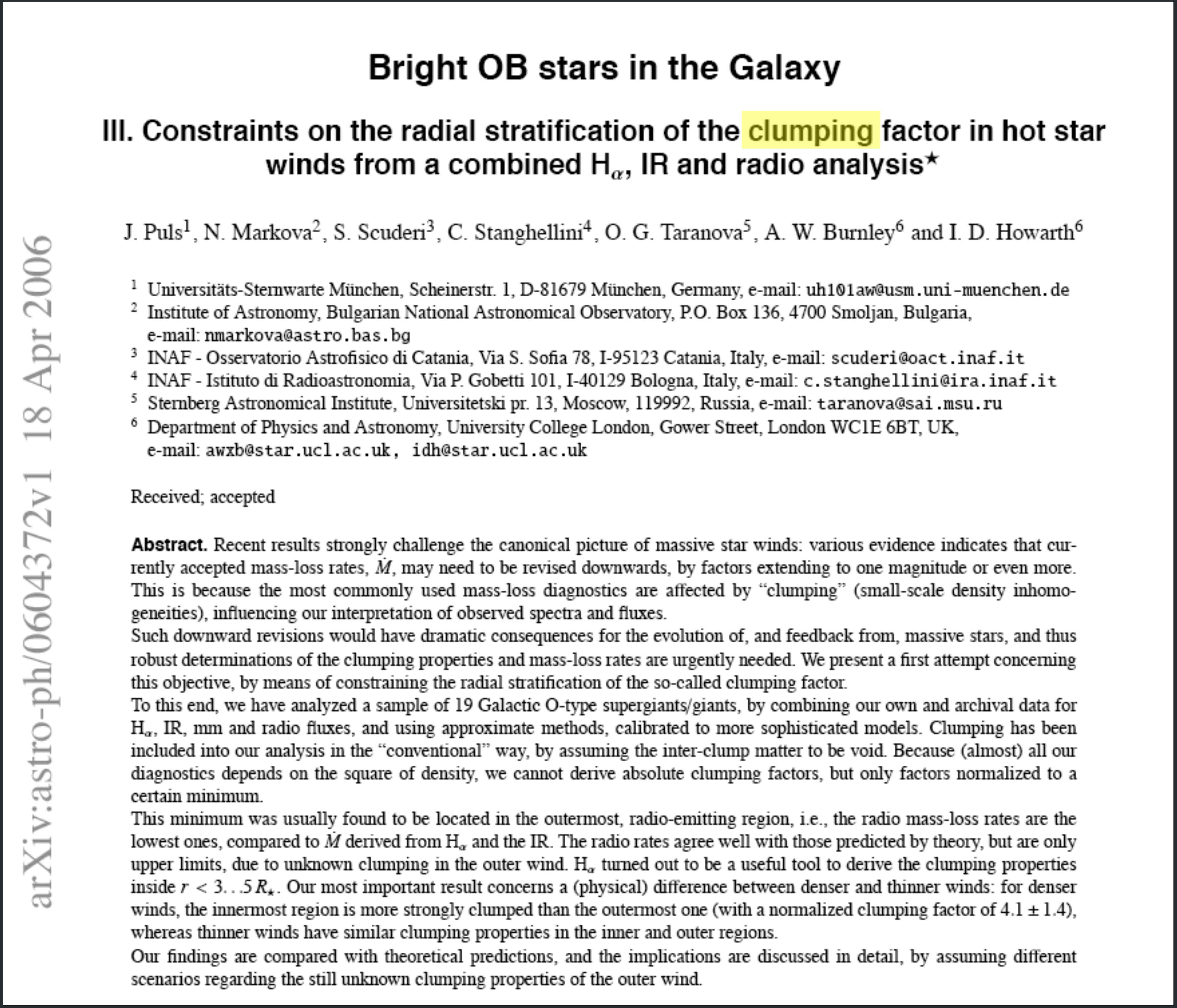

Bright OB stars in the Galaxy

III. Constraints on the radial stratification of the clumping factor in hot star winds from a combined H_α, IR and radio analysis*

J. Puls[1], N. Markova[2], S. Scuderi[3], C. Stanghellini[4], O. G. Taranova[5], A. W. Burnley[6] and I. D. Howarth[6]

[1] Universitäts-Sternwarte München, Scheinerstr. 1, D-81679 München, Germany, e-mail: uh101aw@usm.uni-muenchen.de
[2] Institute of Astronomy, Bulgarian National Astronomical Observatory, P.O. Box 136, 4700 Smoljan, Bulgaria, e-mail: nmarkova@astro.bas.bg
[3] INAF - Osservatorio Astrofisico di Catania, Via S. Sofia 78, I-95123 Catania, Italy, e-mail: scuderi@oact.inaf.it
[4] INAF - Istituto di Radioastronomia, Via P. Gobetti 101, I-40129 Bologna, Italy, e-mail: c.stanghellini@ira.inaf.it
[5] Sternberg Astronomical Institute, Universitetski pr. 13, Moscow, 119992, Russia, e-mail: taranova@sai.msu.ru
[6] Department of Physics and Astronomy, University College London, Gower Street, London WC1E 6BT, UK, e-mail: awxb@star.ucl.ac.uk, idh@star.ucl.ac.uk

Received; accepted

Abstract. Recent results strongly challenge the canonical picture of massive star winds: various evidence indicates that currently accepted mass-loss rates, $\dot{M}$, may need to be revised downwards, by factors extending to one magnitude or even more. This is because the most commonly used mass-loss diagnostics are affected by "clumping" (small-scale density inhomogeneities), influencing our interpretation of observed spectra and fluxes.
Such downward revisions would have dramatic consequences for the evolution of, and feedback from, massive stars, and thus robust determinations of the clumping properties and mass-loss rates are urgently needed. We present a first attempt concerning this objective, by means of constraining the radial stratification of the so-called clumping factor.
To this end, we have analyzed a sample of 19 Galactic O-type supergiants/giants, by combining our own and archival data for H_α, IR, mm and radio fluxes, and using approximate methods, calibrated to more sophisticated models. Clumping has been included into our analysis in the "conventional" way, by assuming the inter-clump matter to be void. Because (almost) all our diagnostics depends on the square of density, we cannot derive absolute clumping factors, but only factors normalized to a certain minimum.
This minimum was usually found to be located in the outermost, radio-emitting region, i.e., the radio mass-loss rates are the lowest ones, compared to $\dot{M}$ derived from H_α and the IR. The radio rates agree well with those predicted by theory, but are only upper limits, due to unknown clumping in the outer wind. H_α turned out to be a useful tool to derive the clumping properties inside $r < 3 \ldots 5 R_\star$. Our most important result concerns a (physical) difference between denser and thinner winds: for denser winds, the innermost region is more strongly clumped than the outermost one (with a normalized clumping factor of 4.1 ± 1.4), whereas thinner winds have similar clumping properties in the inner and outer regions.
Our findings are compared with theoretical predictions, and the implications are discussed in detail, by assuming different scenarios regarding the still unknown clumping properties of the outer wind.

ζ Pup: radially varying clumping

for $\dot{M} = 4.2 \times 10^{-6}\ M_{sun}/yr$

$f_{cl} = 1$ @ $r < 1.12\ R_*$
$f_{cl} = 5.5$ @ $1.12 < r < 1.5\ R_*$
$f_{cl} = 3.1$ @ $1.5 < r < 2\ R_*$
$f_{cl} = 2$ @ $2 < r < 15\ R_*$
$f_{cl} = 1$ @ $r > 15\ R_*$

Hα IR radio

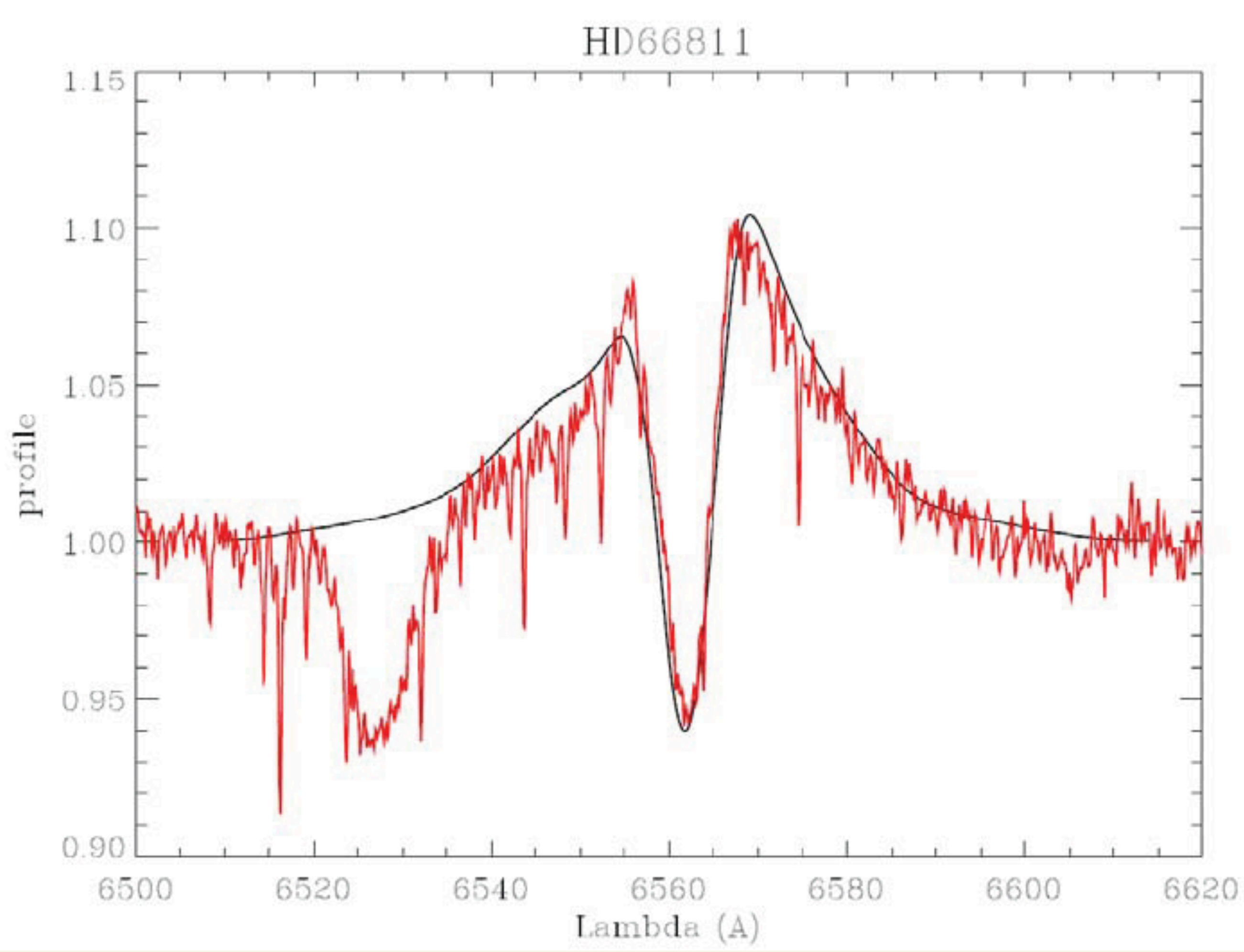

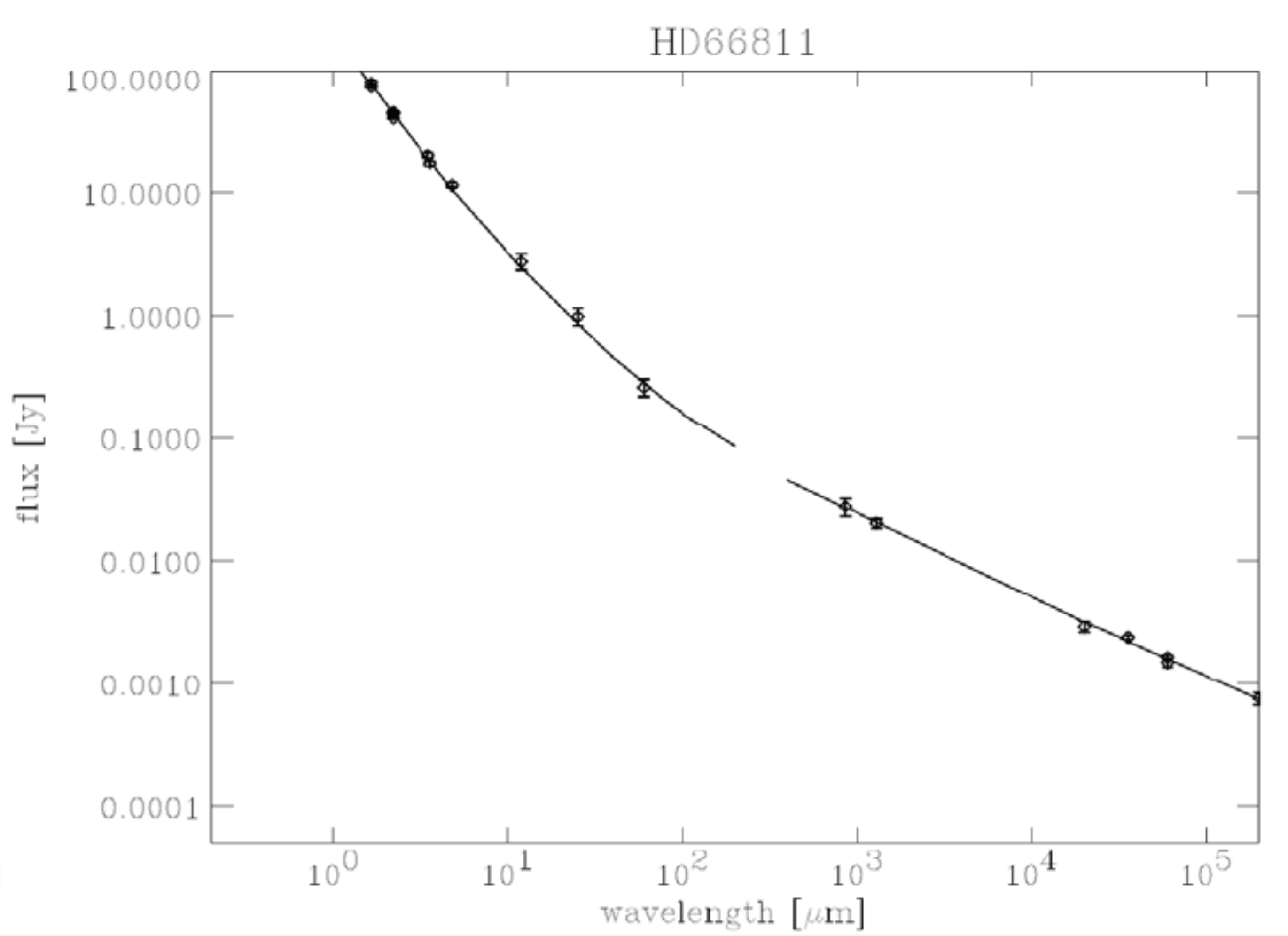

ζ Pup: radially varying clumping

for $\dot{M} = 4.2 \times 10^{-6}\ M_{sun}/yr$

scale up slightly:

$f_{cl} \sim 6$ in the Hα region

$f_{cl} = 1$ @ $r < 1.12\ R_*$

$f_{cl} = 5.5$ @ $1.12 < r < 1.5\ R_*$

$f_{cl} = 3.1$ @ $1.5 < r < 2\ R_*$

$f_{cl} = 2$ @ $2 < r < 15\ R_*$

$f_{cl} = 1$ @ $r > 15\ R_*$

Hα

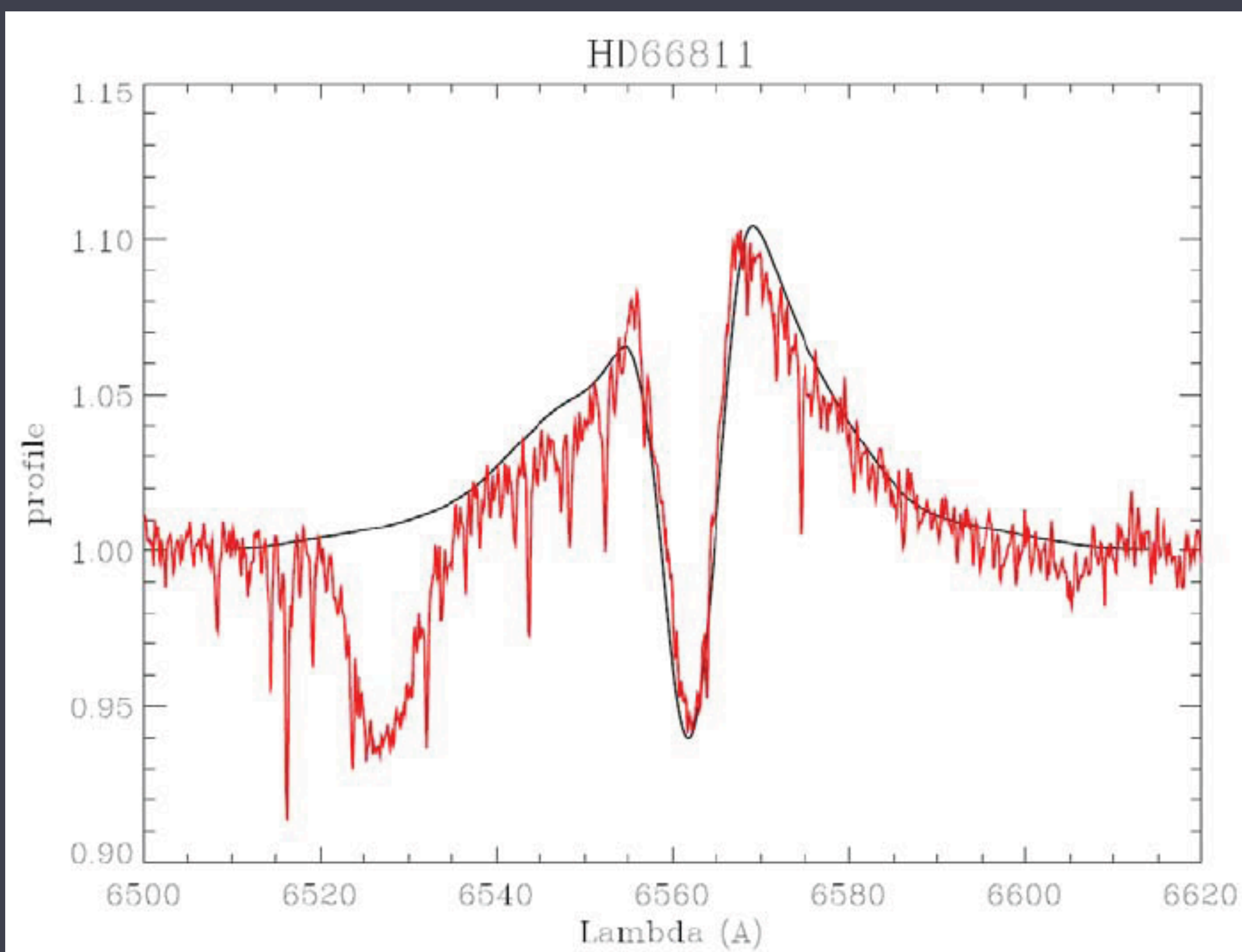

IR

radio

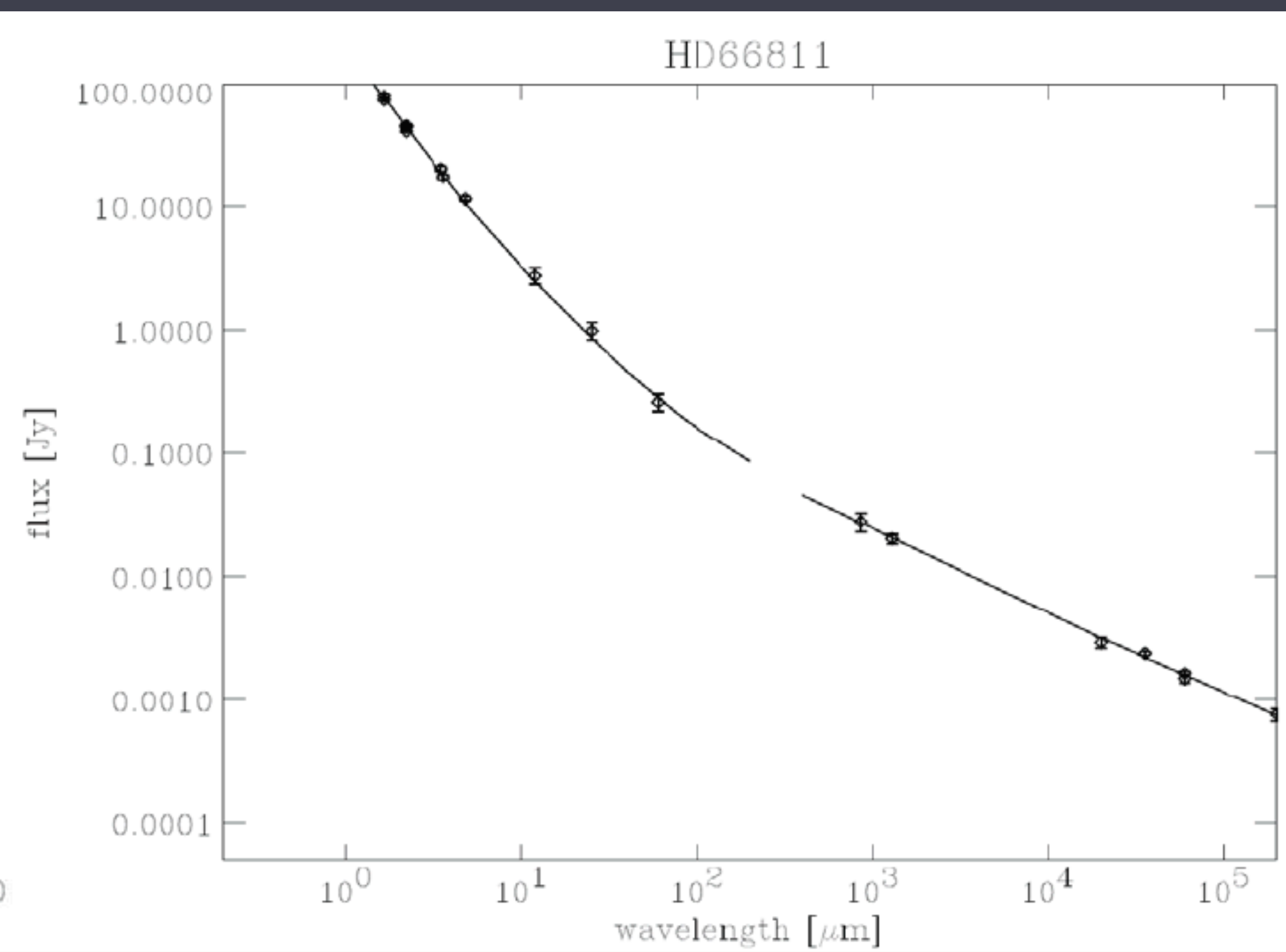

ζ Pup

for $\dot{M} = 3.5 \times 10^{-6}\ M_{sun}/yr$

$\dot{M}_{cl} \equiv \dot{M}_{smooth} / f_{cl}^{0.5}$

scale up slightly:
$f_{cl} \sim 6$ in the Hα region

$3.5 \times 10^{-6}\ M_{sun}/yr =$
$(8.3 \times 10^{-6}\ M_{sun}/yr)/6^{0.5}$

Hα IR radio

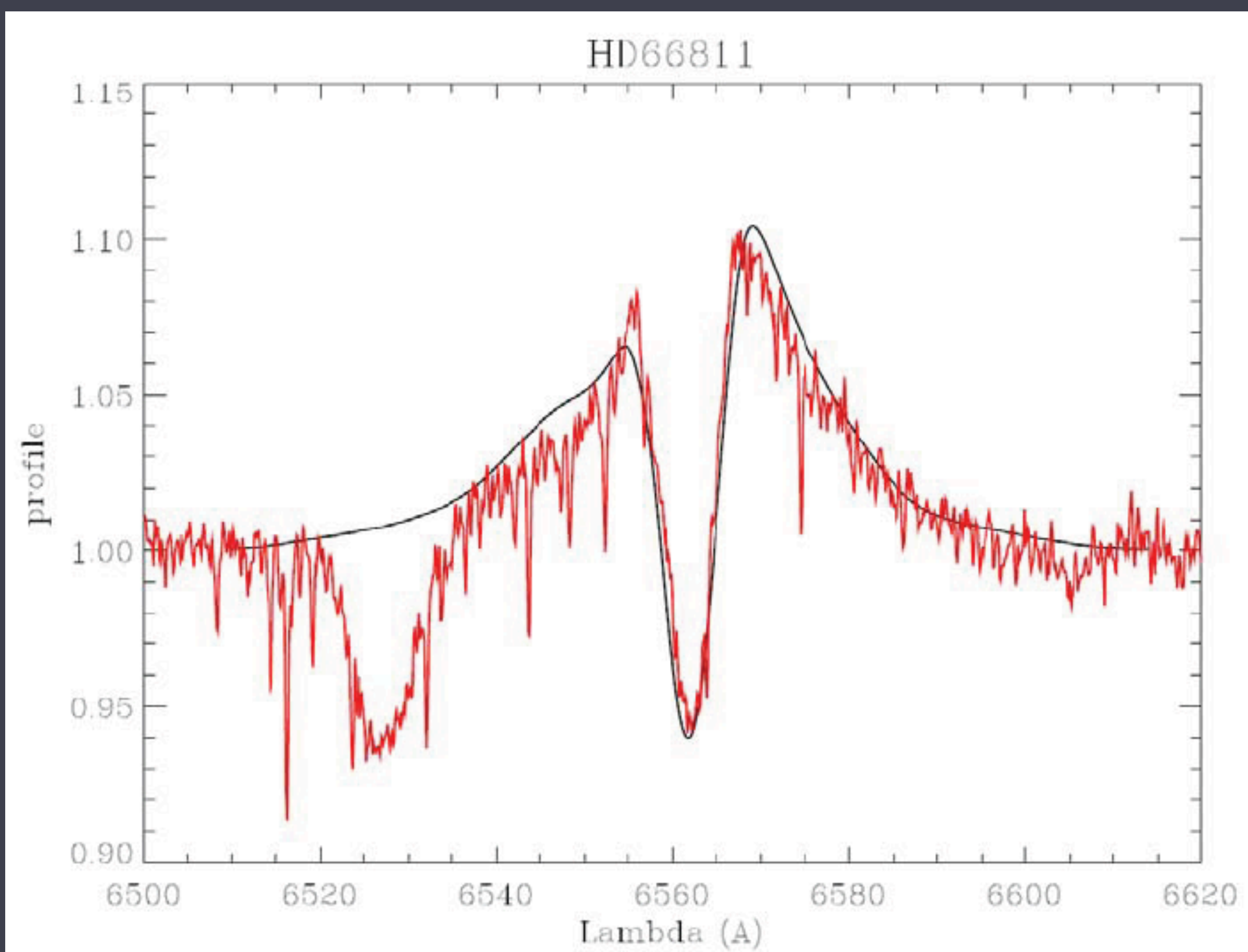

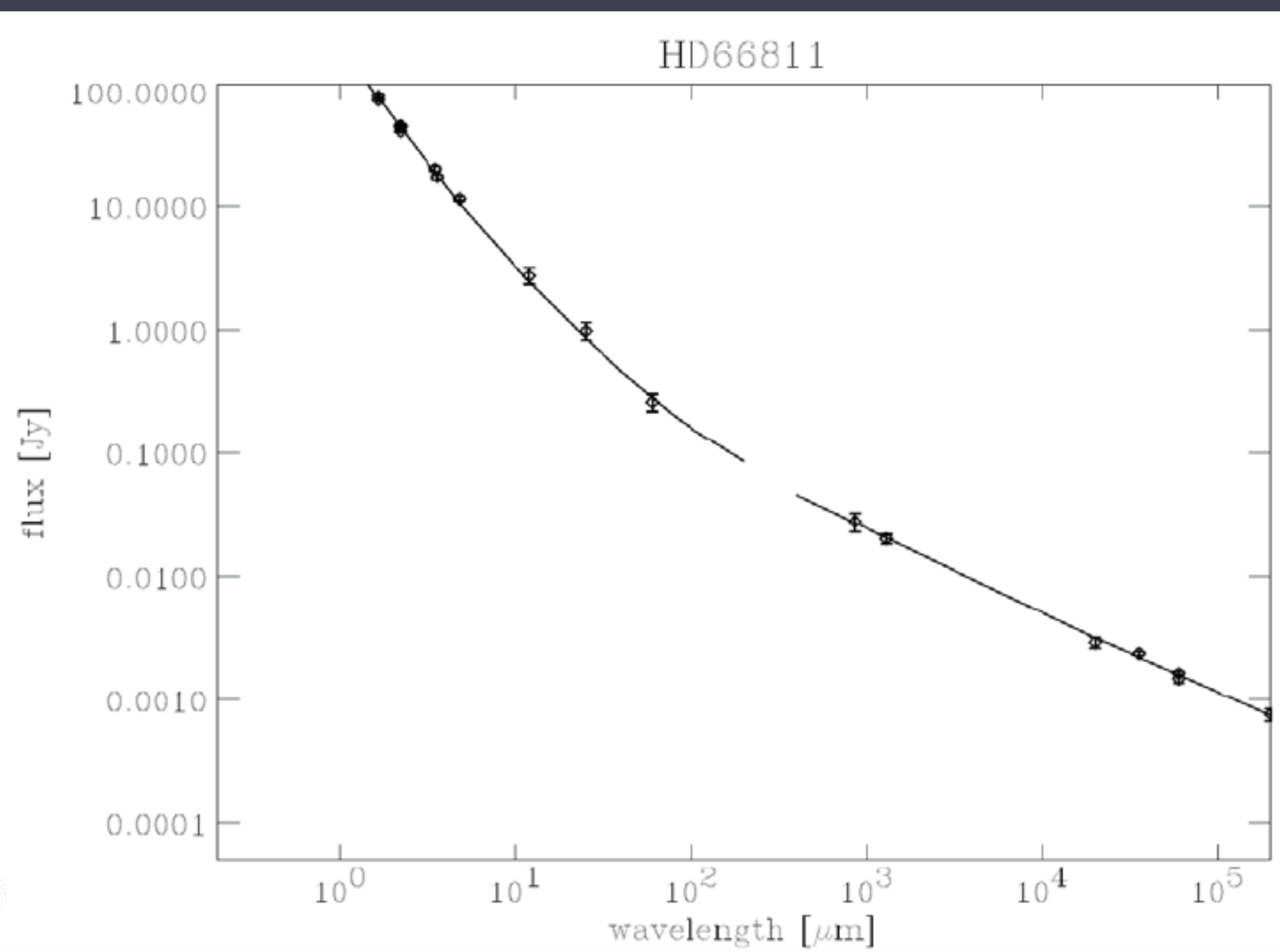

ζ Pup: radially varying clumping

for $\dot{M} = 3.5 \times 10^{-6}\ M_{sun}/yr$

$f_{cl} = 1.3$ @ $r < 1.12\ R_*$
$f_{cl} = 6.0$ @ $1.12 < r < 1.5\ R_*$
$f_{cl} = 3.7$ @ $1.5 < r < 2\ R_*$
$f_{cl} = 2.6$ @ $2 < r < 15\ R_*$
$f_{cl} = 1.3$ @ $r > 15\ R_*$

Hα IR radio

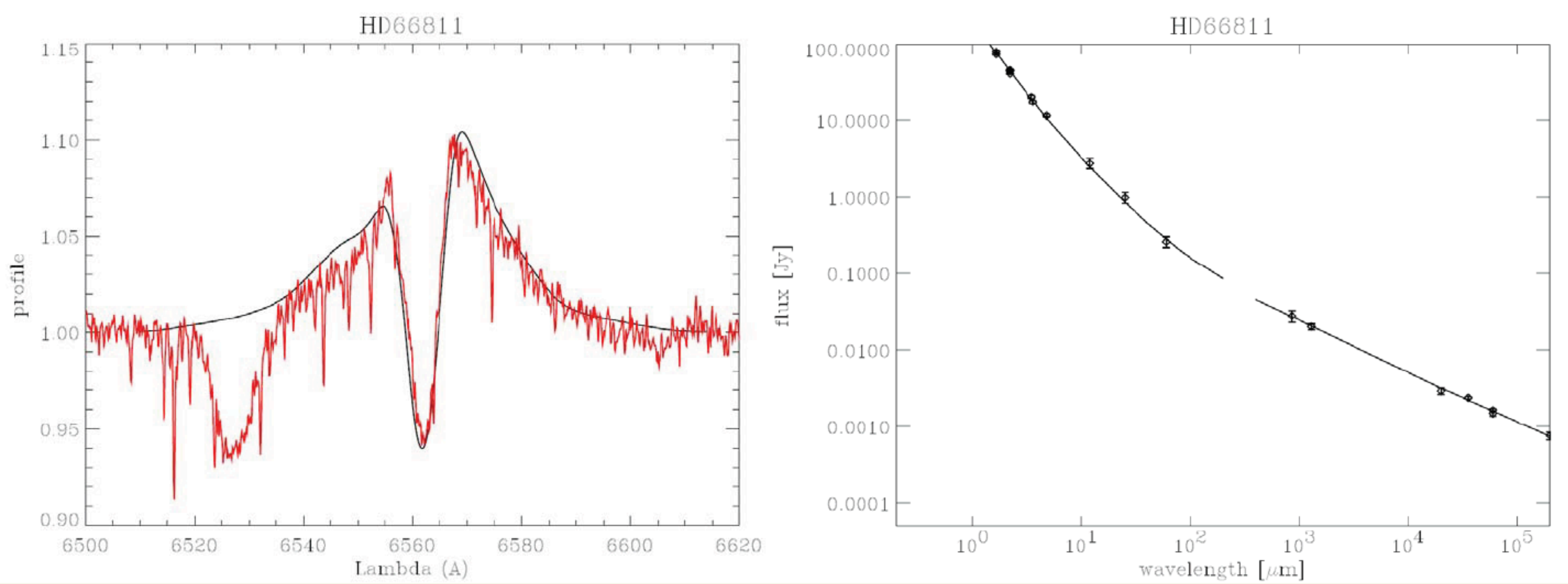

ζ Pup: radially varying clumping

for $\dot{M} = 3.5 \times 10^{-6}\ M_{sun}/yr$

consistent multi-wavelength fit with a single mass-loss rate

$f_{cl} = 1.3$ @ $r < 1.12\ R_*$
$f_{cl} = 6.0$ @ $1.12 < r < 1.5\ R_*$
$f_{cl} = 3.7$ @ $1.5 < r < 2\ R_*$
$f_{cl} = 2.6$ @ $2 < r < 15\ R_*$
$f_{cl} = 1.3$ @ $r > 15\ R_*$

Hα IR radio

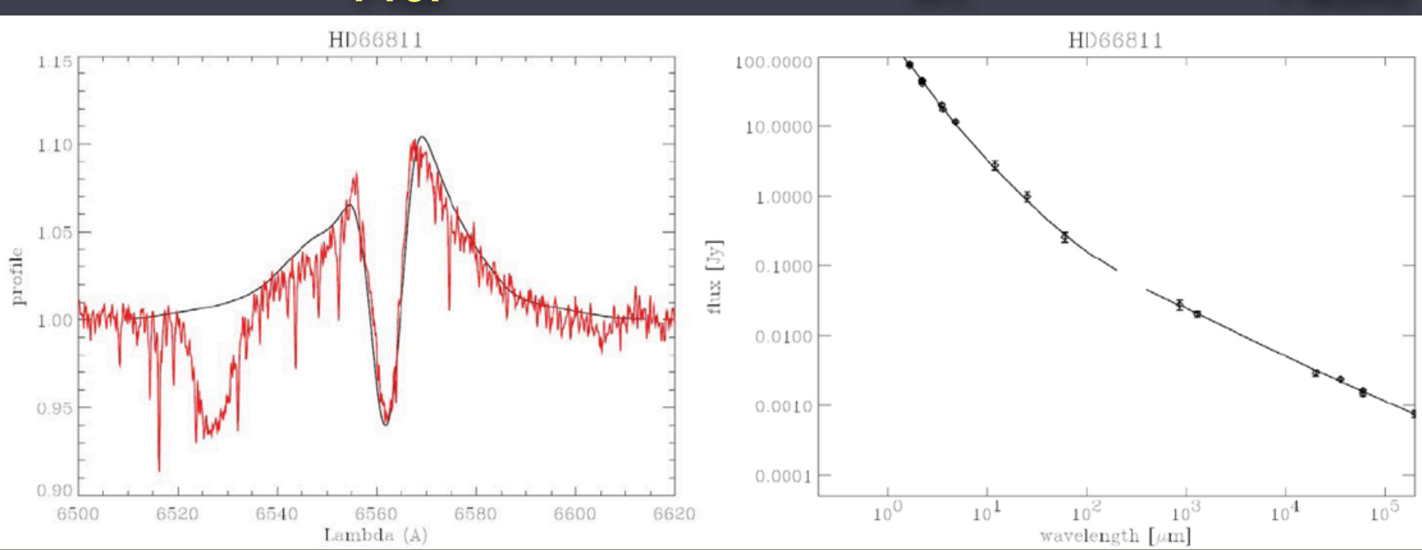

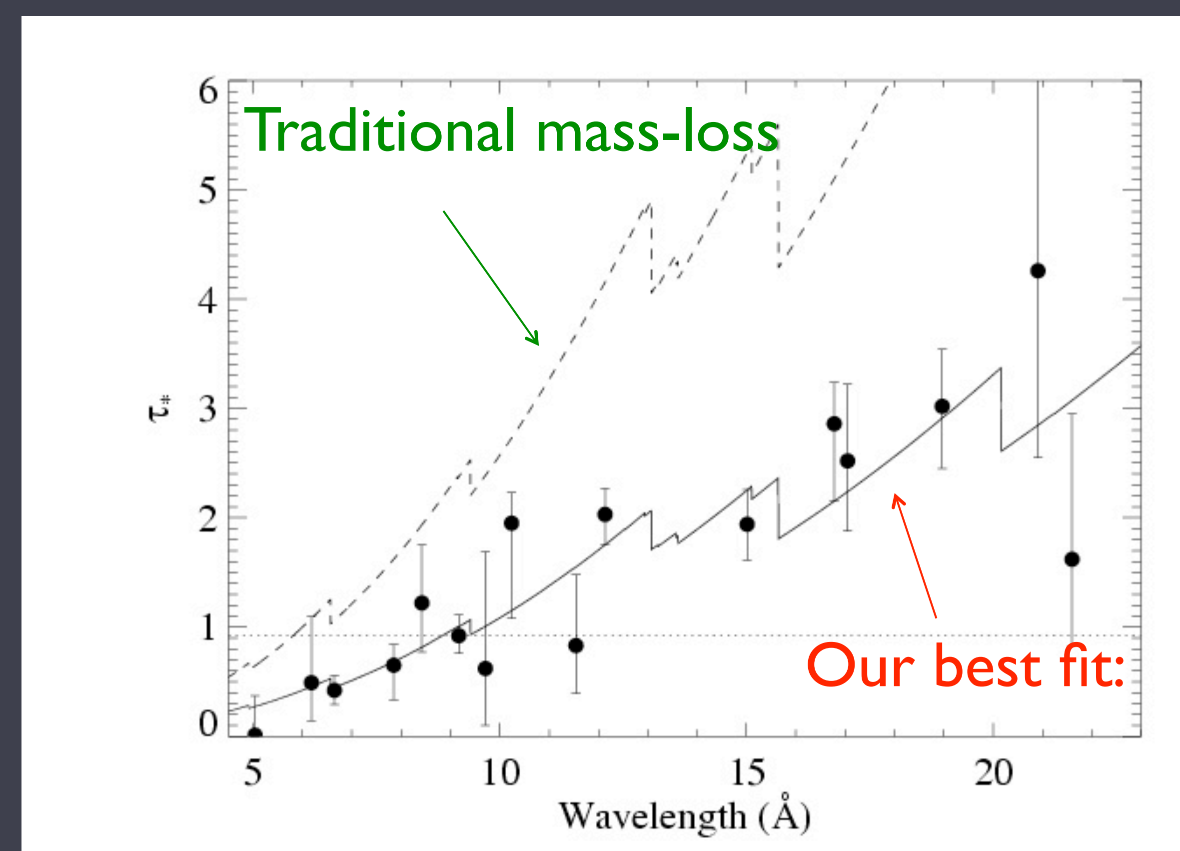

ζ Pup: radially varying clumping

for $\dot{M} = 3.5 \times 10^{-6}\ M_{sun}/yr$

$f_{cl} = 1.3$ @ $r < 1.12\ R_*$
$f_{cl} = 6.0$ @ $1.12 < r < 1.5\ R_*$
$f_{cl} = 3.7$ @ $1.5 < r < 2\ R_*$
$f_{cl} = 2.6$ @ $2 < r < 15\ R_*$
$f_{cl} = 1.3$ @ $r > 15\ R_*$

consistent multi-wavelength fit with a single mass-loss rate

h ~ 0; *no* significant porosity

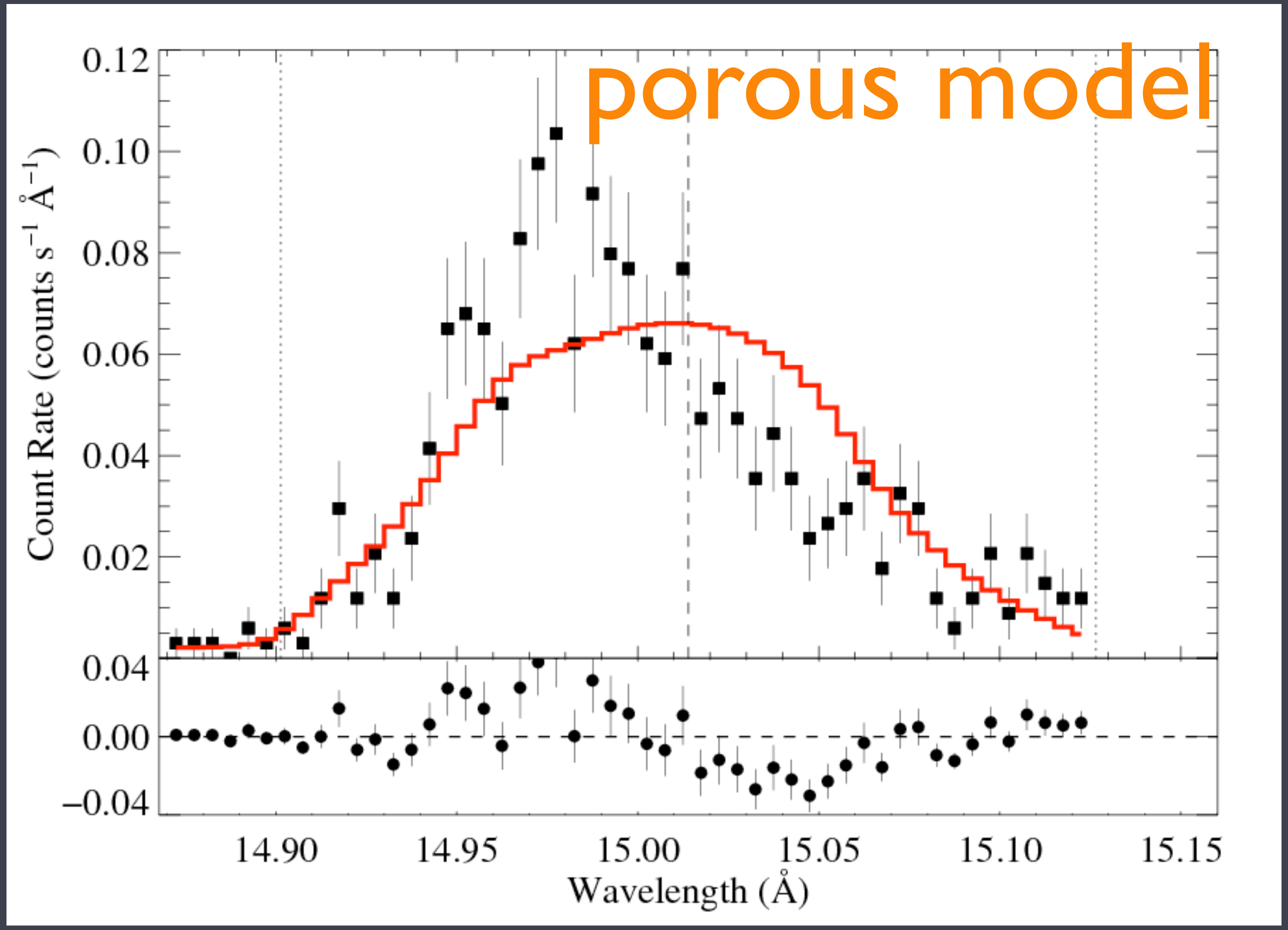

Conclusions

1. Clumped? Yes! Porous? No!
2. X-ray attenuation (from line profile shapes), is a good clumping-insensitive mass-loss rate diagnostic
3. For ζ Pup, $\dot{M} = 3.5 \times 10^{-6}\ M_{sun}/yr$; $f_{cl} \sim 6$ (at $r < 1.5\ R_{\star}$); and $h \sim 0$
4. Anisotropic porosity is ruled out by the non-detection of the Venetian blind effect
5. Isotropic porosity? Only at a level where the effect on the mass-loss rate is negligible

Extra Slides

UV variability

19 Cep (O9.5 Ib) : Si IV

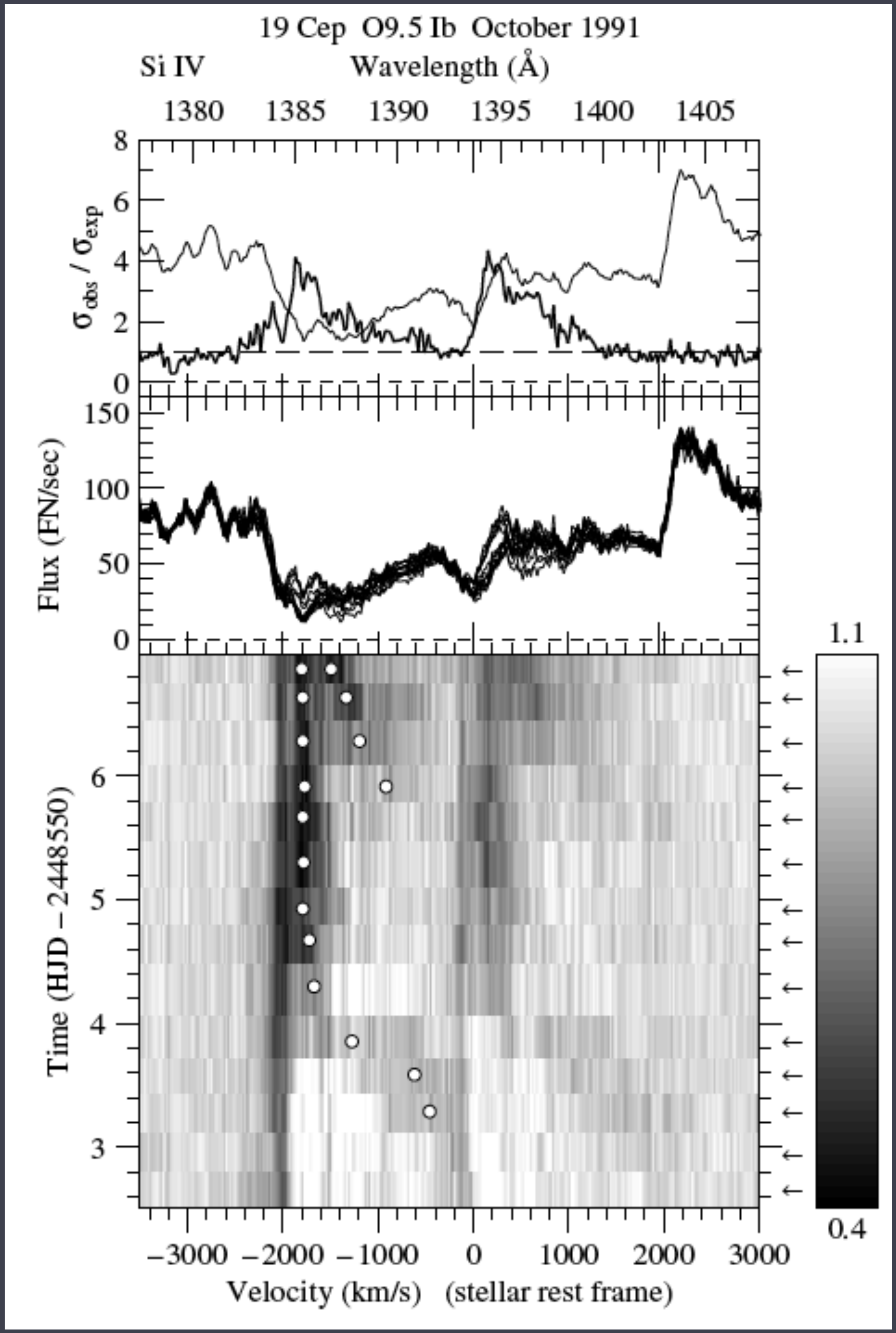

(Kaper et al. 1997)

ξ Per (O7.5 III) : Si IV

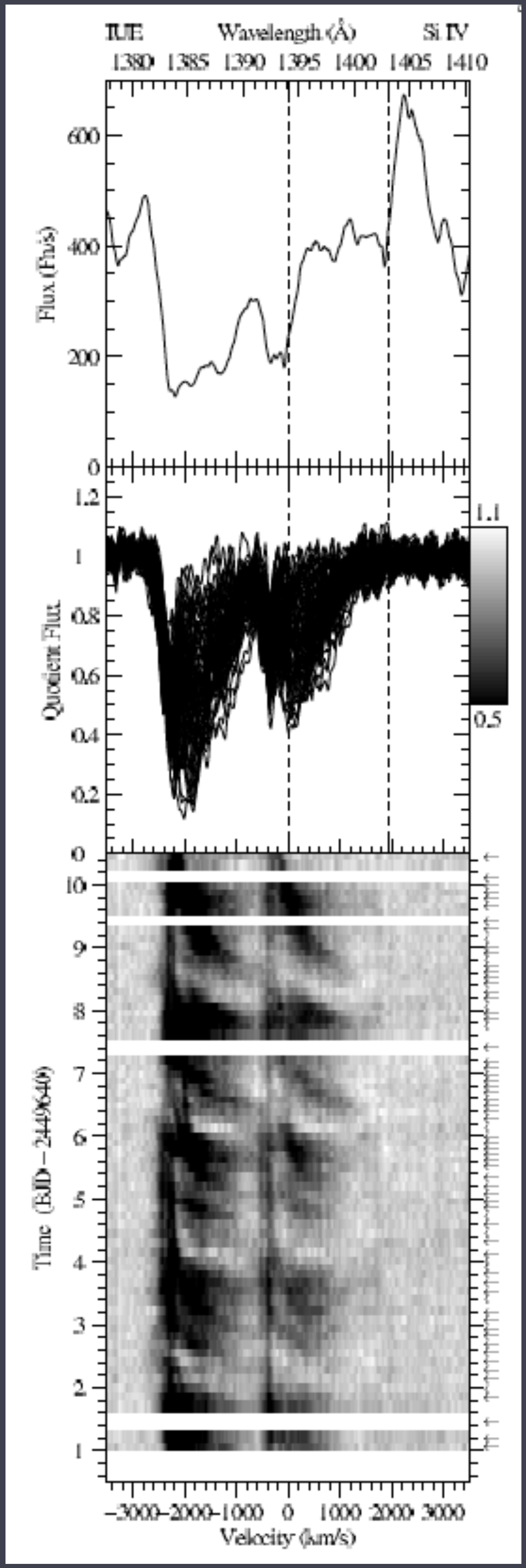

(de Jong et al. 2001)

ζ Pup: radially varying clumping

for $\dot{M} = 4.2 \times 10^{-6}\ M_{sun}/yr$

1-D hydro simulations do not reproduce the observed trend

$f_{cl} = 1$ @ $r < 1.12\ R_*$

$f_{cl} = 5.5$ @ $1.12 < r < 1.5\ R_*$

$f_{cl} = 3.1$ @ $1.5 < r < 2\ R_*$

$f_{cl} = 2$ @ $2 < r < 15\ R_*$

$f_{cl} = 1$ @ $r > 15\ R_*$

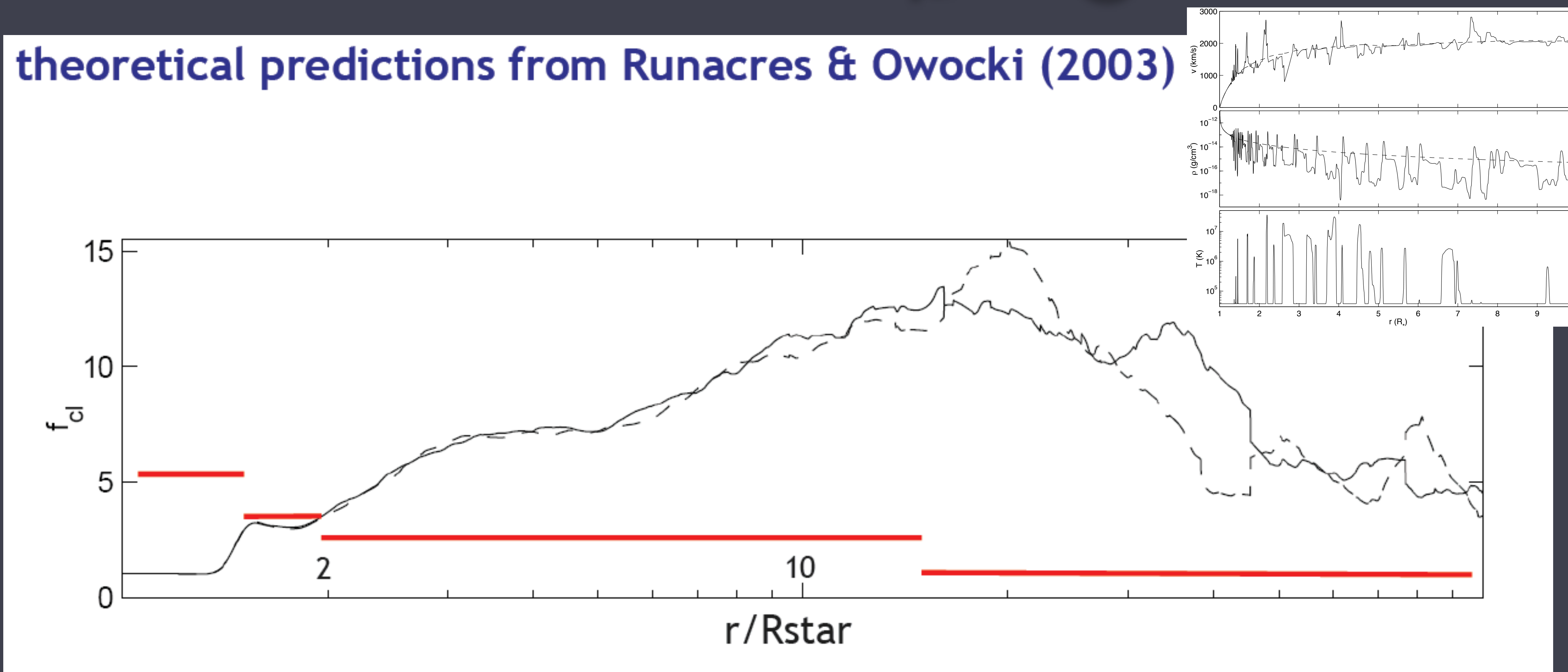

Illumination from isovelocity surfaces

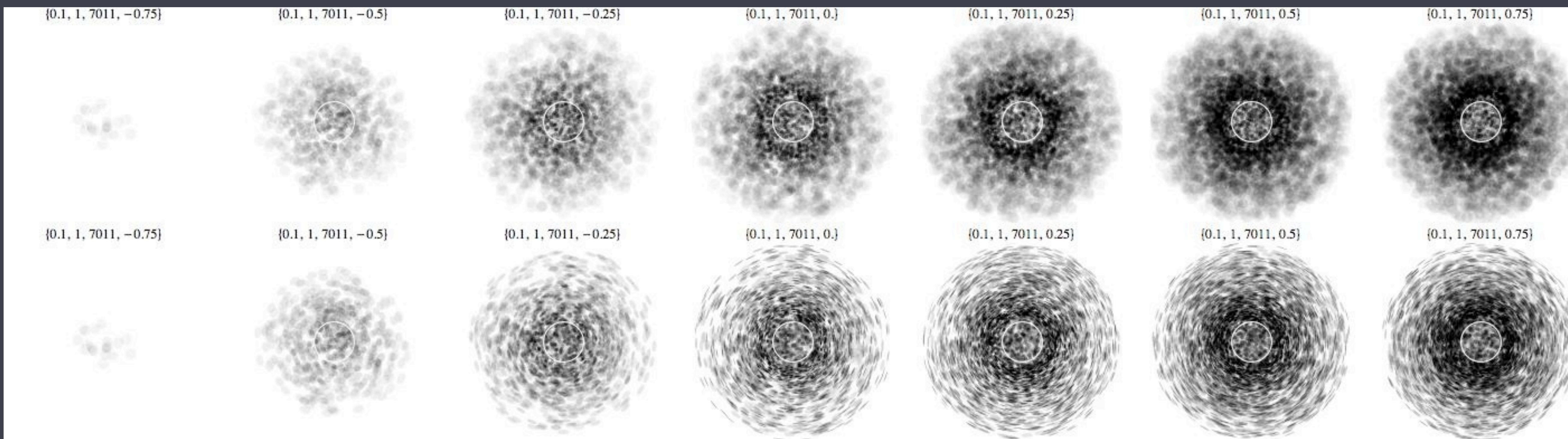

X-ray line profiles can be synthesized directly from hydro simulations

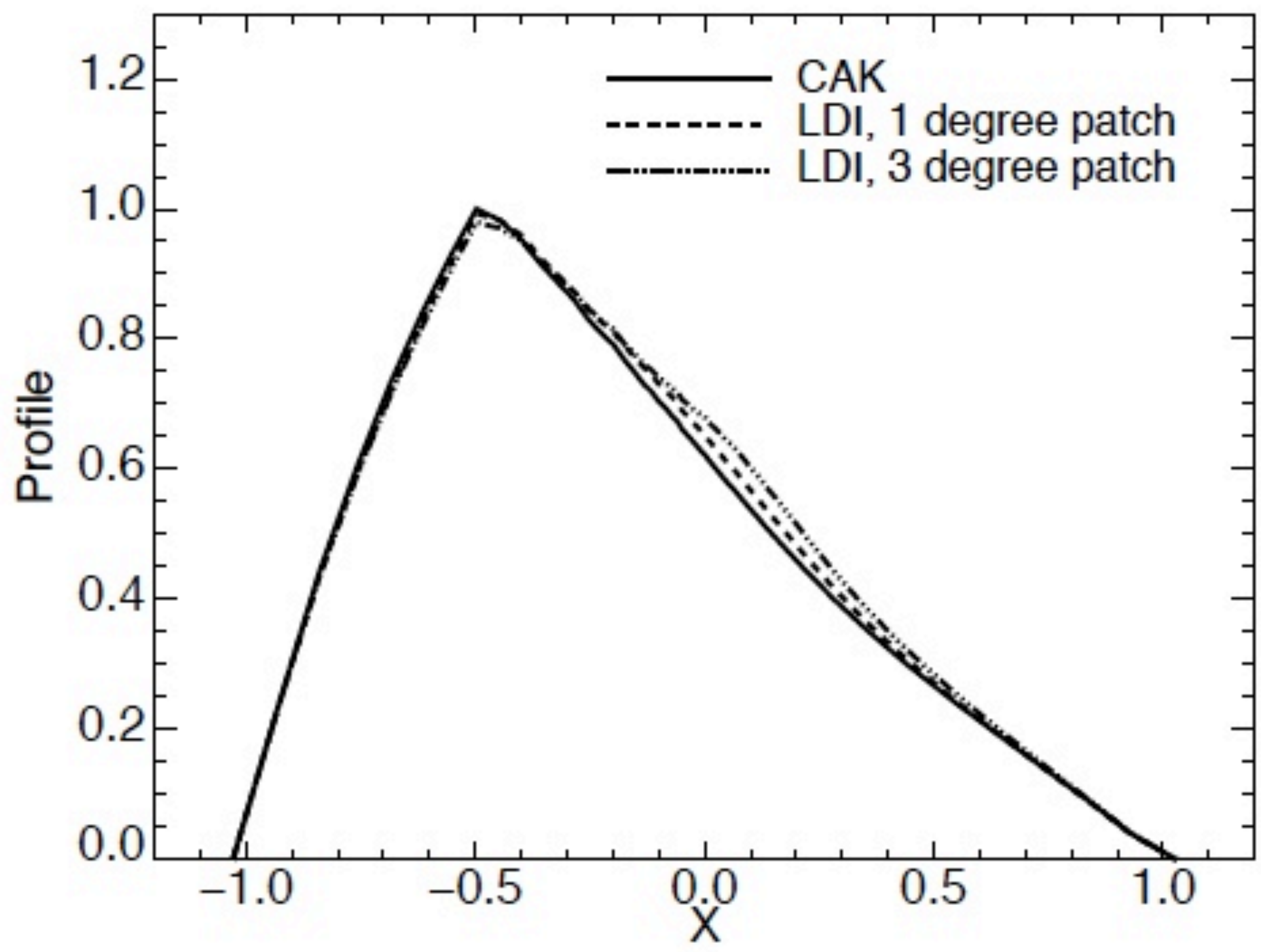

Figure 6. Line profiles for $\tau_\star = 2.5$, calculated from a smooth CAK model and structured LDI models with patch sizes 1 and 3 degrees (see text), as labelled.